BRUNEL UNIVERSITY

Spectral and wave function statistics in Quantum *di*graphs

by

Rodrigo Megaides

A thesis submitted for the degree of
Doctor of Philosophy

in the
School of Inf. Systems, Computing and Mathematics
Mathematical Sciences

July 2012

"They bark, Sancho: a sign that we are moving."

Don Quixote (apocryphal)

BRUNEL UNIVERSITY

Abstract

School of Inf. Systems, Computing and Mathematics
Mathematical Sciences

Spectral and wave function statistics of the quantum *directed* graph, QdG, are studied. The crucial feature of this model is that the direction of a bond (arc) corresponds to the direction of the waves propagating along it. We pay special attention to the full Neumann *di*graph, FNdG, which consists of pairs of antiparallel arcs between every node, and differs from the full Neumann graph, FNG, in that the two arcs have two incommensurate lengths.

The spectral statistics of the FNG (with incommensurate bond lengths) is believed to be universal, i.e. to agree with that of the random matrix theory, RMT, in the limit of large graph size. However, the standard perturbative treatment of the field theoretical representation of the 2-point correlation function [1, 2] for a FNG, does not account for this behaviour.

The nearest-neighbor spacing distribution of the closely related FNdG is studied numerically. An original, efficient algorithm for the generation of the spectrum of *large* graphs allows for the observation that the distribution approaches indeed universality at increasing graph size (although the *convergence* cannot be ascertained), in particular "level repulsion" is confirmed.

The numerical technique employs a new *secular equation* which generalizes the analogous object known for undirected graphs [3, 4], and is based on an adaptation to digraphs of the idea of wave function continuity.

In view of the contradiction between the field theory [2] and the strong indications of universality, a non-perturbative approach to analysing the universal limit is presented. The substitution of the FNG by the FNdG results in a field theory with fewer degrees of freedom. Despite this simplification, the attempt is inconclusive. Possible applications of this approach are suggested.

Regarding the wave function statistics, a field theoretical representation for the spectral average of the wave intensity on an fixed arc is derived and studied in the universal limit. The procedure originates from the study of wave function statistics on disordered metallic grains [5] and is used in conjunction with the field theory approach pioneered in [2].

Foreword

At the end of a long road, plagued with potholes, road works, fake speed cameras, real speed cameras, and much more, this project has finally come to a conclusion. I intended to write a few pages with the details, but now I think I would rather be content with the British road metaphor and move on.

First and foremost, I would like to express my gratitude to my parents, *Inmaculada A.S.* and *Fabien M.*, as I acknowledge the fact that a heavy load had fallen upon them, the burden of my doubts and the occasional moments when lack of purpose or loss of direction were lurking. They were trapped behind a glass from where they could sense my despair, and felt powerless. "Oh dear, I just wish I knew what to do, I just wish I knew anything..." I remember my mother saying. She did know, and she was right. I am so grateful to her for having a faith in me that is much stronger than my own.

I have enjoyed plenty of advice and support from *Alex M.*, whose wisdom and friendship have been crucial during the last stages of my PhD, when I had to take important decisions in the face of contradictory considerations and uncertain outcomes. At that time, "material" obstacles reached a peak, and it all contributed to creating a somewhat surrealistic picture. But life had him and my old friend *Bernard K.* ready to help. While I will do my best to completely forget those days, I will not forget you guys.

I have learnt a lot on the road.

For a start, I have learnt a lot of Maths and Physics. And I have learnt to learn better. I am less dependent on my own "instinctive" ways of understanding, less reluctant to approach the unknown from previously unusual directions, less prone to mistrust what I have not yet understood, more aware of my many weaknesses... I owe a great part of that to my supervisor, *Igor S.*, to whom I am grateful.

That was only the start, but the rest would take too long to recount and it would perhaps be perceived as out of purpose, so I will skip it then.

Many people have contributed to the completion of this manuscript and to the successful end of my studies, one way or another. Like any person that ever wrote a thesis, out of fear of forgetting somebody I will not try to mention every one of you, but I sincerely thank you all. And I will point out now that the responsibility

for the likely mistakes is fully mine, a statement that I would like to emphasize here beyond the mere protocol.

It is undeniable that the decision to undertake this work, and then conclude it no matter what, has been so overreaching that it has affected everything, and viceversa. As a result I feel as if every person with whom I have ever been in contact has had some influence, good, bad or mixed. But what matters now, I think, is that the immense majority of you share some of the satisfaction that I am enjoying at this very moment. To you I feel grateful, so much that, had that slot not been taken by my recent nieces, to all of you I would be tempted to dedicate my thesis. With the exception of the first page, which I would dedicate to the rest, while I remind myself of their irrelevance.

Contents

List of Figures

List of Tables

Abbreviations

DOS	**D**ensity **O**f **S**tates
FNG	**F**ull **N**eumann **G**raph
FNdG	**F**ull **N**eumann **di**G**r**aph
LSD	**L**evel **S**pacing **D**istribution
POT	**P**eriodic **O**rbit **T**heory
QFT	**Q**uantum **F**ield **T**heory
QG	**Q**uantum **G**raph
QdG	**Q**uantum **di**G**r**aph
RMT	**R**andom **M**atrix **T**heory

Symbols

ι	imaginary constant
V	total number of vertices
B	total number of bonds (pairs of arcs) in a graph (digraph)
d^v	degree of vertex v
k	wave number
d(k)	density of states
Δ $(1/\Delta)$	mean level spacing (mean density of states)
F	Classical graph propagator
Σ	Quantum scattering matrix
U(k)	Quantum propagator
str	*super*trace
sdet	*super*determinant
tr*	trace without the invariant eigenspace

Dedicated to Sara and Miriam.
I don't know you yet but I'm looking forward to it...

Chapter 1

Introduction

1.1 Historical background

1.1.1 Quantum physical systems and chaos

The quantum *eigenstates*, $\psi_1, \psi_2, \ldots$, and *eigenenergies*, $E_1, E_2, \ldots$, of a physical system described by a Hamiltonian H, are solutions of the Schrödinger equation

$$H\psi_i = E_i\psi_i, \tag{1.1}$$

where the Hamiltonian, or Schrödinger operator, may be constructed, in the case of a system of N spatial degrees of freedom, $x_1, \ldots, x_N$, as

$$H = \sum_{i=1}^{N} \frac{-\hbar^2}{2m_i}\frac{\partial^2}{\partial x_i^2} + V(x_1, \ldots, x_N), \tag{1.2}$$

and acts on wave functions $\psi(x_1, \ldots, x_N)$.

The dynamics of a *classical* Hamiltonian system is described by the Hamilton-Jacobi (HJ) equation [6], which is obtained from Eq. (1.1) in the $\hbar \to 0$ limit, where $\hbar$ is the Planck constant. In this case, the system is said to be *chaotic* if the phase-space trajectories (given by the solutions to the HJ equation) follow certain properties [7], of which the one usually mentioned is the high sensitivity to initial

conditions [8], or "butterfly effect", manifest by two initially very close trajectories diverging exponentially with time[1].

The subject of *Quantum Chaos* is the quantum mechanical behavior exhibited by physical systems which are classically chaotic. Specifically, the question asked is: "what features of a quantum mechanical system would indicate the chaotic nature of its classical counterpart?". A HJ equation is always non-separable (equivalently, non-integrable) when its solutions exhibit chaotic (as opposed to regular) dynamics, and importantly, non-integrability is transferred from the HJ equation to the Schrödinger equation corresponding to the same physical system, thus non-separability can be seen as the "deepest characterization of chaos" [9]. However, in classical systems, chaos is a property of *phase-space trajectories*, i.e. it characterizes the *solutions* of the HJ equation (as mentioned in the paragraph above). It ensues indeed from non-integrability, but the integrability criterium does not tell us anything about quantum *states* $(\psi_1, \psi_2 \ldots)$ or energies[2]. To rephrase, then, the question above, "what features of the quantum states of a system reflect its chaotic/regular classical dynamics?".

Percival [12] first suggested that the energy spectrum of quantum systems shows two distinct behaviours associated, respectively, with regions of the classical phase space with regular and with chaotic dynamics. In this connection, it was (empirically) established (see [13, 14] and [9] and references therein) that neighboring energy levels of classically integrable systems (with more than one degrees of freedom) tend to cluster, while neighboring levels of non-integrable systems whose phase-space is dominated by chaos tend to "repel" each other. Moreover the strength of the repulsion was seen to fall into *universality classes*, each depending only on certain symmetries and otherwise completely system-independent.

It is well known that eigenvalues from matrices with random components tend to exhibit repulsion, and that this phenomenon is highly independent from the specific random distribution. Under mild conditions on the explicit probability distribution of matrix components, the degree of eigenvalue repulsion of Hermitian

[1] The others are that any region of the phase-space, evolving under a chaotic Hamiltonian, will overlap any other region ("topological mixing") and that any point of the phase space is approached arbitrarily closely by a closed phase space trajectory ("density of periodic orbits").

[2] An analog to the butterfly effect is not expected in quantum systems [10], although the closely related phenomenon of the divergence of two *identical states* under slightly different Hamiltonians does occur [11].

random matrices can be easily found [9] to be

$$P(S) \propto S^{\beta}, \quad S \sim 0, \tag{1.3}$$

where $P(S)$ is the probability of finding consecutive eigenvalues at a distance S, and $\beta = 2$. Further adding the restriction that the random matrix be symmetric, one would find[3] $\beta = 1$. Bohigas, Gianonni and Schmit [15], based on their study of classically chaotic systems with few degrees of freedom (Sinai's billiard) put in contact, on one hand, the "random matrix physics", i.e. the average quantum physics of systems that can be modelled by ensembles of Hamiltonians with appropriate symmetries, and before thought to be applicable only to "complex" physical situations (i.e. those involving many degrees of freedom) and on the other hand, chaotic classical physics. They conjectured explicitly that "spectra of time reversal invariant systems show the same fluctuation properties as predicted by the Gaussian orthogonal ensemble (GOE)" of Random Matrix Theory (RMT -see chapter 2).

Since the eighties, understanding *why* classically chaotic systems possess such quantum-mechanical universal features has become a focus of major research, mostly within the field of *semiclassical analysis* which characterizes quantum systems (in this context, their spectral correlations) in the limit of small Planck's constant. Taking this approach, Gutzwiller [16, 17] could express the distribution of *quantum* energy levels as a sum over *classical* periodic orbits (*trace formula*), and from there any measure of fluctuations in quantum levels can be expressed in terms of constructive interference between sufficiently close periodic orbits. Gutzwiller *periodic-orbit theory*, POT, is essentially a semiclassical approximation to classically chaotic quantum systems, and completes the picture of the *old quantum mechanics* only applicable to integrable systems[4].

[3]The parameter β is related to the "co-dimension of a level crossing", that is, the number of independent parameters that one needs to adjust in order to collapse into each other the two eigenvalues of a 2×2 matrix. This number is easily shown to be one fewer than the total number of independent parameters of the matrix itself: 4 independent parameters in a Hermitian matrix give rise to a co-dimension equal to 3, while 3 parameters in symmetric matrices give rise to a co-dimension 2. Incidentally, 2×2 quaternion Hermitian matrices have 6 independent parameters and a co-dimension 5. A straightforward calculation produces the result shown in Eq. (1.3), with the exponent β being equal to co-dimension minus 1 ([9]).

[4]In fact, the domain of applicability of the old quantum mechanics was identified already by Einstein [18] to consist of physical systems with orbits which, passing a possibly infinite number of times over a small region, they do so only with a *finite* number of different momenta. He pointed out as well that the number of constants of motion needs to, at least, equal the number of degrees of freedom. Although not known at the time, these two properties of classical dynamics are themselves directly related to a system *not* displaying chaos.

The first step in understanding quantum spectral correlations from the investigation of classical periodic orbits correlations was taken by Berry [19] who calculated the contribution from *one-loop* orbits, i.e. orbits with no crossing points ("diagonal approximation"). The contribution of one-loop orbits is dominant in the limit of periodic orbits which are short compared to the typical system size, or in other words in the limit of small time compared to the Heisenberg time; for this reason, the *short time* contribution accounts only for the universal (i.e. RMT like), *large scale* structure of the spectral correlations (i.e. correlations between eigen-levels further apart than the typical level spacing). Sieber and Richter [20, 21] calculated the contribution from *two-loop* orbits (orbits with one single crossing point), finding the next-to-leading order in the short time expansion of the universal correlations. The complete calculation has been achieved recently by Müller *et al.* [22].

In parallel with the POT, another approach was taken, based on Quantum field theory (QFT) techniques, for the study of *average* spectral properties of *ensembles* of chaotic systems such as small[5] metallic grains, where one averages over distributions of impurities and lattice defects ("disorder" in the literature). By giving up on obtaining results for single-sample systems ("clean" systems in the literature), the method, developed by Efetov [23][6], reproduces the RMT results[7] beyond the Heisenberg time, hence resolving the important *small scale* spectral structure, indispensable in order to account for the highly universal *level repulsion* mentioned in a previous paragraph. Incidentally, it was based on an analogy with disordered systems [28] that Sieber and Richter (see above) suggested that two-loop orbits account for the next-to-leading order in the short time expansion, and the authors of [22] took their insight from that direction as well.

1.1.2 Quantum graphs

A *Quantum graph* (QG) consists of a Schrödinger operator (often just a Laplacian) acting on a metric graph. Such a model was first used in Physics by Pauling [29] in the context of quantum organic chemistry, representing non-localised electrons

[5] "Small" here means that the typical system dimension is much shorter than the *inelastic* mean free path of conducting electrons, hence preserving *coherence* of their wave function.

[6] Based on initial work by Schafer and Wegner [24, 25] and Verbaarschot *et al.* [26].

[7] Although these were *conjectured* for such systems much earlier by Gor'kov and Eliashberg [27].

moving inside a network-shaped domain that mimics the molecule. Ruedenberg and Scherr [30] used QGs in the same context, and were the first to consider the construction of wave equations with appropriate boundary conditions on the metric graph. They considered the QG as the limit, when the cross-section of the wires tends to zero (i.e. becoming metric links of the graph), of a network of thin wires (or wave-guides) attaching to each other in positions which would become, in the limit, the vertices of the graph[8]. They were introduced to the Quantum chaos community by Kottos and Smilansky [3].

In the last 15 years, quantum graph models and the universality (or lack of it) of their spectral statistics have been studied extensively. Those models are often not intended to represent any specific physical system, rather, they are used to shed light on the general phenomena of quantum chaos. In this context, QGs are convenient because they are "simple enough" to allow some level of analytical treatment (and great level of numerical exploration) while rich enough to show a plethora of interesting quantum-chaotic features. Kottos and Smilansky [3, 4] introduced the tools, in the frame of the POT, for their analytical study and derived a *trace formula*[9] similar to the Gutzwiller trace formula for chaotic Hamiltonian systems, but with the added benefit of being exact as opposed to asymptotic in the Planck constant. The authors found as well the first numerical evidence of good agreement between the spectral statistics of individual graphs and that predicted by the RMT. Tanner [36] found a condition for ensembles of QGs to follow Wigner-Dyson statistics in the diagonal approximation (i.e. large scale spectral correlations), and conjectured universality at all spectral scales under the same condition. Berkolaiko *et al* [37, 38] performed the periodic orbit counting beyond the diagonal approximation and could reproduce shorter scale contributions under a slight generalization of that conjecture.

Gnutzmann and Altland [1, 2] pioneered the implementation of the already mentioned QFT technique on QGs. Unlike in the previously mentioned case of disordered systems, the authors managed to work on a *single* QG and mapped their

[8] In the context of QGs, a network of thin (finite) wires is currently called a *fat quantum graph*, for a recent work on the interplay of Quantum graphs and fat Quantum graph see [31]. Alternatively, one can imagine the links as the center of an attractive potential for the electron whose wave function one models, those graphs are called *leaky graphs* because the electron is not locked on the links (it can in fact tunnel from a link to another), but becomes so in the limit of infinitely attractive potential [32]. QGs have been applied to a variety of physical systems (see the bibliography in [33]) and have been simulated experimentally [34].

[9] A trace formula for quantum graphs had already been derived, by Rot [35], in a different manner and with less general boundary conditions.

problem to a super-symmetric nonlinear σ-model of Efetov's type [23], by using a variant of the technique developed by Zirnbauer[10] [40]. The authors found a more restrictive condition for universality than the previous studies [36–38], but could reproduce the universal statistics at all scales. The same field theoretical method was later used in order to investigate the wave function statistics on the QG by Gnutzmann *et al.* [41, 42].

1.2 Motivation and outline

Quantum graphs, as we consider them here, are characterized by three aspects. First, the *topology*, i.e. the merely graph-theoretical aspect. Second, the *lengths* which are associated with the links. And third, the *boundary conditions* at the nodes, related to the Schrödinger operator. Since the work by Kottos and Smilansky, a type of QG that is often studied by the Quantum Chaos community is the one characterized in its topology by having every node connected to every other, i.e. being a *full graph*, and by having *Neumann*-type boundary conditions. The so called *full Neumann graph* (FNG) then, possesses two features which oppose each other in terms of their dynamical behaviour: chaotic (universal) dynamics tends to dominate in the presence of high connectivity, while it is inhibited by the Neumann boundary conditions, which strongly favor back-scattering at the nodes.

It is believed that the FNG has universal spectral statistics, as it satisfies Tanner criterium [36] and the POT approach leads to universal results as well [37]. The QFT criterium [2], however, is not satisfied. These two facts lead us to further investigate the Gnutzmann and Altland field theory *for the specific case* of the FNG, with the aim of devising a theory which, being model-specific, would allow us to recover the expected universal result. An additional complication in the field theory of the FNG is the presence of certain degrees of freedom whose non-universal contribution, contrary to other cases of QGs, cannot be easily neglected in the large size limit. The strength of that contribution is directly related to the strength of backscattering, and is thus inescapable because the Neumann boundary conditions are the ones we wish to study. The *existence* of those degrees of freedom, however, has a totally different origin: they arise from the fact that, when travelling across

[10]Interestingly, in more general circumstances Zirnbauer's technique does resort to ensemble averaging: it is needed *after* the mapping to the field theory, in order to be able to justify the reduction to its mean-field part, reproducing the universal result (see [39]).

a link, waves accumulate the same phase *irrespective of the direction*. Therefore, with the aim of simplifying the problem, we consider a model in which such phases are uncorrelated. This is accomplished by substituting, in the usual metric graph, every *bi-directional* bond and its corresponding length, by a pair of anti-parallel, *mono-directional* bonds with two different lengths, hence transforming it into a metric directed graph.

Two methods of constructing a QG can be found in the Quantum Chaos literature (see [33] for a review). The first one consists in assigning a unitary matrix to every node, with a matrix component assigned to every pair of links branching from that node. This is the *scattering approach*: a wave function on those links is viewed as a superposition of waves travelling in opposite directions, and being scattered to other links in correspondence with the above mentioned unitary matrix. As pointed out by Tanner [43], this approach does *not* rely on the links being bi-directional: one can *a priori* assign directions *to the waves* traveling on a link. This is the concept that we denote by *quantum digraph*, QdG: the direction of the link (or *arc*) signals precisely the direction of the waves that are on it. We construct the QdG, following this approach, in chapter 3, where we review as well some elementary results. The second approach consists in solving the Schrödinger equation on the graph, usually[11] imposing the condition that the wave function is continuous on the graph. This second method has the advantage that the stationary waves on the graph are described by *only* V parameters, V being the number of vertices, usually much smaller than the number of bonds, B. This scheme is much better suited for the numerical generation of the spectrum, but its generalization for QdGs was not known. A suitable scheme is newly implemented in chapter 6. In chapter 7 we use the result of the previous chapter in order to numerically generate the spectrum of large full Neuman digraphs, FNdG, and study their spacing distribution, LSD. In this chapter, we present an efficient algorithm for spectrum generation, and confirm the indications of universality for complete Neumann graph, by means of a systematic study of how the LSD approaches universality at increasing graph size.

In chapter 4, we present the (incomplete) non-perturbative study of the universal 2-point correlation function from Gnutzmann and Altland [2] field theory applied to the FNdG.

[11] But not always, see [44] for "generalized" boundary conditions.

In chapter 5 we derive a functional for wave intensity statistics, applicable to general digraphs, and study the universal limit.

Chapter 2

Preliminaries I: spectral sequences and Random Matrix Theory

2.1 Introduction

In this introductory chapter, we develop the tools and the language that we will need in order to characterize the spectral fluctuations of the quantum digraph.

In the literature about the subject of random matrix theory, one usually finds the description of the random matrix ensembles at an early stage, followed by the derivation of their spectral statistical properties. Here, we prefer to consider the sequence of eigenvalues of a given operator (in our case, a single quantum graph) first, due to two reasons. On the one hand, from an "experimental" perspective, this is really the object that is observed and studied: sequences of resonances of complex nuclei, sequences of eigen-energies of small metallic particles, sequences *numerically* generated eigenvalues of a specific operator (in our case, they will be wave numbers of stationary waves in the graph), etc. On the other hand, the *theoretical* treatment that we give to our system, the QdG, will be based on averages over the spectrum of *single samples*. How the statistical properties of these sequences compare to that from the spectra of random matrices, is what one investigates a posteriori. Hence our focus on the description of spectral sequences,

which occupies the section 2.2. Only afterwards, in 2.3, we touch upon the few properties of random matrix ensembles that we need for the rest of this text.

2.2 Characterization of spectral sequences

2.2.1 Basic definitions

Let us consider a sequence of N *real* numbers,

$$-\infty < \lambda_1 < \lambda_2 < \ldots < \lambda_N < \infty.$$

We will denote these numbers by "levels", and the sequence by "spectrum" (as they could represent, for example, the eigenvalues of a $N \times N$ hermitian matrix). Let us characterize such sequence, by the following combinations of delta functions:

$$r_1(x) \equiv \sum_{i=1}^{N} \delta(x - \lambda_i), \tag{2.1}$$

$$r_2(x_1, x_2) \equiv \sum_{i_1=1}^{N} \sum_{i_2 \neq i_1} \delta(x_1 - \lambda_{i_1}) \delta(x_2 - \lambda_{i_2}), \tag{2.2}$$

$$\ldots \equiv \ldots, \tag{2.3}$$

$$r_n(x_1, x_2, \ldots, x_n) \equiv \sum_{\{i_1, \ldots, i_n;\ i_j \neq i_k\}} \delta(x_1 - \lambda_{i_1}) \delta(x_2 - \lambda_{i_2}) \ldots \delta(x_n - \lambda_{i_n}), \tag{2.4}$$

$$\ldots \equiv \ldots, \tag{2.5}$$

$$r_N(x_1, x_2, \ldots, x_N) \equiv \sum_{\{i_1, \ldots, i_N;\ i_j \neq i_k\}} \delta(x_1 - \lambda_{i_1}) \delta(x_2 - \lambda_{i_2}) \ldots \delta(x_N - \lambda_{i_N}), \tag{2.6}$$

where $\sum_{\{i_1, \ldots, i_n;\ i_j \neq i_k\}}$ represents a sum over all, $\frac{N!}{(N-n)!}$, combinations of n indices which take values from 1 to N, *without repetitions*. We can call r_n the *n-point density function*. It is obvious that r_n integrates to the number of possible combinations of indices, i.e.

$$\int_{\mathbb{R}^n} r_n(x_1, \ldots, x_n) dx_1 \ldots dx_n = \frac{N!}{(N-n)!}. \tag{2.7}$$

It is clear as well that the *densities* are symmetric under permutation of their variables, and that one can obtain r_n from r_{n+1} by integrating any one of the $n+1$

variables in the latter, i.e.

$$r_n(x_1,\ldots,x_n) = \frac{1}{N-n}\int_{\mathbb{R}} r_{n+1}(x_1,x_2\ldots,x_n,x_{n+1})dx_{n+1}. \tag{2.8}$$

The n-density can be calculated from combinations of products of $n-1,\ldots,\ 2,\ 1$ densities, for example

$$r_2(x_1,x_2) = r_1(x_1)r_1(x_2) - \delta(x_1-x_2)r_1(x_1), \tag{2.9}$$

$$r_3(x_1,x_2,x_3) = r_1(x_1)r_2(x_2,x_3) + r_1(x_2)r_2(x_1,x_3) + r_1(x_3)r_2(x_1,x_2) \tag{2.10}$$

$$- 2r_1(x_1)r_1(x_2)r_1(x_3) + \delta(x_1-x_2)\delta(x_1-x_3)r_1(x_1), \tag{2.11}$$

but one needs to add terms such as $\delta(x_1-x_2)$ (for example in Eq. (2.9)) due to the fact that the densities $r_2,\ r_3$ etc do *not* include summands such as $\sum_i \delta(x_1-\lambda_i)\delta(x_2-\lambda_i),\ \sum_i \delta(x_1-\lambda_i)\delta(x_2-\lambda_i)\delta(x_3-\lambda_i)$, etc.

The integration of the one-point density, r_1, over a domain[1] $D\in\mathbb{R}$ produces the number, N_D, of levels within this domain. More generally, the integral

$$\int_{D^n} r_n(x_1,\ldots,x_n) = \frac{N_D!}{(N_D-n)!}, \tag{2.12}$$

counts the number of groupings with exactly n levels that can be formed with the N_D levels lying in D, with different orderings of the same values being counted as different groupings.

The following bi-variate distributions are also important:

$$l(n;x_1,x_2) \equiv \sum_{i=1}^{N-(n+1)} \left(\delta(x_1-\lambda_i)\delta(x_2-\lambda_{i+n+1}) + \delta(x_2-\lambda_i)\delta(x_1-\lambda_{i+n+1})\right). \tag{2.13}$$

$r_2(x_1,x_2)$ can be recovered from these distributions through

$$r_2(x_1,x_2) = \sum_{n=0}^{N-2} l(n;x_1,x_2). \tag{2.14}$$

[1]This domain should be chosen in such a way that all the levels are properly accounted for.

2.2.2 Spectral average and mean level spacing

Let us average the distribution $l(0; x_1, x_2)$, Eq. (2.13), *over the spectrum*. By this we mean the integral

$$\bar{l}(y) \equiv \int_{\mathbb{R}} l(0; x, x+y)dx, \quad y \geq 0, \tag{2.15}$$

i.e.

$$\bar{l}(y) = \sum_{i=1}^{N-1} \delta(y - (\lambda_{i+1} - \lambda_i)). \tag{2.16}$$

The function $\bar{l}(y)$ produces a "spike" every time that y coincide with the distance of any two consecutive levels, hence (when properly normalized) it could be interpreted so that $\int_x^{x+s} \bar{l}(y)dy$ represents the probability of finding the spacing between any two consecutive levels to lie between x and $x+s$. However, since universal features affecting the spectral statistics of quantum operators are *local*, namely they are valid within regions of consecutive levels of the spectrum with a specific *average* spacing, the distribution Eq. (2.15) is not convenient because it averages "blindly" over the entire spectrum. It could lead us, for example, to describe a region where the levels are more "packed" as one with less *level repulsion*. Therefore any distance between two specific levels needs to be weighted with respect to the *mean level spacing* in their region of the spectrum. We will define the *mean level spacing* over a region of length X centered around a point x, as

$$\Delta_X(x) \equiv \frac{X}{\int_{x-\frac{X}{2}}^{x+\frac{X}{2}} r_1(x')dx'} \tag{2.17}$$

$$\equiv \frac{X}{N_X(x)}, \tag{2.18}$$

where $N_X(x)$ is the number of levels in the above mentioned region. The interval, X, needs to be large enough for $N_X(x) \gg 1$, so that $\Delta_X(x)$ is smooth[2] on x, but small enough so as to allow $\Delta_X(x)$ to reflect global variations. When such ideal interval can be found (we refer to [9] for more details), one can use it to define the *mean level spacing*, $\Delta(x)$, and its inverse, the *average density of state*. It is now possible to transform the entire level sequence, or to "unfold the spectrum", as[3]

$$\lambda_i \to \frac{\lambda_i}{\Delta(\lambda_i)}, \tag{2.19}$$

[2]This means that it varies very little over intervals typically encompassing a few levels.
[3]There are other possible transformations of this type (see [9]).

so that one has now a spectrum with mean level spacing $\Delta = 1$. *We will assume from this point that such transformation has been performed in our sequences.*

The spectral averaged *two-point correlation function* is defined as[4],

$$\bar{r}_2(s) \equiv \frac{1}{N}\int_{\mathbb{R}} r_2(x, x+s)dx, \quad s \geq 0 \tag{2.20}$$

$$= \frac{1}{N}\sum_{i<j}\delta(s-(\lambda_j-\lambda_i)) \tag{2.21}$$

$$= \frac{1}{N}\sum_{i,j}\delta(s-(\lambda_j-\lambda_i)) - \delta(s) \tag{2.22}$$

$$= \frac{1}{N}\int_{\mathbb{R}} r_1(x)r_1(x+s)dx - \delta(s), \tag{2.23}$$

where Eq. (2.23) is analogous to Eq. (2.9). Defining as well the *spacing distributions*

$$\bar{l}(0;s) \equiv \frac{1}{N}\int_{\mathbb{R}} l(0;x,x+s)dx, \quad y \geq 0 \tag{2.24}$$

$$\bar{l}(1;s) \equiv \frac{1}{N}\int_{\mathbb{R}} l(1;x,x+s)dx, \quad y \geq 0 \tag{2.25}$$

$$\bar{l}(2;s) \equiv \frac{1}{N}\int_{\mathbb{R}} l(2;x,x+s)dx, \quad y \geq 0 \tag{2.26}$$

$$\ldots \equiv \ldots \tag{2.27}$$

which are called, respectively, *nearest-neighbor spacing distribution* (or *level spacing distribution*, LSD), *next-nearest neighbor spacing distribution*, etc, and noticing that

$$\bar{l}(n;s) = \frac{1}{N}\sum_{i=1}^{N-(1+n)}\delta(s-(\lambda_{i+1+n}-\lambda_i)), \tag{2.28}$$

we recover a version of Eq. (2.14):

$$\bar{r}_2(s) = \sum_{n=0}^{N-2} l(n;s). \tag{2.29}$$

[4]This definition would be of little use is the spectrum had qualitatively different regions, corresponding, for example, to zones which are "regular" and zones which are "chaotic" as explained in the previous chapter. However this is not going to be our case when studying the QdG spectrum.

2.2.3 Spectral levels as random variables

If the levels are drawn from a joint probability distribution, $P(\lambda_1, \ldots, \lambda_N)$, with the property

$$P(\pi(\lambda_1, \ldots, \lambda_N)) = P(\lambda_1, \ldots, \lambda_N), \tag{2.30}$$

being $\pi(\lambda_1, \ldots, \lambda_N)$ any permutation of the N variables, we define

$$\begin{aligned} R_1(x) &\equiv \int_{\mathbb{R}^N} r_1(x) P(\lambda_1, \ldots, \lambda_N) d\lambda_1 \ldots \lambda_N && (2.31)\\ &= \sum_{i=1}^{N} \int \delta(x - \lambda_i) P(\lambda_1, \ldots, \lambda_N) d\lambda_1 \ldots \lambda_N && (2.32)\\ &= N \int_{\mathbb{R}^{N-1}} P(x, \lambda_2, \ldots, \lambda_N) d\lambda_2 \ldots d\lambda_N, && (2.33) \end{aligned}$$

where in the third line, we employ Eq. (2.30). For any $n \leq N$, the *n-point correlation function* reads similarly

$$\begin{aligned} R_n(x_1, \ldots, x_n) &\equiv \int_{\mathbb{R}^N} r_n(x_1, \ldots, x_n) P(\lambda_1, \ldots, \lambda_N) d\lambda_1 \ldots \lambda_N && (2.34)\\ &= \frac{N!}{(N-n)!} \int_{\mathbb{R}^{N-n}} d\lambda_{n+1} \ldots d\lambda_N P(x_1, \ldots, x_n, \lambda_{n+1}, \ldots, \lambda_N). && (2.35) \end{aligned}$$

The second line, Eq. (2.35), is the original definition by Dyson [45].

2.3 Random Matrix Theory

In order to reproduce the strong correlations in resonance spectra of complex nuclei, Wigner [46] introduced the idea of modeling them by the spectral correlations or random, 2×2 symmetric matrices *with independent entries*. The level spacing distribution obtained in this way, called *Wigner surmise*, reads

$$l_{\mathrm{W}}(s) = \frac{\pi s}{2} e^{-\frac{\pi s^2}{4}}, \tag{2.36}$$

and reproduces quite accurately the level repulsion observed between the above mentioned resonances[5]. Following Wigner's idea, a general *Random Matrix Theory* was developed, the cornerstone of which is the Wigner-Dyson classification of

[5] Eq. (2.36) compares naturally to Eq. (1.3) with $\beta = 1$.

Gaussian matrix ensembles[6]. Those are characterized by a probability density distribution such as

$$P(\beta; H)dH \propto e^{-\frac{\beta}{2}\mathrm{tr}H^2}dH, \tag{2.37}$$

where H is a $N \times N$ symmetric matrix[7] ($\beta = 1$ in this case), complex Hermitian matrix ($\beta = 2$), or real quaternion matrix ($\beta = 4$). The above ensembles are called, respectively, Orthogonal, Unitary and Symplectic, due to the transformations of H under which $P(H)dH$ is invariant. Invariance of the probability distribution on its own implies that $P(H)$ depends only on the traces $\mathrm{tr}H, \mathrm{tr}H^2, \ldots, \mathrm{tr}H^{N-1}, \mathrm{tr}H^N$, while the requirement that entries of H be statistically independent restricts $P(H)$ even more so as to become Gaussian [48], as in Eq. (2.37). Physical systems with time reversal invariance are modeled by the orthogonal ensemble, while systems without such invariance are modelled by the unitary ensemble, or if they have half integer spin and broken rotational symmetry, by the symplectic ensemble.

The rotations (unitary, for example, in the $\beta = 2$ case) diagonalizing H can be integrated out easily in Eq. (2.37) [48, 49], leaving the probability distribution for the eigenvalues

$$P(\beta; \lambda_1, \ldots, \lambda_N) \propto \prod_{i<j} \mid \lambda_i - \lambda_j \mid^{\beta} e^{-\frac{\beta}{2}\sum_i^N \lambda_i}. \tag{2.38}$$

We will focus on the *Gaussian Unitary Ensemble*, GUE, because it is relevant for the thesis. Substituting $P(2; \lambda_1, \ldots, \lambda_N)$ in Eq. (2.34) [48, 49], one can calculate any correlation function. In the $N \to \infty$ limit,

$$R_2(s) = 1 - \frac{\sin^2(\pi s)}{(\pi s)^2}. \tag{2.39}$$

The *spectral form factor* is defined as the Fourier transform of $R_2(s) - 1 + \delta(s)$. For the GUE ensemble, it reads

$$K(\tau) \equiv \int_{\mathbb{R}} \left(\delta(s) - \frac{\sin^2(\pi s)}{(\pi s)^2}\right) e^{\iota 2\pi s\tau} ds \tag{2.40}$$

$$= \begin{cases} \tau & : \tau < 1 \\ 1 & : \tau \geq 1 \end{cases}. \tag{2.41}$$

[6] as well as the circular ensembles introduced by Dyson [45, 47].

[7] Making $N = 2$ Eq. (2.36) can be derived from Eq. (2.37).

The *small frequency* expansions of the spacing distributions for the GUE ensemble (we do not worry here about the large frequency asymptotics) valid up to $s \sim 2.3$ [50], reads:

$$L_{\mathrm{GUE}}(0;s) = \frac{\pi^2 s^2}{3} - \frac{2\pi^4 s^4}{45} + \frac{\pi^6 s^6}{315} - \frac{\pi^6 s^7}{4050} - \frac{2\pi^8 s^8}{14175} + \frac{11\pi^8 s^9}{496125} + \dots \tag{2.42}$$

$$L_{\mathrm{GUE}}(1;s) = \frac{\pi^6 s^7}{4050} - \frac{11\pi^8 s^9}{496125} + \dots \tag{2.43}$$

$$L_{\mathrm{GUE}}(2;s) = O(s)^{14} \tag{2.44}$$

$$L_{\mathrm{GUE}}(3;s) = O(s)^{23} \tag{2.45}$$

$$L_{\mathrm{GUE}}(4;s) = O(s)^{34} \tag{2.46}$$

$$L_{\mathrm{GUE}}(5;s) = O(s)^{47}. \tag{2.47}$$

Expanding $R_2(s)$ from Eq. (2.39),

$$\begin{aligned} R_2(s) = \frac{\pi^2 s^2}{3} - \frac{2\pi^4 s^4}{45} + \frac{\pi^6 s^6}{315} - \frac{2\pi^8 s^8}{14175} \\ + \frac{2\pi^{10} s^{10}}{467775} - \frac{4\pi^{12} s^{12}}{42567525} + \frac{\pi^{14} s^{14}}{638512875} - \frac{2\pi^{16} s^{16}}{97692469875} + O\left(s^{17}\right), \end{aligned} \tag{2.48}$$

one can check that Eq. (2.29) is reproduced up to some order (odd powers of s cancel each other). We will need mainly $R_2(s)$ and $L(0;s)$, which, from the above equations, are equivalent up to sixth order in the frequency.

Chapter 3

Preliminaries II: quantum *di*graphs

3.1 Introduction

In this chapter, our aim is to present some known results on Quantum digraphs (QdGs). In particular, we will be interested in the quantization scheme by Tanner [36, 43] and Pakonski *et al.* [51], who showed that the method[1] of Kottos and Smilansky [3] can be generalized and be applicable also for directed graphs (digraphs). Tanner explained [43] that such generalization is twofold. On the one hand, *arbitrary* unitary transition matrices are associated to the vertices, as opposed to such matrices being the *result* of solving the Schrödinger equation on the graph. On the other hand, the transition matrices in Tanner's model act on *directed* bonds (*arcs* in our language), this having the precise meaning that waves traveling on a given arc are *a priori* restricted to the direction of that arc. In order to understand how this restriction generalizes the QG, one simply needs to notice that a bi-directional bond between two vertices can be reproduced, in a QdG, with a pair of *parallel* arcs (i.e. arcs connecting the same two vertices) with opposite directions. We carry out this scheme in section 3.4. Before doing this, we state the basic graph-theoretical ideas that we need, section 3.2, and review some basic features of the classical dynamics on digraphs, section 3.3. Some POT results for QdGs are then described in section 3.5.

[1] In the introduction (page 7), we referred to these two schemes as the first and the second method, respectively, of constructing a QG.

3.2 The directed graph: basic definitions

A *directed* graph, or *digraph*, G is a set of V vertices, labeled $1, 2, \ldots, i-1, i, i+1, \ldots, V-1, V$, and a set, $A(G)$, of *arcs*, which are defined as *ordered* pairs of vertices. The *connectivity matrix*, $C(G)_{V\times V}$, is defined as

$$C(G)_{ij} \equiv \begin{cases} 1 & \text{if } ij \in A(G), \\ 0 & \text{otherwise.} \end{cases} \tag{3.1}$$

We say that an arc ij "exists" *iff* $C_{ij} = 1$, or, equivalently *iff* $ij \in A$.
For a generic vertex, i, one defines the *in-degree*, d^i_{in}, and the *out-degree*, d^i_{out}, as the number of arcs incoming to, and outgoing from i, respectively. Formally

$$d^i_{\text{in}} \equiv \sum_{j=1}^{V} C_{ji}, \tag{3.2}$$

$$d^i_{\text{out}} \equiv \sum_{j=1}^{V} C_{ij}. \tag{3.3}$$

If the adjacency matrix is *symmetric*, that is, if $C(G)_{ij} = C(G)_{ji}$, we will say by *definition* that the digraph G *is, itself*, symmetric. Obviously, in the case of symmetric digraphs the arc ji exists *iff* ij exists, and we will say that ij and ji are *anti-parallel*[2]. In this regard, we can define a (undirected) *graph* as a symmetric digraph, and simply think of every pair of anti-parallel arcs as a bi-directional *bond*[3].
We define a *complete* directed graph, or *full* digraph, as one for which every vertex i reaches every other vertex j through arcs ij *and* is reached itself by every vertex k through arcs ki. By construction, *a complete directed graph* is made of anti-parallel connections and *is* therefore *symmetric*.
The digraph that will constitute our model possesses no "loops", i.e. $C_{ii} = 0$ for all i. It is also *connected*, i.e. for *every* subset $H \subset G$, there exists at least one arc in A connecting a vertex in H to another that is *not* in H, and another arc

[2]It is clear from the definition Eq. (3.1) that we have excluded "parallel" connections in the usual, undirected graph-related sense.

[3]In the framework of *metric* graphs, where arcs are given *lengths*, an extra restriction is needed: a *metric graph* is a symmetric, metric digraph with the particularity that the *lengths of anti-parallel arcs coincide*. This will be an essential distinction in the context of *quantum* digraphs.

connecting vertex not in H to vertex[4] in H. The latter is equivalent to stating that there exists some power, C^n, of the adjacency matrix such that $C^n_{ij} \neq 0$ for every pair of nodes i and j, an it implies that there are no "isolated" nodes, i.e. *no column, or row, in C is made entirely of zeros*[5].

3.3 Classical propagation in a digraph

3.3.1 Vertex propagator and digraph propagator

Let us introduce the concept of *vertex propagator*. To every vertex v belonging to the digraph G, we will associate a $d^v_{\text{out}} \times d^v_{\text{in}}$ matrix P^v. Components of this matrix are indexed using $1, 2, ..., c_{\text{in}}, ..., d^v_{\text{in}}$ and $1, 2, ..., c_{\text{out}}, ..., d^v_{\text{out}}$, where every c_{in} (c_{out}) represents a vertex $v(c_{\text{in}})$ with a connection *towards* v (a vertex $v(c_{\text{out}})$ with a connection *outgoing from* v). Considering arcs as random variables, and using stochastic language we may say that the component $P^v_{c_{\text{out}}c_{\text{in}}}$ represents the probability of arc $vv(c_{\text{out}})$ given arc $v(c_{\text{in}})v$. In our language, this will be the *transition probability* from the former arc to the latter, formally:

$$P^v_{c_{\text{out}}c_{\text{in}}} \equiv P(v(c_{\text{in}})v \to vv(c_{\text{out}})). \tag{3.4}$$

P^v naturally needs the properties

$$P^v_{c_{\text{out}}c_{\text{in}}} \geqq 0, \tag{3.5}$$

$$\sum_{c_{\text{out}}=1}^{d^v_{\text{out}}} P^v_{c_{\text{out}}c_{\text{in}}} = 1 \ \forall c_{\text{in}}. \tag{3.6}$$

"Stochasticity", i.e. Eq. (3.6), ensures "probability conservation": given any d^v_{in}-dimensional vector x,

$$\sum_{c_{\text{out}}=1}^{d^v_{\text{out}}} (P^v x)_{c_{\text{out}}} = \sum_{c_{\text{in}}=1}^{d^v_{\text{in}}} x_{c_{\text{in}}}. \tag{3.7}$$

[4]This type of "both ways" connectivity is sometimes called *strong* connectivity in digraphs.

[5]To state this differently, for every vertex v, there is some vertex i for which iv exists, and also some vertex j for which vj exists. While this precision may not be important in the case of undirected graphs, it is crucial concerning digraphs because one needs both "out-connections" from every vertex in order to be able speak of *probability conservation*, as we do already in the next section (see Eq. (3.6)), and "in-connections" to speak of *bi-stochasticity* (see page 21), which is an essential feature of QdGs.

One can "artificially" extend every vertex propagator P^v to a card$A \times$ card$A$ propagator, F^v, acting on the entire space of arcs, simply introducing *vanishing components* for every two arcs that are *not* connected through v. Let v, i, j, k, l be vertices in G, then we define:

$$F^v_{ij,kl} \equiv \delta_{li}\delta_{vi}F^v_{vj,kv}, \quad \text{if } ij, kl \text{ both exist, and} \tag{3.8}$$

$$F^v_{vj,kv} \equiv P^v_{c_{\text{out}}(j)c_{\text{in}}(k)}. \tag{3.9}$$

From the above definition, one should keep in mind that F^v acts on existing *arcs*, but we are indexing its components according to the *vertices* related to those arcs. This type of notation is the one we use mainly in this work, another typical notation that we employ as well consists in labeling the arcs themselves.

It is now possible to define the *graph propagator* simply as the sum of all V vertex propagators,

$$F \equiv \sum_{v=1}^{V} F^v. \tag{3.10}$$

Component by component,

$$F_{ij,kl} = \delta_{i,l}F_{ij,ki}, \quad \text{and} \tag{3.11}$$

$$F_{ij,ki} = F^i_{ij,ki} \tag{3.12}$$

$$= P^i_{c_{\text{out}}(j),c_{\text{in}}(k)}. \tag{3.13}$$

It is clear from the definitions that F^i has the property Eq. (3.6), i.e. $\sum_j F^i_{ij,ki} = 1$, and F inherits it as well: F is a *stochastic* matrix that directs a Markov process on the *entire* space of arcs.

3.3.2 The classical phase space

We will think of an arc ij as a *coordinate*, giving both the "position" (between vertices i and j) and the "momentum" (moving from i to j), within the *phase-space* constituted by the set $A(G)$, with a volume card$A$. A classical, card$A$-dimensional *state vector*, ρ, with components $\rho_{ij} \geq 0$, will be subjected to a discrete-time dynamics determined by the propagator F, in such a way that the state at time

t, ρ^t, *evolves* to ρ^{t+n} through n successive applications of F:

$$\rho^{t+n} \equiv F^n \rho^t. \tag{3.14}$$

The vector ρ may represent a discrete probability distribution, e.g. ρ_{ij} being the likelihood of finding a particle at ij, or it may represent a distribution of "fluid" on the digraph, so that the component ρ^t_{ij} is the mass of fluid lying on the arc ij at time t.
Due to the stochasticity of F, the total mass is *conserved*:

$$\sum_{ij} \rho^{t+n}_{ij} = \sum_{ij} \rho^t_{ij}, \tag{3.15}$$

where the sum is understood to run over *existing* arcs, although, as usual, we name the arcs as ordered pairs of nodes.
In the same manner as "global" stochasticity follows from the "local" stochasticity at every node, the total mass (or probability) conservation, Eq. (3.15), follows from the conservation at every node,

$$\sum_{i} \rho^t_{ij} = \sum_{i} \rho^{t+1}_{ji}. \tag{3.16}$$

The "Kirchoff law", Eq. (3.16), can be read as *the sum of incoming probabilities toward j at time t equals the sum of outgoing probabilities in the next time-step.*

3.3.3 Bi-stochasticity, digraph symmetry and time-reversal

The matrices P^v defined in Eq. (3.4) are often[6] *bistochastic*, i.e. a property similar to Eq. (3.6) holds for the *in*-components as well:

$$\sum_{c_{\text{in}}=1}^{d^v_{\text{in}}} P^v_{c_{\text{out}} c_{\text{in}}} = 1 \ \forall c_{\text{out}}. \tag{3.18}$$

[6]They are *always* bi-stochastic in the context of quantum graphs, where a unitary matrix U^v directs a quantum scattering process through the node v, and P^v, interpreted as the classical analogue of U^v, is defined as

$$P^v_{c,c'} = |U^v_{c,c'}|^2. \tag{3.17}$$

The propagators that one obtains in this way are called unitary-stochastic, or uni-stochastic, a property which implies bi-stochasticity: one recovers both Eq. (3.6) and Eq. (3.18) from Eq. (3.17).

This has two obvious implications, one is[7]

$$d^v_{\text{in}} = d^v_{\text{out}}, \tag{3.19}$$

the other is that the transpose matrices $(P^v)^T$, $(F^v)^T$ are stochastic, and so is F^T in the (usual) case that *all* P^v's are. As a result, one can consider F^T as the *backward* evolution[8] associated with F.
Mowever, in the case of an undirected graph, or equivalently a *symmetric* directed graph in our language, one can define a *time-reversal* operation simply by "reflecting" every arc, $\rho_{ij} \to \rho_{ji} \equiv (R\rho)_{ij}$, with

$$R_{ij,ki} \equiv \delta_{k,j}. \tag{3.20}$$

For a symmetric digraph and a bi-stochastic propagator associated to it, it is possible to ask whether time-evolution followed by time-reversal is equivalent to time-reversing first and then evolving "backwards", i.e. whether

$$RF^n\rho = \left(F^T\right)^n R\rho. \tag{3.21}$$

When Eq. (3.21) is satisfied for every number, n, of time-steps, and for every vector ρ, the (classical) evolution on the symmetric digraph is then said to be *time reversal invariant*. Naturally, this is equivalent to

$$F = RF^TR. \tag{3.22}$$

If one was to consider *metric* digraphs (i.e. graphs with a length l_{ij} associated to every arc ij), and if the arc lengths were to play any role[9], time reversal symmetry would also require that the lengths of antiparallel arcs coincide. In the context of *quantum* digraphs (see section 3.4), the arc length *is* important and quantum time reversal is broken when $l_{ij} \neq l_{ji}$, even if classical time reversal is not (i.e. even if Eq. (3.22) holds).

[7]Simply summing Eq. (3.18) over c_{out}, summing Eq. (3.6) over c_{in} and then equating both results.

[8]Although "involution" cannot be defined for F, which directs an irreversible process.

[9]They usually do not, in the context classical evolution on graphs, because only *discrete*, bond-to-bond hopping (such as it is represented in Eq. (3.14)) is considered, but see [52] for an exception.

3.3.4 Long time dynamics: ergodicity and mixing

The long time evolution of a probability distribution, $\rho_{ij}^t \geq 0$, as we will show below, is determined by the eigenvalue of F with the highest absolute value. Let us denote by $f_0, f_1, \ldots, f_{\mathrm{card}A}$ and by $\varrho^0, \varrho^1, \ldots, \varrho^{\mathrm{card}A}$, respectively, the eigenvalues and eigenvectors of F. The eigenvalues are inversely ordered in modulus: $|f_0| \geq |f_1| \geq \ldots \geq f_{\mathrm{card}A}$.

To the propagator F, we can apply directly the Perron-Frobenius Theorem for *non-negative, irreducible* matrices[10] [53]. This states that f_0 is unique, real and positive, and that:

$$\max_a \sum_{b=1}^{\mathrm{card}A} F_{ba} \leq \mathrm{f}_0 \leq \max_a \sum_{b=1}^{\mathrm{card}A} F_{ab}. \tag{3.23}$$

It is obvious, from the *bi*-stochasticity of F (i.e. Eq. (3.6) and Eq. (3.18)) and the previous theorem, Eq. (3.23), that $f_0 = 1$. Therefore the "zero mode", ϱ^0 is the "invariant measure" of the matrix F [54], and it is as well the *uniform mode*, i.e.

$$\varrho^0 \equiv \mathrm{const.}, \tag{3.24}$$

due again to bi-stochasticity Eq. (3.18), as can be seen checking that Eq. (3.24) solves the eigen-equation $F\varrho^0 = \varrho^0$.

From the stochasticity of F, one can also infer that, for any non-zero eigenmode, i.e. for $\varrho^a \neq \varrho^0$,

$$\sum_{b=1}^{\mathrm{card}A} \varrho_b^a = 0, \tag{3.25}$$

simply summing over vector-components in the eigen-equation, $F\varrho^a = f_a\varrho^a$.

From Eq. (3.25) and Eq. (3.24), we see that any state-vector ρ can be written *uniquely* as the sum of a uniform mode plus a combination of "fluctuating" modes: $\rho \equiv \varrho^0 + \sum_{a=1}^{\mathrm{Card}A-1} \varrho^a$. Using this mode decomposition, the time evolution of a

[10] We note that the irreducibility of F is implied by the fact that our propagator is associated to a (strongly) connected digraph, hence, for some $n \in \mathbb{N}$, $F_{ab}^n \neq 0$ for all arcs a, b.

initial distribution ρ^0 can be expressed as

$$\rho^n = F^n \rho^0 \tag{3.26}$$

$$= F^n \left(\varrho^0 + \sum_{a=1}^{\mathrm{Card}A-1} \varrho^a \right) \tag{3.27}$$

$$= \varrho^0 + \sum_{a=1}^{\mathrm{Card}A-1} f_a^n \varrho^a. \tag{3.28}$$

The second summand in Eq. (3.28) decides the long time evolution of the probability vector. If the eigenvalues of F (except $f_0 = 1$) are *inside* the unit circle, then $f_a^n \to 0$ as $n \to \infty$ for all a, hence $\rho^n \to \varrho_0$. This situation, in which any initial ρ^0 decays to ϱ^0 is called *mixing* dynamics. If f_1 is the next-to-leading eigenvalue, i.e. $1 > |f_1| \geq |f_a|$ $(a \neq 0)$, the speed of the decay towards equi-distribution is given by

$$|\rho^n - \varrho^0| \underset{n\to\infty}{\propto} |f_1|^n \tag{3.29}$$

$$= e^{n \ln |f_1|} \tag{3.30}$$

$$= e^{-n\left(1-|f_1|+(1-|f_1|)^2+\ldots\right)}, \tag{3.31}$$

hence

$$n^{\mathrm{mix}} = \frac{1}{1-|f_1|}, \tag{3.32}$$

sets the mixing timescale.

A function defined on the phase space constituted by the digraph, is a card$A$-dimensional vector, μ, with a value, μ_a, associated with every arc a. Its *phase average* at time n, over a probability vector ρ^n, is defined as the scalar product $\mu \cdot \rho^n$. Its *time average*, along the discrete-time evolution of a probability vector ρ, is defined as,

$$\lim_{n\to\infty} \frac{1}{n} \sum_{m=0}^{n-1} \mu \cdot \rho^m = \mu \cdot \lim_{n\to\infty} \frac{1}{n} \sum_{m=0}^{n-1} \rho^m. \tag{3.33}$$

The dynamic induced by the propagator is said to be *ergodic* when the time average coincides with the phase average over the uniform distribution, $\mu \cdot \varrho^0$. From Eq. (3.33), this clearly is independent of μ, and relies only on

$$\lim_{n\to\infty} \frac{1}{n} \sum_{m=0}^{n-1} \rho^m = \varrho^0. \tag{3.34}$$

This property follows from mixing, but it is more general: ergodicity can occur with eigenvalues of F, besides $f_0 = 1$, lying on the unit circle. As can be seen from the following reasoning, the rate of ergodic decay is determined by the eigenvalue that is closest to 1. If $f_1 = e^{\imath\phi_1}$ is such eigenvalue, from a set of l eigenvalues on the unit circle, we have

$$\frac{1}{n}\sum_{m=1}^{n}\rho^m - \varrho^0 = \frac{1}{n}\sum_{m=1}^{n}\left(\varrho^0 + e^{\imath m\phi_1}\varrho^1 + \ldots + e^{\imath m\phi_l}\varrho^l\right) - \varrho^0 \tag{3.35}$$

$$= \frac{1}{n}\sum_{m=1}^{n}\left(e^{\imath m\phi_1}\varrho^1 + \ldots + e^{\imath m\phi_l}\varrho^l\right) \tag{3.36}$$

$$\underset{n\to\infty}{\propto} \frac{1}{n}\sum_{m=1}^{n} e^{\imath m\phi_1}\varrho^1, \tag{3.37}$$

where $\frac{1}{n}\sum_{m=1}^{n} f_1^m$ will start adding up to zero when[11] $n\phi > 2\pi$. Therefore the timescale of the ergodic decay is

$$n_{\text{erg}} \propto \frac{1}{\phi} \lessapprox \frac{1}{|1 - f_1|}. \tag{3.38}$$

3.3.5 The case of a *symmetric* digraph.

3.3.5.1 Continuity equation

We will write a "continuity equation", derived from Eq. (3.16), but involving "node variables" and "currents along bonds". For this purpose, we restrict ourselves to *symmetric digraphs*. For these, trivially

$$d^v_{\text{in}} = d^v_{\text{out}} \equiv d^v \text{ for all } v. \tag{3.39}$$

We call d^v the *degree*, or the *coordination number* of the vertex v (even though v is connected to $2 \times d^v$ *arcs*).

We define the *node density* at vertex i as the *sum of outgoing densities from*

[11] Incidentally, another consequence of the Perron-Frobenius theorem is that the eigenvalues of F in the unit circle are necessarily roots of 1 [53]. Being of the form $e^{\imath\frac{2\pi}{m}}$, the contribution of such an eigenvalue actually cancels *exactly* after m steps, although this is not an essential requirement for ergodicity.

i, that is

$$\rho_i \equiv \sum_j \rho_{ij}, \tag{3.40}$$

and, taking into account the symmetry of the graph, the *current from i to j* as

$$\vec{\jmath}_{ij} \equiv \rho_{ij} - \rho_{ji}. \tag{3.41}$$

Naturally, $\vec{\jmath}_{ji} = -\vec{\jmath}_{ij}$.
Now we can define a "divergence" for every node i, denoted $\vec{\nabla}_i \cdot \vec{\jmath}$, such that

$$\vec{\nabla}_i \cdot \vec{\jmath} \equiv \sum_j \vec{\jmath}_{ij}, \tag{3.42}$$

and from this (and Eq. (3.16), Eq. (3.40)) follows the *continuity equation*

$$\vec{\nabla}_i \cdot \vec{\jmath}^{\,t} = -\delta_t \rho_i, \tag{3.43}$$

where we have introduced the notation $\delta_t \rho \equiv \rho^{t+1} - \rho^t$.[12]

3.3.5.2 Diffusion

The definitions just presented do not rely on any properties of F except for the stochasticity. The concept of the node density, Eq. (3.40), however, is especially convenient for *purely diffusive* graphs, that is, for graphs in which every vertex scatters any incoming current *equally* through all its bonds. In this situation, the discrete-time propagation through a vertex i is given by

$$\rho_{ij}^{t+1} = \frac{1}{d^i} \sum_{k=1}^{d^i} \rho_{ki}^t \quad \text{for all} \quad j, \tag{3.44}$$

For such graphs, the V node densities, ρ_i^t, as defined in Eq. (3.40), contain the same information as the card$A$ original components, ρ_{ij}^t, of the state vector, because if an initial distribution is given a $t = 0$, from time-step $t = 1$ onward *the outgoing densities around vertex i all coincide* and, as can easily be checked

$$\rho_{ij}^t = \frac{1}{d^i} \rho_i^t \ \forall j. \tag{3.45}$$

[12] that is, we use ∇ for variation in "space" and δ for variation in time.

Further restricting the generality of our digraph by imposing *regularity*, i.e. the requirement that *the coordination number is constant*, the definition Eq. (3.41) allows us to write $\vec{\jmath}_{ij} = \frac{1}{d}(\rho_i - \rho_j)$, for a graph with coordination number d. Defining a *gradient* on node variables[13], as

$$\vec{\nabla}_{ij}\rho \equiv \rho_j - \rho_i, \tag{3.46}$$

we can derive a discrete "Ficks law",

$$\vec{\jmath}_{ij} = -D\vec{\nabla}_{ij}\rho, \tag{3.47}$$

with a "diffusion constant"

$$D \equiv \frac{1}{d}. \tag{3.48}$$

In a manner similar to the definition, Eq. (3.42), of a discrete divergence of the currents "around" a node i, one naturally defines the discrete Laplacian in i as the divergence of the gradients around such node:

$$\nabla_i^2\rho \equiv \vec{\nabla}_i \cdot \vec{\nabla}\rho \tag{3.49}$$

$$= \sum_{j=1}^{d} \vec{\nabla}_{ij}\rho \tag{3.50}$$

$$= \sum_{j=1}^{d} (\rho_j - \rho_i). \tag{3.51}$$

From the Ficks law, Eq. (3.47), and the continuity equation, Eq. (3.43), we find the *diffusion equation* (simply by summing Eq. (3.47) over j):

$$\delta_t \rho_i = D\nabla_i^2 \rho^t. \tag{3.52}$$

[13]We note that the *divergence* is a vertex function, defined over a single index, ∇_i, while the *gradient* is a bond function (two indices). Also, we are using the obvious notation $\nabla_{ijk\ldots}f$ for $(\nabla f)_{ijk\ldots}$.

3.3.5.3 Diffusion and reflection

Let us now consider a digraph with a fixed coordination number, d, and the time evolution be driven by a Neumann classical propagator[14], defined as

$$F_{ij,ki} \equiv \left(1 - \frac{4}{d}\right)\delta_{j,k} + \left(\frac{4}{d^2}\right). \tag{3.53}$$

Under this propagator the discrete time evolution is given by

$$\rho_{ij}^{t+1} = \left(1 - \frac{4}{d}\right)\rho_{ji}^{t} + \frac{4}{d^2}\sum_{k}\rho_{ki}^{t} \tag{3.54}$$

$$= \left(1 - \frac{4}{d}\right)\rho_{ji}^{t} + \frac{4}{d^2}\rho_{i}^{t+1}, \tag{3.55}$$

where we use Eq. (3.16) in the second line, resulting in something very different from Eq. (3.44) or Eq. (3.45). In the present case we will have neither a Ficks law (we cannot infer the currents from the node variables only, at least if we consider only a single time-step...) nor a Diffusion equation. We can however employ the notation just introduced and derive an equation *on the node variables*.
The first step is to derive an equation analogous to Eq. (3.47), that is, currents as function of node densities. For that we calculate $\vec{\mathrm{J}}_{ij}^{\,t+1}$ (subtracting ρ_{ji}^{t+1} from Eq. (3.55)) and obtain

$$\vec{\mathrm{J}}_{ij}^{\,t+1} = \left(\frac{4}{d} - 1\right)\vec{\mathrm{J}}_{ij}^{\,t} - \frac{4}{d^2}\vec{\nabla}_{ij}\rho^{t+1}, \tag{3.56}$$

as a "non-diffusive Fick's law", in the sense that we have related currents to density gradients. Incidentally, Eq. (3.56) becomes exactly the Fick's law, Eq. (3.47), for $d = 4$; however, as d tends to ∞ the "diffusion current", $-\frac{4}{d^2}\vec{\nabla}_{ij}\rho^{t}$, gets suppressed and the current bounces back and forth (as one would expect from the dominance of "back scattering" in the definition Eq. (3.53)), $\vec{\mathrm{J}}_{ij}^{\,t+1} = -\vec{\mathrm{J}}_{ij}^{\,t} + O(\frac{1}{d})$.
The second step is to calculate the divergence around the node i. Summing Eq. (3.56) over j, we obtain

$$\vec{\nabla}_i \cdot \vec{\mathrm{J}}^{\,t+1} = \left(\frac{4}{d} - 1\right)\vec{\nabla}_i \cdot \vec{\mathrm{J}}^{\,t} - \frac{4}{d^2}\nabla_i^2\rho^{t+1}. \tag{3.57}$$

[14]The reason for using this name will become clear in the next section.

After applying the continuity equation Eq. (3.43), the result is

$$\delta_{t+1}\rho_i = \left(\frac{4}{d} - 1\right)\delta_t\rho_i + \frac{4}{d^2}\nabla_i^2\rho^{t+1}, \tag{3.58}$$

which is our node-variable-only equation. Eq. (3.43) becomes Eq. (3.52) in the case that $d = 4$, but otherwise it contains the extra time derivative on the r.h.s. We need to modify the derivatives in Eq. (3.43) so that they have the same time dependence as the Laplacian. For this purpose, we introduce now the "second time-derivative"[15],

$$\delta_{t+1}^2\rho \equiv \delta_{t+1}\rho - \delta_t\rho \tag{3.59}$$

$$= \rho^{t+2} + \rho^t - 2\rho^{t+1}. \tag{3.60}$$

Using this definition on Eq. (3.58) we obtain the final equality, :

$$\left(2 - \frac{4}{d}\right)\delta_t\rho_i - \left(1 - \frac{4}{d}\right)\delta_t^2\rho_i = \frac{4}{d^2}\nabla_i^2\rho^t, \tag{3.61}$$

analogous to the diffusion equation Eq. (3.52) in the sense that it is a linear equation in node variables that relates time variations to space variations, but it contains an extra second derivative w.r.t. the time variable.

3.4 The digraph quantization

A necessary condition for a digraph to be quantizable in the way shown below ([55, 56]) is that every vertex be connected to the same number of incoming and outgoing arcs, i.e.

$$d_{\text{in}}^v = d_{\text{out}}^v \equiv d \text{ for all } v. \tag{3.62}$$

We are interested in quantum *symmetric digraphs* (for which Eq. (3.62) is obviously satisfied), therefore we will employ the notation that is familiar from the undirected QGs, and use the word *bond* to refer to a pair of antiparallel arcs, and use the symbol B to refer to the *total number of bonds*, i.e.

$$B \equiv \frac{\text{card}A}{2}. \tag{3.63}$$

[15] This is a time Laplacian applied at $t + 1$.

Following Severini and Tanner, [55], to our *symmetric digraph* we associate a *quantum digraph* by

1. assigning to every arc ij a positive definite *length*, l_{ij}, along which waves propagate freely but *constrained in direction to the ordering of the pair* ij, and

2. assigning to every vertex v a unitary, $d^v \times d^v$ "vertex scattering matrix" σ^v, that will control the transitions from every incoming arc iv to every outgoing one vj.

In concordance with the above, a (complex) probability *amplitude* a_{iv} at the starting end of iv will "propagate" through the arc and become $a_{iv}e^{\iota \mathrm{k} l_{iv}}$ at the v end. The set of all such amplitudes incoming towards the vertex v, indexed with $c_{\mathrm{in}} = 1, \ldots, d^v$, will propagate then to the outgoing arcs, vj, indexed with $c_{\mathrm{out}} = 1, \ldots, d^v$, according to

$$a_{c_{\mathrm{out}}} = \sum_{c_{\mathrm{in}}=1}^{d^v} \sigma^v_{c_{\mathrm{out}} c_{\mathrm{in}}} e^{\iota \mathrm{k} l_{c_{\mathrm{in}}}} a_{c_{\mathrm{in}}}. \tag{3.64}$$

The component $\sigma^v_{c_{\mathrm{out}} c_{\mathrm{in}}}$, where the indices $c_{\mathrm{out}}, c_{\mathrm{in}}$ are associated with vertices, say j and i respectively, connected to v, represents the transition probability amplitude for a wave coming through the arc iv to be scattered in v to the arc vj.
A unitary *(di)graph scattering* matrix will be constructed assembling the σ^v's, in the same fashion as we constructed the (di)graph propagator, F, starting from vertex propagators, P^v. For a total of V vertices in the graph:

$$P^1, \ldots, P^v, \ldots, P^V \longrightarrow F^1, \ldots, F^v, \ldots, F^V \longrightarrow F \equiv \sum_v F^v$$
$$\sigma^1, \ldots, \sigma^v, \ldots, \sigma^V \longrightarrow, \Sigma^1, \ldots, \Sigma^v, \ldots, \Sigma^V \longrightarrow \Sigma \equiv \sum_v \Sigma^v.$$

It is worth mentioning, however, that if a classical propagator, F, is already associated to the digraph, and the scheme above has to be consistent with the classical dynamics, it is necessary that F be uni-stochastic and that is related to Σ by

$$F_{ij,ki} = |\Sigma_{ij,ki}|^2 . \tag{3.65}$$

For example, the purely diffusive digraph treated in subsection 3.3.5.2 can be quantized with scattering matrices

$$\sigma^v_{c_{\text{out}}c_{\text{in}}} \equiv \frac{e^{2\pi\iota\frac{c_{\text{out}}c_{\text{in}}}{d^v}}}{\sqrt{d^v}} \quad \text{(DFT)}, \tag{3.66}$$

which are called *discrete Fourier transform* matrices. The strongly reflective digraph in subsection 3.3.5.3 is quantized with matrices

$$\sigma^v_{c_{\text{out}}c_{\text{in}}} \equiv \frac{2}{d^v} - \delta_{c_{\text{out}}c_{\text{in}}} \quad \text{(Neumann)}, \tag{3.67}$$

which we call Neumann matrices for reasons that become clear in the next chapter. Regrouping all the existing arcs into a single vector with dimension $2B$, for every vertex scattering matrix σ^v we define

$$\Sigma^v_{ij,kl} \equiv \delta_{v,i}\delta_{v,l}\Sigma^v_{vj,kv} \text{ for every existing arcs, } ij, kl \text{ and} \tag{3.68}$$

$$\Sigma^v_{vj,kv} \equiv \sigma^v_{c_{\text{out}}(j)c_{\text{in}}(v)}. \tag{3.69}$$

Thus Σ^v acts on every *existing* arc, its components simply vanishing when two arcs are not connected through v. The different vertex scattering matrices like Σ^v, all act on the same space, therefore we can add them to form the $2B \times 2B$ *graph scattering matrix* Σ, as

$$\Sigma \equiv \sum_{v=1}^{V} \Sigma_v, \tag{3.70}$$

or, *for existing arcs* ij, kl,

$$\Sigma_{ij,kl} \equiv \delta_{il}\sigma^i_{c_{\text{out}}(j)c_{\text{in}}(k)}. \tag{3.71}$$

We can as well re-group the arc lengths, into a $\text{card}A \times \text{card}A$ (or $2B \times 2B$) *diagonal* matrix $\mathcal{L}$,

$$\mathcal{L}_{ij,ij} \equiv l_{ij}. \tag{3.72}$$

The phases accumulated by the wave, with wave number k, traveling along the arcs are contained in the matrix

$$T \equiv e^{\iota \text{k}\mathcal{L}}. \tag{3.73}$$

The vector of all probability amplitudes, $\vec{a}^{\,t}$ at time t, propagates according to

$$\vec{a}^{\,t+1} = U(\mathrm{k})\vec{a}^{\,t}, \tag{3.74}$$

where

$$U \equiv \Sigma T, \tag{3.75}$$

is the analogue to the "quantum map", [33], in undirected QGs. In fact, in the context of quantum *symmetric digraphs*, a usual quantum *graph* is the particular case defined by the equality

$$l_{ij} = l_{ji} \quad \text{for all existing } ij, \tag{3.76}$$

which involve the corresponding symmetry in the matrices $\mathcal{L}$ and T.
The eigenstates of the QdG are defined as the $2B \times 2B$ vectors $\vec{a}$ which are stationary under Eq. (3.74), i.e.

$$\vec{a} = U(\mathrm{k})\vec{a}. \tag{3.77}$$

Solutions of Eq. (3.77) exist for k values which satisfy the *secular equation*

$$\det(1 - U(\mathrm{k})) = 0. \tag{3.78}$$

The equation Eq. (3.78) is central in the analytical treatment of the spectral statistics on QGs (or QdGs), as it is used for the generation of the spectral density (see below). We will use it for the field theoretical treatment of spectral averages in chapters 4 and 5.

3.5 Periodic Orbit Theory of quantum digraphs

3.5.1 Incommensurability of arc-lengths and k-average

Since Kottos and Smilansky [3] pioneered the POT of quantum graphs, it has been customary to to work with bond-lengths which are *rationally independent*, or equivalently *incommensurate*. From our point of view, the main advantage[16] of substituting a symmetric QdG for a QG, is precisely that we can push the

[16] We make use of it in chapters 4 and 5.

rational independence further by giving different lengths to antiparallel arcs. If $\vec{l}$ is the $2B$-dimensional vector of arc-lengths, and $\vec{n} \in \mathbb{Z}^{2B}$, we will assume the condition

$$\vec{n} \cdot \vec{l} = 0 \iff \vec{n} = \vec{0} \in \mathbb{Z}^{2B}. \tag{3.79}$$

When one encounters k-dependent functions, $f(\mathrm{k})$, they can often be written as a function of the $2B$ phases,

$$f(\mathrm{k}) \equiv F(\mathrm{k}l_1, \ldots, \mathrm{k}l_{2B}) \equiv F\left(\mathrm{k}\vec{l}\right). \tag{3.80}$$

Such is the case, for example, of the l.h.s. of Eq. (3.78), the *spectral determinant*. Because $F(\vec{x})$ ($\vec{x}$ having now independent components) is periodic in each of its variables, with period 2π, we can write

$$F\left(\mathrm{k}\vec{l}\right) = F\left(\mathrm{k}\vec{l}\mathrm{mod}2\pi\right), \tag{3.81}$$

where $\mathrm{k}\vec{l}\mathrm{mod}2\pi \equiv \mathrm{k} \cdot (\mathrm{l_1 mod}2\pi, \ldots, \mathrm{l_{2B} mod}2\pi)$. We have then a linear "flow" $\mathrm{k}\vec{l}$, parameterized by k, in the torus $T^{2B} \equiv [0, 2\pi]^{2B}$. Thanks to the incommensurability condition, Eq. (3.79), the flow is *ergodic*:

$$\lim_{K\to\infty} \frac{1}{K} \int_0^K f(\mathrm{k}) d\mathrm{k} = \frac{1}{(2\pi)^{2B}} \int_{T^{2B}} d\vec{\phi} F\left(\vec{\phi}\right). \tag{3.82}$$

In order to show this, first we transform integrand on the l.h.s. of Eq. (3.82) as

$$f(\mathrm{k}) = \int_{T^{2B}} d\vec{\phi} F\left(\vec{\phi}\right) \delta_{2\pi}\left(\vec{\phi} - \mathrm{k}\vec{l}\right) \tag{3.83}$$

$$= \frac{1}{(2\pi)^{2B}} \int_{T^{2B}} d\vec{\phi} F\left(\vec{\phi}\right) \sum_{\vec{p}\in\mathbb{Z}^{2B}} e^{\iota\vec{p}\cdot\left(\vec{\phi}-\mathrm{k}\vec{l}\right)} \tag{3.84}$$

$$= \frac{1}{(2\pi)^{2B}} \sum_{\vec{p}\in\mathbb{Z}^{2B}} \left(e^{-\iota \mathrm{k}\vec{p}\cdot\vec{l}} \int_{T^{2B}} d\vec{\phi} F\left(\vec{\phi}\right) e^{\iota\vec{p}\cdot\vec{\phi}} \right). \tag{3.85}$$

The first two steps, Eq. (3.83), Eq. (3.84), obviously, are formal, while the third step can be done under mild conditions on f which make the series in the r.h.s of Eq. (3.85) convergent. The k-integration can be now easily carried out on the r.h.s. of Eq. (3.85). The key fact is that, due to the rational independence of the

lengths, Eq. (3.79),

$$\lim_{K\to\infty}\frac{1}{K}\int_0^K d\mathrm{k}e^{-\iota \mathrm{k}\vec{p}\cdot\vec{l}} = \begin{cases} 1 & \text{if } \vec{p}=\vec{0} \\ 0 & \text{otherwise,} \end{cases} \tag{3.86}$$

from which we conclude that Eq. (3.82) is satisfied.

3.5.2 The density of states and the trace formula

The set of wave numbers, $\mathrm{k}_1, \mathrm{k}_2, \ldots$, fulfilling Eq. (3.78) is the *spectrum* of the QdG characterized by $U(k)$. The *density of states*, DOS, is defined as

$$d(\mathrm{k}) \equiv \sum_{s=1}^{\infty}\delta(\mathrm{k}-\mathrm{k}_s), \tag{3.87}$$

where the sum is over the spectrum. Noticing that

$$\det\left(\iota U^{1/2}-\iota U^{-1/2}\right) = \det\left(-\iota U^{-1/2}\right)\det\left(1-U\right) \tag{3.88}$$

$$= \det(-U)^{-1/2}\det\left(1-U\right), \tag{3.89}$$

is a *real* function of the wave number k, and vanishes *iff* k is in the spectrum, one uses the logarithmic derivative of the r.h.s. of Eq. (3.89) to generate the delta functions:

$$d(\mathrm{k}) = \frac{-1}{\pi}\lim_{\epsilon\to 0}\mathrm{Im}\frac{d}{d\mathrm{k}}\left(\log\det\left(-U(\mathrm{k})\right)^{-1/2}+\log\det\left(1-U(\mathrm{k}+\iota\epsilon)\right)\right) \tag{3.90}$$

$$= \frac{1}{2\pi}\mathrm{tr}\mathcal{L}+\frac{1}{\pi}\lim_{\epsilon\to 0}\mathrm{Re}\ \mathrm{tr}\frac{U(\mathrm{k}+\iota\epsilon)}{1-U(\mathrm{k}+\iota\epsilon)}\mathcal{L} \tag{3.91}$$

$$\equiv \frac{1}{\Delta}+\delta d(\mathrm{k}). \tag{3.92}$$

The result is as usual divided into Weil part, or mean DOS, and fluctuating part, and is identical to the undirected QG ([33]). The *mean level spacing* (mls) is

$$\Delta = \frac{2\pi}{\mathrm{tr}\mathcal{L}} = \frac{\pi}{B\bar{l}}, \tag{3.93}$$

with $\bar{l}$ being the average length.

The fluctuating part of the DOS, as written in Eq. (3.91), was found by Kottos and Smilansky [3]. This *trace formula* can be expressed as a sum over *orbits*, i.e.

closed paths made of connected arcs. Expanding the fraction in Eq. (3.91),

$$\delta d(\mathrm{k}) = \frac{1}{\pi}\mathrm{Re}\sum_{n=1}^{\infty}\mathcal{L}U(k+\iota\epsilon)^n \tag{3.94}$$

$$= \frac{1}{\pi}\mathrm{Re}\sum_{p} L_p \sum_{r=1}^{\infty}\left(A_p e^{\iota(\mathrm{k}+\iota\epsilon)L_p}\right)^r, \tag{3.95}$$

where the outermost sum in Eq. (3.95) is over *primitive* orbits, i.e., orbits which *cannot* be written as repetitions of a shorter orbit, and the innermost one is a sum over *repetitions*. L_p is the sum of the arc-lengths involved in the primitive orbit p (it arises from the fact that the orbit can be started from any of its arcs, and every such starts comes with a length given by $\mathcal{L}$ in Eq. (3.94)). A_p is the *amplitude* of p, given by the product of the graph scattering matrix components associated to every arc-to-arc transmission along the orbit. The details are identical as for QGs (see [4] or [33]).

Let us mention a little detail: while $B\bar{l}$ is the *total length* of an undirected QG with B bonds, it is only *half* the total length of a QdG with the same number, B, of pairs of (antiparallel) connections. This is consistent, because one can view a symmetric QdG as a QG in which one would have split every bond into two arcs, one for every direction, each with a length similar to the original bond. Therefore one could convert our QdG model into a QG (making $l_{ij} = l_{ji}$ for all connections) and the present expressions would all be maintained, with the same meaning for the symbols. In particular, the mean level spacing remains unchanged.

3.5.3 The spectral form factor and diagonal approximation

Let us consider the spectral sequence $k_1, k_2, \ldots$ as having average spacing $\Delta = 1$ (after a re-scaling, as shown in 2.2.2). The spectral form factor associated with this sequence is given, *for moderate bond-lengths fluctuations*, by [33][17]

$$K(\tau = \frac{n}{2B}) = K_n \tag{3.96}$$

$$= \frac{1}{2B}\langle \mathrm{tr}U(\mathrm{k})^n \mathrm{tr}U(\mathrm{k})^{\dagger n}\rangle_{\mathrm{k}}, \tag{3.97}$$

[17] This quantity is the spectral form factor associated to the density of eigenphases of $U(\mathrm{k})$. The spectral statistics and the eigenphase statistics coincide [33].

where $\langle \ldots \rangle_{\mathrm{k}} = \lim_{K\to\infty} \frac{1}{K} \int_0^K (\ldots) d\mathrm{k}$. The form factor can be expressed as a *double* sum over periodic orbits. For *small* τ, self-crossing orbits are negligible (this is the *diagonal approximation*) and the one-loop orbits contribution is obviously given by

$$K_n^{\mathrm{diag}} = \frac{n}{2B} \mathrm{tr} F^n \tag{3.98}$$

$$= \tau \mathrm{tr} F^{\tau 2B}, \tag{3.99}$$

where F is the Perron-Frobenius, or classical propagator, associated to the graph,

$$F_{ij,ki} = |\Sigma_{ij,ki}|^2. \tag{3.100}$$

From Eq. (3.99) and Eq. (2.41), it is clear that short time universality, expected in the large size limit, relies on

$$\lim_{B\to\infty} \mathrm{tr} F^{\tau 2B} = 1, \tag{3.101}$$

which, as noticed by Tanner [36], it is *not* equivalent to mixing (see 3.3.4) because, importantly, the limit $B \to \infty$ acts on F itself, not just on the exponent. If the spectral gap, i.e. the denominator in the r.h.s. of Eq. (3.32) remains constant as the dimensionality of F increases, then clearly the reasonings in 3.3.4 can be applied and Eq. (3.101) holds. However, if this is not the case, the effect the eigenvalues inside the unit circle needs to be taken into account. Let us introduce the notation

$$\mathrm{tr} F \equiv 1 + \mathrm{tr}^* F, \tag{3.102}$$

where

$$\mathrm{tr}^* F = \sum_{a=1}^{2B-1} f_a, \tag{3.103}$$

can be read as "trace without the contribution of the eigenvalue 1" (we have already established the convention $|f_{2B-1}| \leq \ldots \leq |f_3| \leq |f_2| \leq |f_1| < 1$). The effect of the eigenvalues inside the unit circle on the l.h.s. of Eq. (3.101) is given by

$$|\mathrm{tr}^* F^{\tau 2B}| \leq \mathrm{tr}^* |F^{\tau 2B}| \leq 2B |f_1|^{\tau 2B}. \tag{3.104}$$

If $|f_1|$ approaches 1 (in the $B \to \infty$ limit) as $|f_1| \sim \left(1 - \frac{1}{B^\alpha}\right)$, we can only be certain that $\mathrm{tr}^* F \to 0$, and hence that Eq. (3.101) holds, if

$$2B\left(1 - \frac{1}{B^\alpha}\right)^{2B\tau} = 2B\left(1 - \frac{1}{B^\alpha}\right)^{2B^\alpha \tau B^{1-\alpha}} \tag{3.105}$$

$$\sim 2Be^{-2\tau B^{1-\alpha}} \tag{3.106}$$

$$\to 0, \tag{3.107}$$

for which it is necessary that $0 \leq \alpha < 1$. In order words, a sufficient condition for Eq. (3.101) is that the spectral gap decrease, in the thermodynamic limit, not faster than

$$1 - |f_1| \sim \frac{1}{B^\alpha}, \quad 0 \leq \alpha < 1. \tag{3.108}$$

Tanner conjectured that the inequality in Eq. (3.108) is a sufficient universality criterion, i.e. that it guarantees large-size RMT behaviour beyond the diagonal approximation.

Chapter 4

Field theory of the full Neumman digraph

4.1 Introduction

As we mentioned in the introductory chapter 1, Gnutzmann and Altland ([1, 2]) managed to map *exactly* the spectral average over the two point function of an *individual* quantum graph onto a super-symmetric nonlinear σ-model of Efetov type ([23]). It is well known that the uniform mode of this type of field theory produces the universal results predicted by RMT, and the problem of finding conditions for universality translates into finding conditions for the stability of the fluctuations around such mode. They found that such stability requires that[1]

$$\lim_{B\to\infty} \frac{1}{B^2} \mathrm{tr}^* \left(\frac{1}{1-F} \right)^2 = 0. \tag{4.1}$$

This equation is more restrictive than Eq. (3.101), as an analysis of the effect of the spectrum of F on l.h.s. of Eq. (4.1) leads to a more severe condition than Tanner's, Eq. (3.108), on the spectral gap. Specifically [2], $\alpha < 1$ is enough for Eq. (4.1) only if the number of eigenvalues of F approaching 1 like $1 - \frac{c}{B^\alpha}$ is independent of B, as can be easily checked on Eq. (4.1) by power counting. In the worst case, the number of such modes is "extensive" (linear in the system size B), therefore the general condition for the validity of Eq. (4.1) is $\alpha < \frac{1}{2}$ (again, by simple power counting).

[1] We remind the reader that tr* means "trace without the eigenvalue 1".

The Full Neumann graph, FNG, defined as a full graph with Neumann vertex scattering matrices (as in Eq. (3.67)) at the nodes, does not fulfil Gnutzmann and Altland criterium Eq. (4.1) (in fact, a careful look at the expansion of the action of the field theory in the nearly massless modes shows that the Gaussian approximation that leads to Eq. (4.1) is invalid). This result goes against the common belief that the spectral statistics of the FNG is universal (in the $B \to \infty$ limit) [37].

It was our aim to reconcile these two perspectives. For that reason we have investigated the full Neumann *di*graph, FNdG, (which is "full" according to the definitions in section 3.2, page 18). Breaking the symmetry between the lengths of every two antiparallel arcs simplify considerably the field theory, while retaining the main feature which is that Eq. (4.1) is not satisfied. The full Neumann classical propagator depends only on the topology and the Neumann scattering matrices.

In section 4.2, we restate the scheme developed by Gnutzmann and Altland, i.e. we derive the field-theoretical representation of the 2-point function in a non graph-specific manner. After introducing some notation for the field theory in section 4.3, and deriving some simple algebraic results results regarding the Neumann graph scattering matrix and classical propagator (for example the eigen-mode decomposition of F) in section 4.4, in section 4.5 we concentrate specifically on the FNdG, describing the problem of the massive modes and then showing our attempt to solve it.

4.2 General field theory of the 2-point correlation function

4.2.1 Derivation of the sigma model

Our object of interest is the two point correlation function of the fluctuating density of states, i.e.

$$R(s) \equiv \lim_{K\to\infty} \frac{\Delta^2}{K} \int_0^K \delta d(k + \frac{s}{2}\Delta)\delta d(k - \frac{s}{2}\Delta) d\mathrm{k}. \tag{4.2}$$

Following Gnutzmann and Altland [2] we re-write the fluctuating DOS (second summand in the r.h.s. of Eq. (3.91)) as

$$\delta d(\mathrm{k}) = \frac{-1}{2\pi} \lim_{j\to 0} \mathrm{Im} \frac{d}{dj} \frac{\det\left(1 - U(\mathrm{k}^+ + j)\right)}{\det\left(1 - U(\mathrm{k}^+ - j)\right)}, \tag{4.3}$$

and express the two point function as

$$R(s) = \frac{\Delta^2}{8\pi^2} \lim_{j_\mp \to 0} \frac{\partial^2}{\partial j_+ \partial j_-} \mathrm{Re} \lim_{K\to\infty} \frac{1}{K} \int_0^K \zeta(s, j_+, j_-) dk, \tag{4.4}$$

with the *generating function*

$$\zeta(s, j_+, j_-) = \frac{\det(1 - U(k^+ + p_{\mathrm{f}+}))}{\det(1 - U(k^+ + p_{\mathrm{b}+}))} \frac{\det(1 - U(k^+ + p_{\mathrm{f}-}))^*}{\det(1 - U(k^+ + p_{\mathrm{b}-}))^*}. \tag{4.5}$$

The *sources*, $p_{\mathrm{b}\pm} \equiv (\pm s/2 - j_\pm)\Delta$, $p_{\mathrm{f}\pm} \equiv (\pm s/2 + j_\pm)\Delta$, through the j-terms, prevent the determinants in the denominator canceling with those in the numerator of the r.h.s Eq. (4.5), i.e. they break *super-symmetry* in the field theory jargon that we will use below. The s-terms prevent the determinants from canceling "in the horizontal direction", i.e. through coupling a phase with its complex conjugate, i.e. they break *advance-retarded* symmetry. The equation Eq. (A.21) is the tool we need in order to write the generating function Eq. (4.5) as a following Gaussian *super*-integral:

$$\zeta(s, j_+, j_-) = \int d(\tilde{\psi}_+, \psi_+) e^{-\tilde{\psi}_+(1-U_+)\psi_+} \int d(\tilde{\psi}_-, \psi_-) e^{-\tilde{\psi}_-(1-U_-^\dagger)\psi_-}, \tag{4.6}$$

where we have defined *super*-vectors,

$$\psi_\pm \equiv \begin{pmatrix} \vec{s}_\pm \\ \vec{\chi}_\pm \end{pmatrix}_{\mathrm{bf}} \qquad \psi_\pm^\dagger \equiv \left(\vec{s}_\pm^{\,\dagger}, \vec{\chi}_\pm^{\,\dagger}\right)_{\mathrm{bf}}, \tag{4.7}$$

and *super*-matrices,

$$U_\pm \equiv \begin{pmatrix} U(k^+ + p_{\mathrm{b}\pm}) & 0 \\ 0 & U(k^+ + p_{\mathrm{f}\pm}) \end{pmatrix}_{\mathrm{bf}}, \tag{4.8}$$

where the letters bf indicate that these objects are expressed in *boson-fermion* structure, see A. The integral over the *bosonic* (complex numbers) variables produces the *inverse* determinant of the boson-boson matrix blocks, while the integral over *fermionic* (Grassmann numbers) variables produces the determinant of the

fermion-fermion matrix block.

The spectral average will be performed over the integrand of Eq. (4.6). Assuming the incommensurability of arc-lengths, we use Eq. (3.82) and substitute this average by an integral over independent phases on every arc:

$$\lim_{K\to\infty}\int_0^K \frac{d\mathrm{k}}{K} e^{\tilde{\psi}_+ U_+ \psi_+ + \tilde{\psi}_- U_-^\dagger \psi_-} \equiv \prod_{i=1}^{2B}\int_0^{2\pi}\frac{d\phi_i}{2\pi} e^{L_i(\phi_i)}, \tag{4.9}$$

where, in the l.h.s, we have selected the phase-dependent exponent from Eq. (4.6), and in the r.h.s. we define

$$L_i(\phi_i) \equiv \left((\psi_+^\dagger\Sigma_+)_{\mathrm{b},i}, (\psi_+^\dagger\Sigma_+)_{\mathrm{f},i}, s_{-,i}^*, \chi_{-,i}^*\right) \begin{pmatrix} e^{\iota\phi_i} & 0 & 0 & 0 \\ 0 & e^{\iota\phi_i} & 0 & 0 \\ 0 & 0 & e^{-\iota\phi_i} & 0 \\ 0 & 0 & 0 & e^{-\iota\phi_i} \end{pmatrix} \begin{pmatrix} s_{+,i} \\ \chi_{+,i} \\ (\Sigma_-\psi_-)_{\mathrm{b},i} \\ (\Sigma_-\psi_-)_{\mathrm{f},i} \end{pmatrix}, \tag{4.10}$$

where $\Sigma_\pm \equiv \Sigma e^{i\mathcal{L}p_\pm}$. For every one of the integral factors in Eq. (4.9), following Gnutzmann and Altland [2], one can use the *color-flavor* transformation [40], which substitutes the highly fluctuating phases by smoother variables (to be defined below) at the cost of coupling $+/-$ fields components (decoupled in Eq. (4.6) and Eq. (4.10)). Specifically,

$$\int_0^{2\pi}\frac{d\phi_i}{2\pi} e^{L_i(\phi_i)} = \int D(Z_i,\tilde{Z}_i) e^{L_i(Z_i,\tilde{Z}_i)}, \tag{4.11}$$

where

$$L_i(Z_i,\tilde{Z}_i) \equiv \left((\psi_+^\dagger\Sigma_+)_{\mathrm{b},i}, (\psi_+^\dagger\Sigma_+)_{\mathrm{f},i}, s_{-,i}^*, \chi_{-,i}^*\right) \begin{pmatrix} 0 & 0 & Z_{\mathrm{i,bb}} & Z_{\mathrm{i,bf}} \\ 0 & 0 & Z_{\mathrm{i,fb}} & Z_{\mathrm{i,ff}} \\ \tilde{Z}_{\mathrm{i,bb}} & \tilde{Z}_{\mathrm{i,bf}} & 0 & 0 \\ \tilde{Z}_{\mathrm{i,fb}} & \tilde{Z}_{\mathrm{i,ff}} & 0 & 0 \end{pmatrix} \begin{pmatrix} s_{+,i} \\ \chi_{+,i} \\ (\Sigma_-\psi_-)_{\mathrm{b},i} \\ (\Sigma_-\psi_-)_{\mathrm{f},i} \end{pmatrix}. \tag{4.12}$$

Each of the $2B$ pairs of 2×2 matrices, $Z_i, \tilde{Z}_i$, are restricted so that $\tilde{Z}_{i,\mathrm{bb}} = Z_{i,\mathrm{bb}}^*$ and $\tilde{Z}_{i,\mathrm{ff}} = -Z_{i,\mathrm{ff}}^*$, while the Grassmann components are independent. On the

other hand,

$$\int D(Z_i, \tilde{Z}_i) \equiv \int d(Z_i, \tilde{Z}_i) \mathrm{sdet}(1 - Z_i \tilde{Z}_i) = 1, \tag{4.13}$$

and

$$|Z_{\mathrm{bb}}|^2 < 1. \tag{4.14}$$

Comparing the matrices in the r.h.s. of Eq. (4.10) and the r.h.s. of Eq. (4.12), one can see the effect of the transformation Eq. (4.11) in coupling super-vector components which where previously not connected. Particularly, now complex Gaussian variables, such as $s_{+,i}$, are coupled to anti-commuting variables, such as $(\psi_+^\dagger \Sigma_+)_{\mathrm{f},i}$, through $Z, \tilde{Z}$ matrix components such as $\tilde{Z}_{\mathrm{i,bf}}$. Thus we need now the full generality of Eq. (A.21) in order to integrate the super-vector, $\psi, \psi^\dagger$, and write

$$\int d(\tilde{\psi}_+, \psi_+, \tilde{\psi}_-, \psi_-,) \exp\left(-(\tilde{\psi}_+, \tilde{\psi}_-) \begin{pmatrix} 1 & -\Sigma_+ Z \Sigma_-^\dagger \\ -\tilde{Z} & 1 \end{pmatrix} \begin{pmatrix} \psi_+ \\ \psi_- \end{pmatrix} \right) = \frac{1}{\mathrm{sdet}(1 - \Sigma_+ Z \Sigma_-^\dagger \tilde{Z})}, \tag{4.15}$$

where $Z, \tilde{Z}$ are now $2 \cdot 2B$ super-matrices which are diagonal in the space of arcs ("topological space"). To sum up, we have so far performed the following (exact) transformation:

$$\lim_{K \to \infty} \frac{1}{K} \int_0^K \zeta(s, j_+, j_-) dk = \int \frac{D(Z, \tilde{Z})}{\mathrm{sdet}(1 - \Sigma_+ Z \Sigma_-^\dagger \tilde{Z})}, \tag{4.16}$$

where the restrictions on the $Z, \tilde{Z}$ matrices mentioned above parameterize, as shown by Zirnbauer [40], the Efetov's σ-model manifold of unitary symmetry.

4.2.2 Saddle-point approximation and universality

We employ $\mathrm{str} \ln A = \ln \mathrm{sdet} A$ in order to write the the r.h.s. of Eq. (4.16) as

$$\int \frac{D(Z, \tilde{Z})}{\mathrm{sdet}(1 - \Sigma_+ Z \Sigma_-^\dagger \tilde{Z})} = \int d(Z, \tilde{Z}) e^{-S(Z, \tilde{Z}; s, j_+, j_-)}, \tag{4.17}$$

where we have absorbed the factor $\mathrm{sdet}(1 - Z\tilde{Z})$ in the *action*

$$S = -\mathrm{str} \ln(1 - Z\tilde{Z}) + \mathrm{str} \ln(1 - \Sigma_+ Z \Sigma_-^\dagger \tilde{Z}). \tag{4.18}$$

With the aim to find a saddle point, one usually linearizes the action, S, with respect to the sources. First, we expand $\Sigma_\pm$:

$$\Sigma_\pm = \Sigma + i\Sigma\mathcal{L}p_\pm - \frac{1}{2}\Sigma\mathcal{L}^2 p_\pm^2 + \dots \tag{4.19}$$

$$\simeq \Sigma + i\Sigma\bar{l}\left(\pm\frac{s}{2} - \sigma_3^{\rm bf} j_\pm\right)\Delta \tag{4.20}$$

$$= \Sigma + i\Sigma\frac{\pi}{B}\left(\pm\frac{s}{2} - \sigma_3^{\rm bf} j_\pm\right) \tag{4.21}$$

where we have made the substitution $\mathcal{L}_a \equiv \bar{l}$ for all arcs a, as done by Gnutzmann and Altland, because we are not interested in the effect of arc-lengths fluctuations. We have also retained only those terms which are linear in the frequency, s, because every power of $s \sim 1$ comes with a power of $1/B \to 0$, or linear in the super-symmetry breaking source $j_\pm$, because terms proportional to j_+^2 or to j_-^2 will be eliminated by the limit $j_\pm \to 0$ in Eq. (4.4) (only *exponents* proportional to j_+, j_- or $j_+ j_-$ can survive at the end). The action, S, is now written as the sum a "kinetic" part and a "source action",

$$S = S_{\rm k} + S_p, \tag{4.22}$$

with the "kinetic" part being

$$S_{\rm k} = {\rm str}\ln(1 - \Sigma Z\Sigma^\dagger\tilde{Z}) - {\rm str}\ln(1 - Z\tilde{Z}), \tag{4.23}$$

and the source term being

$$S_p = i{\rm str}\left(p_+\frac{\Sigma Z\Sigma^\dagger\tilde{Z}}{1 - \Sigma Z\Sigma^\dagger\tilde{Z}} - p_-\frac{\tilde{Z}\Sigma Z\Sigma^\dagger}{1 - \tilde{Z}\Sigma Z\Sigma^\dagger}\right). \tag{4.24}$$

In the source action, we have neglected $j_\pm$ terms which would be proportional to

$$\frac{j_+ j_-}{B^2}{\rm str}\Sigma\sigma_3^{\rm bf} Z\sigma_3^{\rm bf}\Sigma^\dagger\tilde{Z}\frac{1}{1 - \Sigma Z\Sigma^\dagger\tilde{Z}}, \tag{4.25}$$

and

$$\frac{j_+ j_-}{B^2}{\rm str}\Sigma\sigma_3^{\rm bf} Z\Sigma^\dagger\tilde{Z}\frac{1}{1 - \Sigma Z\Sigma^\dagger\tilde{Z}}\Sigma Z\Sigma^\dagger\sigma_3^{\rm bf}\tilde{Z}\frac{1}{1 - \Sigma Z\Sigma^\dagger\tilde{Z}}. \tag{4.26}$$

The reason is that the super-trace is only order B and cannot compensate the $1/B^2$ factor[2].

[2]In the case of the uniform $Z, \tilde{Z}$ fields which make up the main contribution to the integral, one can see upon deriving with respect to $j_\pm$, that one deals with B integrals (single trace) for the terms that we neglect, versus B^2 integrals (product of traces) for the terms that we do not

The kinetic action grows with B due to the super-trace, while the source term is of order 1 due to $p_\pm \propto \frac{1}{B}$, thus one finds the saddle point of the action looking for the extremum of the kinetic part only. Varying the kinetic action with respect to $Z, \tilde{Z}$ and equating it to zero, one easily finds the saddle point solution, $Y, \tilde{Y}$, as the uniform $Z, \tilde{Z}$ distribution, i.e.

$$Y_i = Y, \quad \tilde{Y}_i = \tilde{Y} \quad \text{for all arcs } i. \tag{4.27}$$

For the validity of the saddle point approximation, it is necessary that the Gaussian contribution of the non-uniform modes to R, Eq. (4.4), vanishes in the limit $B \to \infty$, that is[3]

$$\lim_{B\to\infty} \lim_{j_\pm \to 0} \frac{\partial^2}{\partial j_+ \partial j_-} \int d(Z,\tilde{Z}) e^{\mathrm{str}^*\left(Z\tilde{Z} - \Sigma Z \Sigma^\dagger \tilde{Z} + p_+ \Sigma Z \Sigma^\dagger \tilde{Z} - p_- \tilde{Z} \Sigma Z \Sigma^\dagger\right)} = 0, \tag{4.28}$$

where the super-trace str* is understood not to include the 0-mode (uniform field). As shown by Gnutzmann and Altland, the above limit amounts to the condition (we do the calculation in appendix B)

$$\lim_{B\to\infty} \frac{1}{B^2} \mathrm{tr}^* \left(\frac{1}{1-F}\right)^2 = 0. \tag{4.29}$$

In section 4.5 we show how this condition is not met by the full Neumann digraph, and show an attempt to derive universality through a different treatment of the field theory.

---

neglect, while we need to compensate for a $1/B^2$ factor in both cases. We touch upon this issue in more detail in the next chapter (subsection 5.2.3).

[3] The complete Gaussian contribution to R can be written as

$$\lim_{j_\pm \to 0} \left(\int d(Y,\tilde{Y}) e^{\mathrm{str} p_+ Y\tilde{Y} - \mathrm{str} p_- \tilde{Y} Y} \frac{\partial^2}{\partial j_+ \partial j_-} \int d(Z,\tilde{Z}) e^{\mathrm{str}^*\left(Z\tilde{Z} - \Sigma Z \Sigma^\dagger \tilde{Z} + p_+ \Sigma Z \Sigma^\dagger \tilde{Z} - p_- \tilde{Z} \Sigma Z \Sigma^\dagger\right)} + \right.$$
$$\left. \int d(Z,\tilde{Z}) e^{\mathrm{str}^*\left(Z\tilde{Z} - \Sigma Z \Sigma^\dagger \tilde{Z} + p_+ \Sigma Z \Sigma^\dagger \tilde{Z} - p_- \tilde{Z} \Sigma Z \Sigma^\dagger\right)} \frac{\partial^2}{\partial j_+ \partial j_-} \int d(Y,\tilde{Y}) e^{\mathrm{str} p_+ Y\tilde{Y} - \mathrm{str} p_- \tilde{Y} Y} \right).$$

The integrals themselves produce 1 under the $j_\pm \to 0$, as can be seen, for example from the r.h.s. Eq. (B.9) in page 123, while integrals that are derived w.r.t *only one* source produce 0 under the limit (as can be inferred as well from the equations in appendix B) and are not considered. The second summand above produce the universal result, therefore the first one is then the one to investigate.

4.3 The $Q/\mathcal{Q}$ notation.

It is convenient to introduce

$$Q \equiv V\Lambda V^{-1} \quad ; \quad \mathcal{Q} \equiv \mathcal{V}\Lambda\mathcal{V}^{-1} \tag{4.30}$$

with

$$V = \begin{pmatrix} 1 & Z \\ \tilde{Z} & 1 \end{pmatrix} \quad ; \quad \mathcal{V} = \begin{pmatrix} 1 & \Sigma Z \\ \Sigma^\dagger \tilde{Z} & 1 \end{pmatrix} \quad ; \quad \Lambda \equiv \begin{pmatrix} 1 & 0 \\ 0 & -1 \end{pmatrix} \tag{4.31}$$

Defining also

$$D = \begin{pmatrix} 1-\Sigma & 0 \\ 0 & 1-\Sigma^\dagger \end{pmatrix} \tag{4.32}$$

the following equalities can easily be checked :

$$\mathcal{V}V^{-1} = 1 + \frac{1}{2} D\Lambda(Q-\Lambda), \tag{4.33}$$

$$V\mathcal{V}^{-1} = 1 + \frac{1}{2} D^\dagger\Lambda(\mathcal{Q}-\Lambda). \tag{4.34}$$

One can use these identities together with

$$S_{\mathrm{k}} = \mathrm{str}\ln \mathcal{V}V^{-1} = -\mathrm{str}\ln V\mathcal{V}^{-1}, \tag{4.35}$$

in order to re-write the kinetic term as

$$S_{\mathrm{k}} = \mathrm{str}\ln\left(1 + \frac{1}{2} D\Lambda(Q-\Lambda)\right) \tag{4.36}$$

$$= -\mathrm{str}\ln\left(1 + \frac{1}{2} D^\dagger\Lambda(\mathcal{Q}-\Lambda)\right). \tag{4.37}$$

A source term can usually be written, for example, as

$$S_p = \mathrm{str}\ p\Lambda(\mathcal{Q}-\Lambda), \tag{4.38}$$

where p is some super-symmetry breaking matrix that depends on the specific problem.

This notation does not rely at all on the structure of the matrices $Z, \tilde{Z}$, and can be employed in other settings where Zirnbauer's method is used in dealing with phase averages, for example in [39], but to our knowledge it has not been used so far.

4.4 Preliminary remarks

4.4.1 Neumann scattering matrix

The full Neumann graph, as well as the full Neumann *symmetric digraph*, has a very particular *graph* scattering matrix Σ (by which we mean Eq. (3.71)). It is trivially obtained from the *vertex* scattering matrices Eq. (3.67). It is convenient to distinguish two parts according to whether or not they have size-dependent components:

$$\Sigma \equiv \mathfrak{T} - \mathfrak{R}. \tag{4.39}$$

The "reflection probability amplitude", $\mathfrak{R}$, is size independent, this is the reason why we consider it separately from "transmission amplitude", $\mathfrak{T}$, which is "isotropic"[4] in the sense that it does not distinguish between different links and decreases with the graph-size as $1/V$. According to our vertex notation,

$$\mathfrak{R}_{ij,kl} = \delta_{il}\delta_{jk}(1-\delta_{ij})\mathfrak{R}_{ij,ji} \tag{4.40}$$

$$\mathfrak{T}_{ij,kl} = \delta_{il}(1-\delta_{ij})(1-\delta_{ik})\mathfrak{T}_{ij,ki}, \tag{4.41}$$

where the non-vanishing components read

$$\mathfrak{R}_{ij,ji} = 1 \tag{4.42}$$

$$\mathfrak{T}_{ij,ki} = \frac{2}{V-1}. \tag{4.43}$$

From the definitions Eq. (4.40) one easily shows that

$$\mathfrak{T} = \mathfrak{R}\mathfrak{T}^T\mathfrak{R} \tag{4.44}$$

$$\left(\frac{1}{2}\mathfrak{T}\mathfrak{R}\right)^2 = \frac{1}{2}\mathfrak{T}\mathfrak{R}. \tag{4.45}$$

For further use, it is convenient to define the following projector:

$$N \equiv \frac{1}{2}\mathfrak{T}\mathfrak{R}, \tag{4.46}$$

[4] In reality $\mathfrak{T}$ does have reflexive component, with the same size dependent contribution as any other component.

whose non-vanishing components are

$$N_{ik,ij} = \frac{1}{V-1}. \tag{4.47}$$

Due to $N^2 = N$, for any matrix A

$$(NA)^n N = (NAN)^n. \tag{4.48}$$

From Eq. (4.44) and Eq. (4.46), we have $N = N^T$ thus N can be written as a the sum of orthogonal projectors,

$$N = \sum_{i=1}^{V} \vec{v}_i \otimes \vec{v}_i^T, \tag{4.49}$$

where

$$(\vec{v}_i)_{kj} \equiv \delta_{ik}(1-\delta_{ij})(\vec{v}_i)_{ij}. \tag{4.50}$$

For any *arc-diagonal* matrix A

$$(NAN)_{ij,ik} = \sum_{l\neq i} N_{ij,il} A_{il} N_{il,ik} \tag{4.51}$$

$$= \frac{\sum_{l\neq i} A_{il}}{V-1} \frac{1}{V-1} \tag{4.52}$$

$$\equiv A_i N_{ij,ik}, \tag{4.53}$$

i.e. N performs *averages over outgoing arcs from a given bond*, according to which we have defined (always referring to arc-diagonal matrices)

$$\frac{\sum_{l\neq i} A_{il}}{V-1} \equiv A_i. \tag{4.54}$$

From Eq. (4.48) and the above definition, for arc-diagonal matrices

$$((NA)^n N)_{ij,ik} = A_i^n N_{ij,ik}, \tag{4.55}$$

holds, and inside a trace

$$\begin{aligned}
\mathrm{str}(NA)^n &= \mathrm{str}(NAN)^n && (4.56)\\
&= \mathrm{str}\sum_{i=1}^{V}\sum_{j\neq i} A_i^n N_{ij,ij} && (4.57)\\
&= \mathrm{str}\sum_{i=1}^{V} A_i^n \sum_{j\neq i} N_{ij,ij} && (4.58)\\
&= \mathrm{str}\sum_{i=1}^{V} A_i^n. && (4.59)
\end{aligned}$$

In Eq. (4.57) we have "unfolded" the str from Eq. (4.56), which involves a usual trace over the space of arcs *and* a super-trace over any other structure (generally Bose-Fermi and Advanced-Retarded), so that str in Eq. (4.57) and followings refers to *only* non topological structures. The property Eq. (4.59) is the one that we need in the remaining of the chapter. In practice, it is used in power series of functions of matrix-variables, such as

$$\begin{aligned}
\mathrm{str} f(NA) &= \mathrm{str}\sum_{n=0}^{\infty}\frac{f^{(n)}(0)}{n!}(NA)^n && (4.60)\\
&= \sum_{n=0}^{\infty}\frac{f^{(n)}(0)}{n!}\mathrm{str}(NA)^n && (4.61)\\
&= \sum_{n=0}^{\infty}\frac{f^{(n)}(0)}{n!}\mathrm{str}\sum_{i=1}^{V} A_i^n && (4.62)\\
&= \mathrm{str}\sum_{i=1}^{V}\sum_{n=0}^{\infty}\frac{f^{(n)}(0)}{n!}A_i^n && (4.63)\\
&= \mathrm{str}\sum_{i=1}^{V} f(A_i) && (4.64)
\end{aligned}$$

4.4.2 Mode decomposition of relevant operators

The $V(V-1)$-dimensional space of arcs can be in principle decomposed in two types of subspaces:

- the subspace of "traceless" modes, that we denote by ϕ, and has dimensions $(V-1)(V-2)-1$. What we call "tracelessness" reads, for every node i :

$$\sum_j \phi_{ij} = 0 \quad \text{and} \tag{4.65}$$

$$\sum_j \phi_{ji} = 0. \tag{4.66}$$

  This space is further subdivided into a space of "symmetric" modes, ϕ^+, with $\frac{(V-1)(V-2)}{2} - 1$ components, and a $(V-1)(V-2)$-dimensional space of "antisymmetric" modes, ϕ^-. They have the properties

$$\phi^{\pm}_{ji} = \pm\phi^{\pm}_{ij}. \tag{4.67}$$

- the subspace of "tracefull" modes, ψ, with dimension $2(V-1)+1$. These have the form

$$\psi_{ij} = a_i + b_j, \tag{4.68}$$

  and we consider three subspaces, ψ_0, ψ^+, ψ^-, which are, respectively, the uniform mode, and the two $(V-1)$-dimensional spaces with the properties

$$\psi^+_{ij} = a_i, \tag{4.69}$$

$$\psi^-_{ij} = b_j, \tag{4.70}$$

  and the restrictions

$$\sum_i^V a_i = \sum_i^V b_i = 0. \tag{4.71}$$

In order to obtain the spectrum of the operators Σ and F, we analyze their action onto these four eigenspaces. The traceless spaces are eigenmodes of these operators, while the tracefull spaces are not, but the remaining eigenspaces can be written in terms of those. Specifically, we will find two $(V-1)$-dimensional eigenspaces with the form

$$\tilde{\psi}^{\pm}_{ij} = a_i + f^{\pm}(a_j), \tag{4.72}$$

f^+, f^- being some linear functions.

4.4.2.1 Eigenvalues of the quantum scattering matrix, Σ

The graph scattering matrix acts on the traceless modes according to

$$(\Sigma\phi^{\pm})_{ij} = -\mathfrak{R}_{ij,ji}\phi^{\pm}_{ji} + \sum_{k\neq i}\mathfrak{T}_{ij,ki}\phi^{\pm}_{ki} \tag{4.73}$$

$$= \mp\phi^{\pm}_{ij}, \tag{4.74}$$

where we have used the definition of the Neumann graph scattering matrix, Eq. (4.39), for Eq. (4.73). From the tracelessness property, Eq. (4.65), follows that $\mathfrak{T}\phi^{\pm} = 0$ and hence Eq. (4.74). Therefore we have the eigenvalues $\lambda^{\pm}_{\phi} = \mp 1$, with degeneracy $(V-1)(V-2)/2 - 1$ and $(V-1)(V-2)/2$, respectively.
In order to find the non-uniform, tracefull modes, $\psi_{ij} = a_i + b_j$ with properties Eq. (4.71), as well as their corresponding eigenvalues, we solve the eigenequation

$$(\Sigma\psi)_{ij} = \lambda_{\psi}\psi_{ij}, \tag{4.75}$$

by working out the effect of Σ on such modes:

$$(\Sigma\psi)_{ij} = -\mathfrak{R}_{ij,ji}\psi_{ji} + \sum_{k\neq i}\mathfrak{T}_{ij,ki}\psi_{ki} \tag{4.76}$$

$$= -a_j - b_i + \frac{2}{V-1}\sum_{k\neq i}(a_k + b_i) \tag{4.77}$$

$$= -a_j + b_i + \frac{2}{V-1}\sum_{k\neq i}a_k \tag{4.78}$$

$$= -a_j + b_i - \frac{2}{V-1}a_i. \tag{4.79}$$

For Eq. (4.79) we have applied the condition Eq. (4.71). Hence, from Eq. (4.75) and Eq. (4.79),

$$a_j - b_i + \left(\frac{2}{V-1} - \lambda_{\psi}\right)a_i - \lambda_{\psi}b_j = 0. \tag{4.80}$$

Summing Eq. (4.80) over i and applying again Eq. (4.71), we obtain

$$b_j = \frac{1}{\lambda_{\psi}}a_j \quad \text{for all} \quad j. \tag{4.81}$$

Summing Eq. (4.80), this time in j, we have

$$\lambda^2_{\psi} - \frac{2}{V-1}\lambda_{\psi} + 1 = 0. \tag{4.82}$$

As a result, the eigenvalue reads

$$\lambda_{\psi}^{\pm} = \frac{1}{V-1} \pm \iota \sqrt{1 - \frac{1}{(V-1)^2}} \tag{4.83}$$

$$\simeq \pm\, \iota + \frac{1}{V-1} \mp \iota \frac{1}{2(V-1)^2} + \dots \tag{4.84}$$

and Eq. (4.72) takes the form

$$b^{\pm} = \left(\frac{1}{V-1} \mp \iota \sqrt{1 - \frac{1}{(V-1)^2}} \right) a \tag{4.85}$$

$$= \mp\, \iota a + \left(\frac{1}{V-1} \pm \iota \frac{1}{2(V-1)^2} + \dots \right) a. \tag{4.86}$$

4.4.2.2 The eigenvalues of the classical propagator, F

The components of the Perron-Frobenius operator are defined as $F_{ij,ki} = |\Sigma_{ij,ki}|^2$, hence from Eq. (4.39)

$$F = \left(1 - \frac{4}{V-1} \right) \mathfrak{R} - \frac{2}{V-1} \mathfrak{T} \tag{4.87}$$

For the traceless modes, $\mathfrak{T}\phi^{\pm}$=0, hence

$$\left(F\phi^{\pm} \right)_{ij} = \pm \left(1 - \frac{4}{V-1} \right) \phi_{ij}^{\pm}, \tag{4.88}$$

i.e.

$$\lambda_{\phi}^{\pm} = \pm \left(1 - \frac{4}{V-1} \right). \tag{4.89}$$

The Full-Neumann classical propagator acts on ψ's as

$$(F\psi)_{ij} = \left(1 - \frac{4}{V-1} \right) \mathfrak{R}_{ij,ji} \psi_{ji} + \frac{2}{V-1} \sum_{k \neq i} \mathfrak{T}_{ij,ki} \psi_{ki} \tag{4.90}$$

$$= \left(1 - \frac{4}{V-1} \right) (a_j + b_i) + \frac{4}{(V-1)^2} \sum_{k \neq i} (a_k + b_i) \tag{4.91}$$

$$= \left(1 - \frac{4}{V-1} \right) a_j + b_i + \frac{4}{(V-1)^2} \sum_{k \neq i} a_k \tag{4.92}$$

$$= \left(1 - \frac{4}{V-1} \right) a_j + b_i - \frac{4}{(V-1)^2} a_i, \tag{4.93}$$

where we have followed the exact same steps as in the preceding subsection. Using Eq. (4.93) in the eigen-equation

$$(\mathrm{F}\psi)_{ij} = \lambda_\psi \psi_{ij}, \tag{4.94}$$

we obtain

$$\left(1 - \frac{4}{V-1}\right) a_j + b_i - \left(\lambda_\psi + \frac{4}{(V-1)^2}\right) a_i - \lambda_\psi b_j = 0. \tag{4.95}$$

Summing Eq. (4.95) on i we have

$$b = \frac{1 - \frac{4}{V-1}}{\lambda_\psi} a, \tag{4.96}$$

and summing in j

$$\lambda_\psi^2 + \left(\frac{2}{V-1}\right)^2 \lambda_\psi + \frac{4}{V-1} - 1 = 0. \tag{4.97}$$

The solutions are

$$\lambda_\psi^\pm = \frac{-2}{(V-1)^2} \pm \sqrt{1 - \frac{4}{V-1} + \frac{4}{(V-1)^4}} \simeq \qquad \pm 1 \mp \frac{2}{V-1} + \dots \tag{4.98}$$

and

$$b \simeq \left(\pm 1 \mp \frac{2}{V-1} + \dots\right) a \tag{4.99}$$

4.5 Nonlinear σ-model action for the FNdG

4.5.1 Analysis of the Gaussian approximation

We know, from [2] (as well as subsection 4.2.2 and appendix B), that the validity of the saddle point approximation to the field theory of the two point function requires

$$\lim_{B\to\infty} \frac{1}{B^2} \mathrm{tr}^* \left(\frac{F}{1-F}\right)^2 = 0. \tag{4.100}$$

However, we also know (see 4.4.2.2) that for the FNdG a $((V-1)(V-2)/2-1)$-degenerate eigenspace of traceless, symmetric modes, ϕ^+, of F exists, with eigenvalues $\lambda_\phi^+ = (1 - 4/(V-1))$. The contribution arising from ϕ^+-modes clearly

makes the limit in the l.h.s. of Eq. (4.100) remain constant, since at infinite size, the trace is

$$\mathrm{tr}^* \left(\frac{F}{1-F}\right)^2 \sim \frac{V^2}{2}\left(\frac{V}{4}\right)^2 = \frac{V^4}{32}. \tag{4.101}$$

This result contradicts the evidence pointing towards universality of the full Neumann graph. One could argue that the Eq. (4.100) being a constant is not the worst possible case (the limit could diverge[5]), but the reality is worse. The numerical results on the level spacing distribution (see chapter 5), despite not being conclusive about the general convergence of the FNdG towards universality, do seem to show that level repulsion exists beyond doubt, while a finite deviation from $R_2(s)$ at $s = 0$ would say otherwise (in the $s \to 0$ limit, the spacing distribution and the two point function are equivalent, as can be inferred from Eq. (2.29)).

Moreover, restricting the kinetic action to symmetric modes, and expanding it beyond 2nd order, the $1/V$ masses of traceless modes seem to completely invalidate the Gaussian approximation. The kinetic action, restricted to symmetric modes, can be easily re-written in terms of the N matrix, as,

$$\begin{aligned} S_{\mathrm{k}} &= -\mathrm{str}\ln(1 - Z\tilde{Z}) + \mathrm{str}\ln(1 - (\mathfrak{T} - \mathfrak{R})Z(\mathfrak{R}\mathfrak{T}\mathfrak{R} - \mathfrak{R})\tilde{Z}) && (4.102)\\ &= -\mathrm{str}\log(1 - Z\tilde{Z}) + \mathrm{str}\log(1 - (1-2N)Z(1-2N)\tilde{Z}), && (4.103) \end{aligned}$$

where we have used $RZ = ZR$. The Gaussian approximation reads[6],

$$\begin{aligned} S_{\mathrm{k}}^{(2)} &= 4\mathrm{str}(NZ - NZN)\tilde{Z} && (4.104)\\ &= \frac{4}{V-1}\mathrm{str}\vec{\tilde{Z}}(1-N)\vec{Z} && (4.105) \end{aligned}$$

[5] Such is the case of the Neumann *star* graph, for which one can easily show that the l.h.s. of Eq. (4.100) diverges as B.

[6] This can be compared with a "well behaved" universal graph, the DFT full graph, for which $S_{\mathrm{k}}^{(2)} = \mathrm{str}\vec{\tilde{Z}}(1-N)\vec{Z}$. The extensive subspace of traceless modes, i.e. modes such that $N\vec{Z} = 0$, has finite masses in the DFT case, while being almost massless in the Neumann case, Eq. (4.104).

The mass $\sim \frac{1}{V}$ of the traceless modes makes Z contribute up to orders $\sqrt{V}$. Further expanding Eq. (4.103), the n^{th} term reads[7], up to constants $a, b, c, \ldots$,

$$S_{\text{k}}^{(n)} = \text{str}\Big(a(N(Z\tilde{Z})^n + N(\tilde{Z}Z)^n) \tag{4.106}$$

$$+ b_1(NZN\tilde{Z}(Z\tilde{Z})^{n-1} + N\tilde{Z}NZ(\tilde{Z}Z)^{n-1}) \tag{4.107}$$

$$+ b_2(NZ\tilde{Z}N(Z\tilde{Z})^{n-1} + N\tilde{Z}ZN(\tilde{Z}Z)^{n-1} + \ldots \tag{4.108}$$

$$+ c_{1,1}(NZN\tilde{Z}N(Z\tilde{Z})^{n-1} + N\tilde{Z}NZN(\tilde{Z}Z)^{n-1}) \tag{4.109}$$

$$+ c_{1,2}(NZN\tilde{Z}ZN\tilde{Z}(Z\tilde{Z})^{n-2} + N\tilde{Z}NZ\tilde{Z}NZ(\tilde{Z}Z)^{n-2}) + \ldots \tag{4.110}$$

$$+ \ldots \tag{4.111}$$

$$+ \frac{4^n}{n}(NZN\tilde{Z})^n \Big). \tag{4.112}$$

The str runs over $V(V-1)$ components, each of which is of order $\sim \frac{1}{V-1} \times$ (order of $Z\tilde{Z}$). The order of $Z\tilde{Z}$ is $\sim V$ as determined by the masses (gaussian approximation). Therefore

$$S_{\text{k}}^{(n)} \sim V^{n-1}, \tag{4.113}$$

which grows with n, completely invalidating the expansion.
This discussion suggests studying the action, restricted to symmetric modes, in order to find alternative ways to recover universality without relying on the Gaussian expansion around the uniform sector of the σ-model manifold.

4.5.2 FNdG σ-model action restricted to symmetric modes

4.5.2.1 Kinetic term

We recall from Eq. (4.103) that the kinetic action restricted to symmetric modes reads

$$S_{\text{k}} = -\text{str}\ln(1 - Z\tilde{Z}) + \text{str}\ln(1 - (1-2N)Z(1-2N)\tilde{Z}), \tag{4.114}$$

[7]However, due to the tracelessness condition, $NZN = N\tilde{Z}N = 0$ and many of the summands would vanish (Eq. (4.107), Eq. (4.109)...).

and consider $1-2N$ to be an effective scattering matrix for the action. Applying the Q formalism, (page 45), we start with

$$S_{\mathrm{k}} = \mathrm{str}\log\begin{pmatrix} 1 & (1-2N)Z \\ (1-2N)\tilde{Z} & 1 \end{pmatrix}\begin{pmatrix} 1 & Z \\ \tilde{Z} & 1 \end{pmatrix}^{-1}, \tag{4.115}$$

where the argument of the logarithm plays the role of the matrix product in the l.h.s. of Eq. (4.33), and we introduce a matrix D analogous to the one in Eq. (4.32)

$$D = \begin{pmatrix} 1-(1-2N) & 0 \\ 0 & 1-(1-2N) \end{pmatrix} = 2N\begin{pmatrix} 1 & 0 \\ 0 & 1 \end{pmatrix}. \tag{4.116}$$

The action, with the format Eq. (4.36), reads

$$\begin{aligned} S_{\mathrm{k}} =& \mathrm{str}\ln\left(1+N\Lambda(Q-\Lambda)\right) \\ =& -\mathrm{str}\sum_{n=1}^{\infty}\frac{1}{n}(-N\Lambda(Q-\Lambda))^n. \end{aligned} \tag{4.117}$$

Due to the fact that Q is an arc-diagonal matrix, we can use the result Eq. (4.64) directly and write the action

$$S_{\mathrm{k}} = \mathrm{str}\sum_{i=1}^{V}\ln\left(\sum_{j\neq i}Q_{ij}\right) \tag{4.118}$$

4.5.2.2 Source term

The full action of the model now reads

$$\mathrm{str}\ln\left(1+N\Lambda(Q-\Lambda)+(1-2N)\Phi\Lambda(Q-\Lambda)\right) \equiv S_{\mathrm{k}}+S_{\Phi}, \tag{4.119}$$

with the linearized source action

$$S_{\Phi} = \mathrm{str}\Phi(1-2N)\Lambda(Q-\Lambda)\frac{1}{1+N\Lambda(Q-\Lambda)} \tag{4.120}$$

$$= \mathrm{str}\Phi(1-2N)D\frac{1}{1+ND} \tag{4.121}$$

$$= S_1 - 2S_2. \tag{4.122}$$

We define $D=\Lambda(Q-\Lambda)=\Lambda Q-1$, which is obviously arc-diagonal, as well as the matrix Φ, which contains the frequency dependence and the super-symmetry

breaking $j_\pm$:

$$\Phi = \frac{-\iota\pi s}{4B} + \frac{\iota\pi}{2B}\begin{pmatrix} j_+ & 0 \\ 0 & j_- \end{pmatrix}_{\mathrm{AR}} \sigma_3^{\mathrm{bf}}. \tag{4.123}$$

Applying the same formalism as before to S_1

$$\begin{aligned} S_1 =& \mathrm{str}\Phi D\frac{1}{1+ND} && (4.124)\\ =& \mathrm{str}\Phi\sum_{i=1}^{V}\sum_{j\neq i} D_{ij} - \mathrm{str}\sum_{i=1}^{V}\frac{1}{V-1}\sum_{j\neq i}(D\Phi D)_{ij}\frac{1}{1+\frac{1}{V-1}\sum_{j\neq i} D_{ij}}, && (4.125)\end{aligned}$$

we see that this part of the action contain the "standard" source term, i.e. the one proportional to $\mathrm{str}\Phi\Lambda Q$. On the other hand, we have for S_2

$$\begin{aligned} S_2 =& \mathrm{str}\Phi ND\frac{1}{1+ND} && (4.126)\\ =& \mathrm{str}\Phi\sum_{i=1}^{V}\frac{\frac{1}{V-1}\sum_{j\neq i} D_{ij}}{1+\frac{1}{V-1}\sum_{j\neq i} D_{ij}}, && (4.127)\end{aligned}$$

hence the entire source action reads

$$\begin{aligned} S_1 - 2S_2 =& \mathrm{str}\Phi\sum_{i=1}^{V}\sum_{j\neq i} D_{ij} && (4.128)\\ & -\mathrm{str}\sum_{i=1}^{V}\frac{1}{V-1}\sum_{j\neq i}\left((D\Phi D)_{ij} + 2\Phi D_{ij}\right)\frac{1}{1+\frac{1}{V-1}\sum_{j\neq i} D_{ij}}. && (4.129)\end{aligned}$$

Let us recover now the Q-notation. On the one hand

$$\frac{1}{1+\frac{1}{V-1}\sum_{j\neq i} D_{ij}} = \frac{V-1}{\Lambda\sum_{j\neq i} Q_{ij}}, \tag{4.130}$$

while on the other

$$\sum_{j\neq i}\left((D\Phi D)_{ij} + 2\Phi D_{ij}\right) = \sum_{j\neq i}\left(\Lambda Q_{ij}\Phi\Lambda Q_{ij} - \Phi + 2\Phi\Lambda Q_{ij} - (\Lambda Q_{ij}\Phi + \Phi\Lambda Q_{ij})\right). \tag{4.131}$$

Therefore, as an alternative notation to the r.h.s. of Eq. (4.120), we can write

$$S_\Phi = \mathrm{str}\Phi(\Lambda Q - 1) + \mathrm{str}\sum_{i=1}^{V}\sum_{j\neq i}(\Lambda\Phi - Q_{ij}\Lambda\Phi Q_{ij})\frac{1}{\sum_{j\neq i} Q_{ij}}. \tag{4.132}$$

In terms *of power counting only*, one sees that, due to the denominator, the non-standard term would be subdominant by $1/V$ compared to the standard one. One also sees that it disappears, as it should, if Q is uniform.

4.5.2.3 Conclusion

The action $S_{\mathrm{k}} + S_{\Phi}$ is still very problematic. Even assuming that we can neglect the non-standard term in the r.h.s. of Eq. (4.132), Q is still non uniform, therefore the standard term is not supposed to produce the universal result. Moreover, the kinetic action is still present *and* dominant, by a factor of V (as we have V traces in the r.h.s. of Eq. (4.118)). Interestingly, it is easy to see that for the case of a (Neumann) *star* graph, the kinetic action would be order 1, the same as the source. In fact, the main part of S_{Φ} does not change, while the kinetic part would become $\mathrm{str}\ln\sum_{i=1}^{B} Q_i \sim 1$.

Among the several attempts made in order to progress from here, the more promising was a change of variables from the original Q-manifold to a new pseudo hermitian one, defined by

$$A_i \equiv \sum_{j\neq i} Q_{ij} \quad \text{for all } i. \tag{4.133}$$

The change is made through the introduction of a Dirac delta, in order to sidestep a complicated and unknown Jacobian. From Fourier transforming the V delta functions, V new Fourier variables, μ_i, arise.

While the Q variable could be integrated out, the remaining ones were challenging. Part of the difficulty comes from the fact that the integration of Q gives rise to interactions between the previously independent Fourier variables. This is due to the fact that every Q_{ij} relates to two nodes, so we have terms like

$$\mathrm{str}\,(\mu_i + \mu_j)\, Q_{ij}. \tag{4.134}$$

This leads us to suggest that this formalism could be adaptable to the Neumann star graph, as there is only a single node in that case. The functional would look similar to

$$\int d\mu \int dA \int dQ\ e^{\iota \mathrm{str}\ \mu\left(A-\sum_i Q_i\right)} e^{-\mathrm{str}\ln A - \mathrm{str}\Phi\Lambda A}, \tag{4.135}$$

and the A integral could be attempted by developing a super-symmetric version of the Itzykson-Zuber integral [57] similar to the one presented in [58] (see as well [59, 60]).

Chapter 5

A functional for wave function statistics

5.1 Introduction

The method pioneered in [1, 2] can be used (see section 5.2) to produce a σ-model functional for the spectral average of the *wave intensity* probability distribution. The wave intensities are determined by the eigenvector components that satisfy the stationarity condition Eq. (3.77)

$$\vec{a}_s = U(\mathrm{k}_s)\vec{a}_s, \tag{5.1}$$

where we are using in Eq. (5.1) $s = 1, 2, \ldots$ (with $\mathrm{k}_{s+1} > \mathrm{k}_s$) for eigenstate indexing, and $\vec{a}_s$ is related to waves traveling on the QdG by

$$\psi(x_{ij}; \mathrm{k}_s) = a_{ij;s} e^{\iota \mathrm{k} x_{ij}}, \qquad \sum_{ij} |a_{ij;s}|^2 l_{ij} \equiv 1. \tag{5.2}$$

The normalization condition sets the scale of the square amplitudes as

$$|a_{ij;s}|^2 \sim \frac{1}{2B\bar{l}}. \tag{5.3}$$

We will denote by x a *fixed* arc of the digraph, and will study the distribution

$$f(t) = \lim_{N\to\infty} \frac{1}{N} \sum_{s=1}^{N} \delta(t - 2B\bar{l}|a_{x;s}|^2), \tag{5.4}$$

which represents the probability of finding a value of t for the wave intensity $|a_x|^2$, when sampling over the entire spectrum.

The *universal* result (that is, the result concerning the eigenvector components of the ensembles of RMT) is that wave *amplitudes* are distributed like Gaussian random variables [9], or in order words, that the random wave hypothesis [61], RWH, holds *on average over the graph eigenstates*.

The average wave intensity on the arc x, i.e. the first moment of $f(t)$, is naturally 1 (this is a *local* version of the Weyl law Eq. (3.93), and can be as well recovered from similar POT arguments). The second moment is the *local* inverse participation ratio, IPR, here *averaged over the spectrum*. This latter quantity, which is a standard measure of eigenstate statistics, has been already studied in the context of quantum graphs, see for example [41, 42, 62, 63]. In particular Gnutzmann *et al.* [41] manage to give universality criteria[1] for the IPR through an analytical treatment of its spectral average for a *single sample*, based on the super-symmetry technique in [2].

We plan to carry out a similar treatment for Eq. (5.4), which will be an adaptation of the work by Falko and Efetov in the context of small disordered conductors[5]. The uniform mode of our theory will reproduce the Gaussian universal result mentioned above, but the reduction to the uniform mode in the thermodynamic limit requires now

$$\lim_{B\to\infty} \frac{1}{B} \mathrm{tr}^* \frac{1}{1-F} = 0, \tag{5.5}$$

which is obviously (much) stronger than Eq. (4.1): an *extensive* number of eigenvalues of F approaching 1 as $1 - \frac{c}{B^\alpha}$ invalidates the Eq. (5.5) for any $\alpha > 0$.

It is worth mentioning that the l.h.s. of Eq. (4.1) is reminiscent of the Gaussian correction to the uniform mode of the sigma-model field theory representation of the 2-point function for small metallic grains ([64]), if one identifies B with the "dimensionless conductance" and the "discrete Laplacian", $1-F$, with the continuous Laplacian ("kinetic term") of the σ-model action that describes disordered systems in the diffusive regime ([23]). Similarly, the fact that the quadratic decay

[1] They actually investigate spectral averages of quantities of the form $\left(\vec{a}_s{}^\dagger M \vec{a}_s\right)^2$ where M is a diagonal matrix representing an observable on the bonds. Naturally, the local IPR to which we refer to here is a special case, corresponding to M not vanishing only for the component M_{xx}.

of spectral fluctuations changes to linear, Eq. (5.5), when studying the wave functions fluctuations decay, is also standard in Efetov's formalism[2] (see [65] for the corrections to the Gaussian wave amplitude statistics, indeed *linear* in the inverse dimensionless conductance).

Much more attainable than Eq. (5.5), the condition

$$\lim_{B\to\infty} \frac{1}{B^2} \mathrm{tr}^* \frac{1}{1-F} M^2 = 0, \tag{5.6}$$

was obtained by Gnutzmann *et al.* [41] as a criterium for *quantum ergodicity*, i.e. the property that

$$\lim_{N\to\infty} \frac{1}{N} \sum_{s=1}^{N} \left(\vec{a}_s{}^{\dagger} \mathcal{L} M \vec{a}_s \right)^2 = \frac{\mathrm{tr}(\mathcal{L}M)^2}{(2B\bar{l})^2}, \tag{5.7}$$

where M is a *diagonal* matrix representing an observable on the space of bonds. From [41] one can also infer that the spectrum-averaged, *second* moment of the distribution of wave amplitudes mentioned above agrees with RWH if $\mathrm{tr}^* \frac{1}{1-F} < B$ in the limit $B \to \infty$, in agreement with[3] Eq. (5.5).

In the next two sections we present, respectively, a careful derivation of the functional representation for the spectral average of Eq. (5.4), and a derivation of the universal limit.

5.2 The functional

5.2.1 Setting up $f(t)$ for the spectral average

Following Fal'ko and Efetov, we define

$$f_{\mathrm{k}}(t) \equiv \sum_s \delta(t - 2B\bar{l}|a_{s,x}|^2)\delta(\mathrm{k} - \mathrm{k}_s), \tag{5.8}$$

from which Eq. (5.4) is recovered upon spectral average,

$$f(t) = \lim_{K\to\infty} \frac{\Delta}{K} \int_0^K f_{\mathrm{k}}(t) d\mathrm{k}. \tag{5.9}$$

[2]We are referring here, and in the entire text, to systems with unitary symmetry (broken time reversal invariance).

[3]In the case of a FNG, substituting M by a constant matrix, one can also infer that the correction Eq. (5.6) is order $1/V$ ($(1/B^2)BV$), greater than the actual Eq. (5.7) which is $\sim 1/B$.

In order to proceed, the first step consists in transforming $f_k(t)$ into a *single* product of two k-dependent factors, both of them representable in terms of "advanced/retarded Green functions" $,\frac{1}{1-U(\mathrm{k})}/\frac{1}{1-U(\mathrm{k})^\dagger}$, so that a spectral average can be performed in a manner similar to the calculation of the 2-point function by the super-symmetry technique. Noticing that the wave amplitude, $|a_{s,x}|^2$, can be obtained from the x, x component of the Green function operator as[4]

$$\lim_{\gamma\to 0}\gamma\left(\frac{1}{1-e^{-\gamma U(\mathrm{k})^\dagger}}\right)_{x,x}=\begin{cases}|a_{s,x}|^2, & \text{if } \mathrm{k}=\mathrm{k}_s \text{ for some eigenstate } s\\ 0, & \text{otherwise,}\end{cases} \tag{5.10}$$

we perform the following steps

$$f_{\mathrm{k}}(t)=\sum_s \delta\left(t-2B\bar{l}\lim_{\gamma\to 0}\gamma\left(\frac{1}{1-e^{-\gamma U(\mathrm{k})^\dagger}}\right)_{x,x}\right)\delta(\mathrm{k}-\mathrm{k}_s) \tag{5.11}$$

$$=\delta\left(t-2B\bar{l}\lim_{\gamma\to 0}\gamma\left(\frac{1}{1-e^{-\gamma U(\mathrm{k})^\dagger}}\right)_{x,x}\right)\sum_s\delta(\mathrm{k}-\mathrm{k}_s) \tag{5.12}$$

$$=\lim_{\gamma\to 0}\delta\left(t-2B\bar{l}\gamma\left(\frac{1}{1-e^{-\gamma U(\mathrm{k})^\dagger}}\right)_{x,x}\right)d(k). \tag{5.13}$$

In Eq. (5.11), we simply apply Eq. (5.10) (the factor $\delta(\mathrm{k}-\mathrm{k}_s)$ will enforce the correct amplitude in the argument of the first delta). The crucial step Eq. (5.12) is possible because the t-dependent delta function loses its explicit dependence on specific eigenstates, due to the trick Eq. (5.10). The expression Eq. (5.13) is simply formal (with a finite γ, the argument of the leftmost delta function is a complex number, and $\lim_{\gamma\to 0}\int dt f_{\mathrm{k}}(t)=0$!) and it has to be understood as a shorthand notation for the expansion of the (Fourier transform of the) leftmost delta in Eq. (5.12), in powers of the γ term. In any case, we have achieved our aim of having a product of k-dependent functions (compare with the integrand in the r.h.s. of Eq. (4.2)). Since the argument of the delta function in Eq. (5.13) is expressed in terms of an advanced (complex conjugate) Green function, we need to locate the retarded part of the DOS in the r.h.s of Eq. (5.13). From Eq. (3.91), we can write

$$d(\mathrm{k})=\frac{1}{2\pi}\lim_{\epsilon\to 0}\left(\mathrm{tr}\mathcal{L}\frac{1}{1-U(\mathrm{k}^+)}+\mathrm{tr}\mathcal{L}\frac{U(\mathrm{k}^+)^\dagger}{1-U(\mathrm{k}^+)^\dagger}\right), \tag{5.14}$$

[4]Simply diagonalizing U, noticing that the γ-factor makes the limit vanish if there is no eigenvalue of U equating unity, and that in the case that there *is* an eigenvalue 1, the eigenvalue matrix becomes a projector onto the corresponding eigenvector.

where we have absorbed the mean DOS into the advanced part of the fluctuating DOS. The first summand in the r.h.s. of Eq. (5.14) will be the only one to contribute to the spectral average. This becomes clear after substituting the *second* summand in Eq. (5.13), giving the term

$$\delta\left(t-2B\bar{l}\gamma\left(\frac{1}{1-e^{-\gamma}U(\mathrm{k})^{\dagger}}\right)_{x,x}\right)\mathrm{tr}\mathcal{L}\frac{U(\mathrm{k}^{+})^{\dagger}}{1-U(\mathrm{k}^{+})^{\dagger}},$$

which does not survive the k-integration. Without loss of generality, we will calculate the spectral average of

$$f_{\mathrm{k}}(t)\equiv\frac{1}{2\pi}\lim_{\gamma,\epsilon\to 0}\delta\left(t-2B\gamma\bar{l}\mathrm{tr}\left(\frac{1}{1-e^{-\gamma}U(\mathrm{k})^{\dagger}}\right)_{x,x}\right)\mathrm{tr}\mathcal{L}\frac{1}{1-U(\mathrm{k}^{+})}. \tag{5.15}$$

5.2.2 The spectral average.

The spectral integration is carried out after expressing Eq. (5.15) through Gaussian super-symmetric averages[5].

The DOS (retarded) part of Eq. (5.15) is readily written as

$$\mathrm{tr}\mathcal{L}\frac{1}{1-U(\mathrm{k}^{+})}=\int d(\psi,\psi^{\dagger})\left(\psi^{\dagger}\mathcal{L}\pi_{\mathrm{b}}\psi\right)\ e^{-\psi^{\dagger}(1-U(\mathrm{k}^{+}))\psi}, \tag{5.16}$$

where we introduce the usual $4B$-dimensional super-vectors $\psi,\psi^{\dagger}$, extend the meaning of the Green function operator as

$$1-U(\mathrm{k})\to\begin{pmatrix}1-U(\mathrm{k}) & 0\\ 0 & 1-U(\mathrm{k})\end{pmatrix}_{\mathrm{bf}}, \tag{5.17}$$

and now define π_{b} as the $4B\times 4B$ projector over the boson-boson sector[6]

Writing the retarded part of $f_{\mathrm{k}}(t)$ in terms of Gaussian super-integrals requires Fourier transforming the Dirac delta in Eq. (5.15), expanding the result[7] in powers of the Green function (i.e. the γ term inside the argument) and writing every such power, separately, as an integral. Crucially, the latter can be done using a simple

[5]We could as well have defined sources, and write Eq. (5.15) as super-determinants to be expressed as Gaussian integrals instead of averages.

[6]In the calculation of the 2-point function, the super-symmetry breaking was "shared" by the numerator and denominator in Eq. (4.5), but for this case we will use only the bosonic part.

[7]Let us remind that this expansion is the *real* meaning of this delta function.

version of the Wick's theorem for (bosonic) Gaussian averages. For the n^{th} term of the expansion we have

$$\left(\left(\frac{1}{1-e^{-\gamma}U(\mathrm{k})^\dagger}\right)_{x,x}\right)^n = \left(\int d(\psi,\psi^\dagger)|\psi_{\mathrm{b},x}|^2 e^{-\psi^\dagger(1-e^{-\gamma}U(\mathrm{k})^\dagger)\psi}\right)^n \tag{5.18}$$

$$= \frac{1}{n!}\int d(\psi,\psi^\dagger)|\psi_{\mathrm{b},x}|^{2n} e^{-\psi^\dagger(1-e^{-\gamma}U(\mathrm{k})^\dagger)\psi}, \tag{5.19}$$

where $\psi_{\mathrm{b},x}$ is the bosonic, x component of the auxiliary ψ-vector[8].

Using Eq. (5.19) in the power expansion of the Dirac delta, we have

$$\delta\left(t - 2B\bar{l}\gamma\left(\frac{1}{1-e^{-\gamma}U(\mathrm{k})^\dagger}\right)_{x,x}\right) = \int_{-\infty}^{\infty} dz e^{2\pi\iota z t}\sum_{n=0}^{\infty}\frac{\left(-4\pi\iota z B\bar{l}\gamma\right)^n}{n!^2}\int d(\psi,\psi^\dagger)|\psi_{\mathrm{b},x}|^{2n}e^{-\psi^\dagger(1-U(\mathrm{k})^\dagger)\psi}. \tag{5.20}$$

Everything is ready now to carry out the spectral average in exactly the same way as it was done in the previous chapter (page 41, equations Eq. (4.9) to Eq. (4.14)). Combining the k-dependent parts of Eq. (5.16) and Eq. (5.20),

$$\lim_{K\to\infty}\frac{\Delta}{K}\int_0^K d\mathrm{k} e^{-\psi_+^\dagger(1-e^{-\gamma}U(\mathrm{k})^\dagger)\psi_+ - \psi_-^\dagger(1-U(\mathrm{k}^+))\psi_-} = \Delta\int d(Z,\tilde{Z})\mathrm{sdet}(1-Z\tilde{Z})e^{-\Psi^\dagger\mathcal{V}_\gamma\Psi}, \tag{5.21}$$

where we introduce

$$\Psi^\dagger\mathcal{V}_\gamma\Psi \equiv \left(\psi_+^\dagger,\psi_-^\dagger\right)\begin{pmatrix}1 & e^{-\gamma/2}\Sigma Z\\ e^{-\gamma/2}\Sigma^\dagger\tilde{Z} & 1\end{pmatrix}\begin{pmatrix}\psi_+\\ \psi_-\end{pmatrix}, \tag{5.22}$$

in advanced/retarded (+/-) blocks. The "Lagrangian" $\Psi^\dagger\mathcal{V}_\gamma\Psi$ now contains interactions between advanced and retarded Ψ-components, and between bosonic and fermionic components as well, therefore the forthcoming integration of the Ψ fields requires some care.

[8]Both in Eq. (5.16) and Eq. (5.19) we make use of $\mathrm{sdet}(1-U(\mathrm{k})) = 1$.

5.2.3 The Gaussian integration.

Recovering the pre-exponential terms appearing in Eq. (5.16) and Eq. (5.19), the first step in the integration will require already an approximation[9]:

$$\int d(\Psi,\Psi^\dagger)\left(\Psi^\dagger\mathcal{L}\pi_{\rm b}\pi_-\Psi\right)|\Psi_{+,{\rm b},x}|^{2n}e^{-\Psi^\dagger\mathcal{V}_\gamma\Psi}\equiv$$
$$\mathrm{sdet}\mathcal{V}_\gamma\int d(\Psi,\Psi^\dagger)\left(\Psi^\dagger\mathcal{L}\pi_{\rm b}\pi_-\Psi\right)e^{-\Psi^\dagger\mathcal{V}_\gamma\Psi}\int d(\Psi,\Psi^\dagger)|\Psi_{+,{\rm b},x}|^{2n}e^{-\Psi^\dagger\mathcal{V}_\gamma\Psi}. \quad (5.23)$$

In applying Wicks theorem[10] to the l.h.s. of Eq. (5.23) we have neglected cross-terms, i.e. pairings of Ψ components that combine advanced *and* retarded components. Falko and Efetov do this as well, and it is in fact a usual step in Efetov's method applied to disordered systems [23]. The argument in that context is that those components correspond to different positions and their average vanishes *in the large size limit*. In our language, two arguments can be constructed which justify Eq. (5.23). The first and main argument is that the scalar product in the integrand of the r.h.s of Eq. (5.23) implies that this integral is actually a sum of $2B$ integrals, while, in contradistinction, the integral that we are neglecting would take the form

$$\int d(\Psi,\Psi^\dagger)\left(\Psi^\dagger\mathcal{L}\pi_{\rm b}\pi_-\Psi\right)|\Psi_{+,{\rm b},x}|^{2}e^{-\Psi^\dagger\mathcal{V}_\gamma\Psi}\int d(\Psi,\Psi^\dagger)|\Psi_{+,{\rm b},x}|^{2(n-1)}e^{-\Psi^\dagger\mathcal{V}_\gamma\Psi}, \quad (5.24)$$

where the *first* integral would, upon applying Wicks theorem again, take the shape of a product proportional to

$$\sum_{a=1}^{2B}\int d(\Psi,\Psi^\dagger)\Psi^\dagger_{-,{\rm b},a}\Psi^2_{+,{\rm b},x}e^{-\Psi^\dagger\mathcal{V}_\gamma\Psi}\int d(\Psi,\Psi^\dagger)\Psi^\dagger_{+,{\rm b},x}\Psi_{-,{\rm b},a}e^{-\Psi^\dagger\mathcal{V}_\gamma\Psi}. \quad (5.25)$$

Despite the sum over the $2B$ arcs, only a number of terms proportional to the degree of the digraph (that is, at most of the order of $\sqrt{B}$ as it would happen in the case of a full digraph) would not vanish, as $\mathcal{V}_\gamma^{-1}$ connects only arcs which coincide in a node. Therefore only arcs connected to the arc $ij\equiv x$ by a single

[9] We introduce here $\pi_\pm$ as projectors over the +/- spaces.

[10] Now, obviously, in the opposite direction as in Eq. (5.19). The sdet factor in the r.h.s. does not equal unity in this case, since $\mathcal{V}_\gamma$ is not super-symmetric.

step will contribute, as can be seen from the typical $+,-$ component[11] of $\mathcal{V}_\gamma^{-1}$:

$$\left(\Sigma Z \frac{1}{1-\Sigma^\dagger \tilde{Z}\Sigma Z}\right)_{ij,ki} = \Sigma_{ij,ki}Z_{ki} + \sum_l \Sigma_{ij,li}Z_{li}\Sigma^\dagger_{li,ik}\tilde{Z}_{ik} + \dots . \tag{5.26}$$

This takes us to a second argument. For the uniform $Z, \tilde{Z}$-configuration, which we call $Y, \tilde{Y}$, there appears a factor $\Sigma_{ij,ik}$ attached to the term Eq. (5.26), which would become $\Sigma \frac{Y}{1-\tilde{Y}Y}$. However, the $+,+$ and $-,-$ terms of V_γ^{-1} become, due to pair-wise cancellation of Σ and $\Sigma^\dagger$, $\frac{Y\tilde{Y}}{1-Y\tilde{Y}}$ and $\frac{\tilde{Y}Y}{1-\tilde{Y}Y}$, losing all dependence on the graph topology. This is relevant because, being $Y, \tilde{Y}$ diagonal in the space of arcs, the $+,-$ and $-,+$ would be subdominant with a term of the order $\Sigma \sim 1/\sqrt{d}$, where d is the typical degree.

To sum up, we have $\sim B$ terms, each with weight ~ 1 in the main term, r.h.s. of Eq. (5.23), against $\sim d \lesssim \sqrt{B}$ terms with weight $\sim \frac{1}{\sqrt{d}}$. Thus Eq. (5.23) is justified and we can continue the process of Gaussian-integrating. We point the reader to the $n!$ that will appear when applying Wicks theorem, now to the second integral in the r.h.s. of Eq. (5.23),

$$\int d(\Psi,\Psi^\dagger)|\Psi_{+,\mathrm{b},x}|^{2n} e^{-\Psi^\dagger \mathcal{V}_\gamma \Psi} = (n!)\mathrm{sdet}\mathcal{V}_\gamma^{n-1}\left(\int d(\Psi,\Psi^\dagger)|\Psi_{+,\mathrm{b},x}|^2 e^{-\Psi^\dagger \mathcal{V}_\gamma \Psi}\right)^n \tag{5.27}$$

$$= n!\mathrm{sdet}\mathcal{V}_\gamma^{-1}\left(\mathcal{V}^{-1}\right)^n_{\mathrm{b},+,x;\mathrm{b},+,x}, \tag{5.28}$$

where[12] $\left(\mathcal{V}^{-1}\right)_{\mathrm{b},+,x;\mathrm{b},+,x}$ denotes the corresponding diagonal component of $\mathcal{V}^{-1}$. The factorial will compensate for the second power in the denominator of the expansion Eq. (5.20), allowing us to formally re-sum the series:

$$\int_{-\infty}^{\infty} dz e^{2\pi\iota t}\sum_{n=0}^{\infty}\frac{\left(-4\pi\iota z B\bar{l}\gamma\right)^n}{n!}\left(\left(\mathcal{V}^{-1}\right)_{+,\mathrm{b},x}\right)^n = \delta\left(t - 2B\bar{l}\gamma\left(\mathcal{V}^{-1}\right)_{\mathrm{b},+,x;\mathrm{b},+,x}\right). \tag{5.29}$$

The first integral in the r.h.s. Eq. (5.23) naturally gives

$$\mathrm{sdet}(\mathcal{V}_\gamma^{-1})\mathrm{str}\mathcal{L}\pi_b\pi_-\mathcal{V}^{-1}, \tag{5.30}$$

[11] See Eq. (4.31).

[12] Outside the super-determinant, we use $\mathcal{V}$ instead on $\mathcal{V}_\gamma$. Although not explicit in the work by Falko and Efetov, this approximation is there as well. It is valid in the limit $B \to \infty$ while $t \sim 1$, because $\mathcal{V}_\gamma^{-1}$ expands as $\mathcal{V}^{-1}$ plus a series of powers of $\gamma\mathcal{V}^{-1}$, and these will become corresponding powers of $\gamma\!\!\!/\frac{t}{\gamma\!\!\!/B}$ upon integration of the non-compact part of the uniform Q-manifold.

so that after the Gaussian integration is completed, we have finally substituted the spectral average by an integral over Efetov's super-space, i.e. $f_{\rm k}(t) \to f_Q(t)$ with $f(t) = \int DQ f_Q(t)$, and we are in the position to write[13]

$$f_Q(t) = \frac{\Delta}{2\pi} \int DQ {\rm sdet} V \mathcal{V}_\gamma^{-1} \left({\rm str} \mathcal{L} \pi_{{\rm b},-} \mathcal{V}^{-1} \right) \delta \left(t - 2B\bar{l}\gamma \left(\mathcal{V}^{-1} \right)_{+,{\rm b},x} \right). \tag{5.31}$$

In order to present a more recognizable form of this functional, we start by noticing that the super-determinant gives rise to the action of the theory, $S \equiv S_{\rm k} + S_\gamma$, with the usual kinetic action, and with[14]

$$\begin{aligned} S_\gamma &= {\rm str} \ln \left(1 + \gamma \frac{\Sigma Z \Sigma^\dagger \tilde{Z}}{1 - \Sigma Z \Sigma^\dagger \tilde{Z}} \right) && (5.32) \\ &= {\rm str} \ln \left(1 + \frac{\gamma}{2} \pi_+ \mathcal{Q} \right) && (5.33) \\ &\approx \frac{\gamma}{4} {\rm str} \Lambda \mathcal{Q}. && (5.34) \end{aligned}$$

Making use of the equation $2\mathcal{V}^{-1} = 1 + \Lambda\mathcal{Q}$, we can as well write

$$\begin{aligned} {\rm str} \mathcal{L} \pi_{{\rm b},+} \mathcal{V}^{-1} &= {\rm str} \mathcal{L} \pi_{{\rm b},-} \frac{1 + \Lambda \mathcal{Q}}{2} && (5.35) \\ &\approx {\rm str} \mathcal{L} \pi_{{\rm b},-} \frac{\Lambda \mathcal{Q}}{2} && (5.36) \\ &\approx \frac{\bar{l}}{2} {\rm str} \pi_{{\rm b},-} \Lambda \mathcal{Q}, && (5.37) \end{aligned}$$

where in Eq. (5.36) we use our prior knowledge of the fact the the 0-mode Q-integration will have a non-compact component which will make the identity matrix irrelevant, and in Eq. (5.37) we are neglecting bond lengths fluctuations, as we are not interested in their effect. The argument of the Dirac delta is treated similarly, and as a result we write

$$f_Q(t) = \frac{\Delta \bar{l}}{4\pi} \int DQ \ {\rm str} \ \pi_{{\rm b},-} \Lambda \mathcal{Q} \ \delta \left(t - B\bar{l}\gamma \left(\Lambda \mathcal{Q} \right)_{+,{\rm b},x} \right) e^{-S_{\rm k} - S_\gamma}. \tag{5.38}$$

[13] The ${\rm sdet}\mathcal{V}_\gamma$ cancel leaving finally a single negative power.

[14] The equation Eq. (5.33) is exact, as $e^{-\gamma} \equiv 1 - \gamma$ can be done anytime. The equation Eq. (5.34) relies on our present knowledge of the fact that γ terms will be substitute by $\sim t/B$ terms upon integration of the mean field part of the Q-manifold, and that $B \to \infty$ while t is finite.

5.3 Universal limit

5.3.1 Mode separation

We define the 0-mode sub-manifold, Q_0, as one which takes uniformly the value that the original Q-manifold takes on the arc x, i.e.

$$(Q_0)_{ij} \equiv Q_x, \tag{5.39}$$

and perform the change of variables $Q \to Q_0, \tilde{Q}$, with

$$Q \equiv T_0 \tilde{Q} \bar{T}_0, \tag{5.40}$$

where T and V matrices are related through

$$T \equiv V \cdot \begin{pmatrix} 1/\sqrt{1 - Z\tilde{Z}} & 0 \\ 0 & 1/\sqrt{1 - \tilde{Z}Z} \end{pmatrix}. \tag{5.41}$$

The condition

$$\tilde{Q}_x \equiv \Lambda, \tag{5.42}$$

prevents the number of degrees of freedom from increasing by 1. In terms of matrices $Y, \tilde{Y}$ and $W, \tilde{W}$ parameterizing Q_0 and $\tilde{Q}$ respectively, this change amounts to

$$Z \equiv \frac{1}{\sqrt{1 - Y\tilde{Y}}} (Y + W) \frac{1}{1 + \tilde{Y}W} \sqrt{1 - \tilde{Y}Y} \tag{5.43}$$

$$\tilde{Z} \equiv \frac{1}{\sqrt{1 - \tilde{Y}Y}} \left(\tilde{Y} + \tilde{W}\right) \frac{1}{1 + Y\tilde{W}} \sqrt{1 - Y\tilde{Y}}, \tag{5.44}$$

with the condition

$$W_x = \tilde{W}_x = 0, \tag{5.45}$$

where "0" is obviously meant as a 2×2 super-matrix with vanishing elements. Except from boundary anomalies to which we will not pay attention, a linear condition such as Eq. (5.45) produces a Jacobian 1 [5, 39]. With these considerations,

the functional Eq. (5.38) can be written as

$$f_{Q_0,\tilde{Q}}(t) = \\ \frac{\Delta\bar{l}}{4\pi}\int D\tilde{Q}DQ_0 \text{ str } \tilde{Q}_{0,(-\text{b})}\xi\tilde{\mathcal{Q}}\xi^\dagger \ \delta\left(t - B\bar{l}\gamma\left(\tilde{Q}_{0,(+\text{b})}\Lambda\right)_{+,\text{b},x} - c\right)e^{-S_\text{k}-S_\gamma}, \quad (5.46)$$

where we use the notation

$$\tilde{Q}_0 \equiv \bar{T}_0\Lambda T_0, \qquad \tilde{Q}_{0,(\pm\text{b})} \equiv \bar{T}_0\pi_{\text{b},\pm}\Lambda T_0, \quad (5.47)$$

and make use of the fact that the equalities

$$\mathcal{Q} = \mathcal{T}_0\tilde{\mathcal{Q}}\bar{\mathcal{T}}_0 = \xi T_0\xi^\dagger\tilde{\mathcal{Q}}\xi\bar{T}_0\xi^\dagger, \quad (5.48)$$

hold[15]. At this stage of the calculation, and writing the γ-action as

$$S_\gamma = \frac{\gamma}{4}\text{str}\tilde{Q}_0\xi^\dagger\tilde{\mathcal{Q}}\xi, \quad (5.49)$$

we realize that the main difference between our functional and Falko and Efetov's one, is the fact that the argument of the delta function does not loose its dependence on the fluctuating modes. This happens due to the term

$$c \equiv \bar{l}\gamma\left(\tilde{Q}_{0,(+\text{b})}\xi\left(\tilde{\mathcal{Q}} - \Lambda\right)\xi^\dagger\right)_{+,\text{b},x}. \quad (5.50)$$

The reason why the non-zero mode dependence disappears from the delta in the disordered systems functional, while it does not in Eq. (5.46), we believe, is rather deep. It is due to the fact that the integration over a sigma model manifold arises there from a completely different transformation, for which the elimination of certain fast degrees of freedom has to be performed beforehand. This implies that the information relating to very small scales, i.e. scales that would correspond to a single bond in the case of a QG, disappears in the process. The price to pay for the exactness of the method developed in [2], in this case, is the term Eq. (5.50).

The rest of the calculation relies on the fact that *only* the the non-compact part of the *uniform* manifold will compensate for the $\gamma \to 0$ term, which can be justified if only the 0-mode is completely massless, a quite general assumption. However, the influence of the term Eq. (5.50) in the corrections to the 0-mode contribution

[15] $\xi, \xi^\dagger$ can be defined in several ways, for example $\xi = \begin{pmatrix} 1 & 0 \\ 0 & \Sigma \end{pmatrix}$.

would have to be determined a posteriori. Now we will simply infer that, because only the $\sim d$ arcs connected to x enter c, the contribution of it *to the Gaussian correction* is negligible as well, and hence we will ignore it in the next subsection.

5.3.2 0-mode integration

The sigma model manifold is conveniently described using "Efetov's parameterization" [23], according to which we decompose the T_x-matrix as[16]

$$\begin{aligned} T_x = &\begin{pmatrix} 1-2\eta\bar{\eta} & 2\eta & 0 & 0 \\ -2\bar{\eta} & 1-2\bar{\eta}\eta & 0 & 0 \\ 0 & 0 & 1+2\kappa\bar{\kappa} & 2i\kappa \\ 0 & 0 & -2i\bar{\kappa} & 1+2\bar{\kappa}\kappa \end{pmatrix} \begin{pmatrix} e^{i\chi} & 0 & 0 & 0 \\ 0 & e^{i\phi} & 0 & 0 \\ 0 & 0 & 1 & 0 \\ 0 & 0 & 0 & 1 \end{pmatrix} \cdot \\ &\cdot \begin{pmatrix} \sqrt{\frac{1}{2}(\lambda_1+1)} & 0 & \sqrt{\frac{1}{2}(\lambda_1-1)} & 0 \\ 0 & \sqrt{\frac{1}{2}(\lambda+1)} & 0 & i\sqrt{\frac{1}{2}(1-\lambda)} \\ \sqrt{\frac{1}{2}(\lambda_1-1)} & 0 & \sqrt{\frac{1}{2}(\lambda_1+1)} & 0 \\ 0 & i\sqrt{\frac{1}{2}(1-\lambda)} & 0 & \sqrt{\frac{1}{2}(\lambda+1)} \end{pmatrix}, \end{aligned} \tag{5.51}$$

and $\bar{T}_x = T_x^{-1}$ can be calculated knowing that pseudo hermitian conjugation is defined so that

$$\bar{M} \equiv \begin{pmatrix} \sigma_0 & 0 \\ 0 & -\sigma_3 \end{pmatrix} M^\dagger \begin{pmatrix} \sigma_0 & 0 \\ 0 & -\sigma_3 \end{pmatrix}. \tag{5.52}$$

The result is

$$\begin{aligned} \bar{T}_x = &\begin{pmatrix} \sqrt{\frac{1}{2}(\lambda_1+1)} & 0 & -\sqrt{\frac{1}{2}(\lambda_1-1)} & 0 \\ 0 & \sqrt{\frac{1}{2}(\lambda+1)} & 0 & -i\sqrt{\frac{1}{2}(1-\lambda)} \\ -\sqrt{\frac{1}{2}(\lambda_1-1)} & 0 & \sqrt{\frac{1}{2}(\lambda_1+1)} & 0 \\ 0 & -i\sqrt{\frac{1}{2}(1-\lambda)} & 0 & \sqrt{\frac{1}{2}(\lambda+1)} \end{pmatrix} \cdot \\ &\begin{pmatrix} e^{-i\chi} & 0 & 0 & 0 \\ 0 & e^{-i\phi} & 0 & 0 \\ 0 & 0 & 1 & 0 \\ 0 & 0 & 0 & 1 \end{pmatrix} \begin{pmatrix} 1-2\eta\bar{\eta} & -2\eta & 0 & 0 \\ 2\bar{\eta} & 1-2\bar{\eta}\eta & 0 & 0 \\ 0 & 0 & 1+2\kappa\bar{\kappa} & -2i\kappa \\ 0 & 0 & 2i\bar{\kappa} & 1+2\bar{\kappa}\kappa \end{pmatrix}. \end{aligned} \tag{5.53}$$

[16] There are several way of doing this. Ours is dependent on the fact that we use bose-fermi ordering as opposed to fermi-bose, and that we use $\mathrm{str} = \mathrm{tr_b} - \mathrm{tr_f}$ and not the other way around. Also, due to the fact that $\bar{\bar{T}} = T$, the parametrization that interchanges our T and $\bar{T}$ is also valid.

The measure of the integration over Q_0 reads[17]

$$\int dQ_0 = \int_{\chi,\phi=0}^{\chi,\phi=2\pi} \int_{\lambda=-1}^{\lambda=1} \int_{\lambda_1=1}^{\lambda_1=\infty} \frac{1}{2^6\pi^2} \frac{d\lambda d\lambda_1}{(\lambda_1-\lambda)^2} d\chi d\phi \; d\eta d\bar{\eta} \; d\bar{\kappa} d\kappa. \tag{5.54}$$

The integral is done easily taking to account that only terms proportional to λ_1 survive the $\gamma \to 0$ limit, or equivalently the $\lambda_1 \to \infty$ limit (this also applies to the pre-exponential super-trace, as it will be seen below). Under this consideration, using Eq. (5.51) and Eq. (5.53), we have *effectively*

$$\tilde{Q}_0 \equiv \lambda_1 \Lambda \Pi_{\mathrm{b}}, \tag{5.55}$$

$$\tilde{Q}_{0,(+\mathrm{b})} \equiv \frac{\lambda_1}{2}(1-4\eta\bar{\eta})\Lambda\Pi_{\mathrm{b}}, \tag{5.56}$$

$$\tilde{Q}_{0,(+\mathrm{f})} \equiv -2\lambda_1 \kappa\bar{\kappa}\Lambda\Pi_{\mathrm{b}}, \tag{5.57}$$

where, in Eq. (5.55) and Eq. (5.56) we simply applied the limit $\lambda_1 \sim \frac{1}{\gamma} \to \infty$, and defined

$$\Pi_{\mathrm{b}} \equiv \begin{pmatrix} 1 & 0 & 1 & 0 \\ 0 & 0 & 0 & 0 \\ 1 & 0 & 1 & 0 \\ 0 & 0 & 0 & 0 \end{pmatrix}, \tag{5.58}$$

while in Eq. (5.57) we have as well neglected terms *not* proportional to $\kappa\bar{\kappa}$ due to the fact that no other such pair exists in the integrand (and the measure Eq. (5.54) needs a pair like that for the integral not to vanish). The pre-exponential super-trace now reads

$$\mathrm{str}\; \tilde{Q}_{0,(-\mathrm{b})}\xi\tilde{\mathcal{Q}}\xi^\dagger \equiv 2\lambda_1\kappa\bar{\kappa}\; \mathrm{str}\; \Lambda\Pi_{\mathrm{b}}\xi\tilde{\mathcal{Q}}\xi^\dagger, \tag{5.59}$$

while the γ action becomes[18]

$$S_\gamma \equiv \frac{\gamma\lambda_1}{4}\mathrm{str}\Lambda\Pi_{\mathrm{b}}\xi^\dagger\tilde{\mathcal{Q}}\xi, \tag{5.60}$$

[17] The ordering of the anti-commuting differentials is important!

[18] We notice that the Grassmann variables disappear from this term.

and the delta term reduces to

$$\delta\left(t - B\bar{l}\gamma\left(\tilde{Q}_{0,(+\mathrm{b})}\Lambda\right)_{+,\mathrm{b},x} - c\right) \equiv \delta\left(t - B\bar{l}\gamma\frac{\lambda_1}{2}(1-4\eta\bar{\eta})\right) \tag{5.61}$$

$$\equiv 2B\bar{l}\gamma\lambda_1\eta\bar{\eta}\frac{d}{dt}\delta\left(t - \frac{B\bar{l}\gamma}{2}\lambda_1\right) \tag{5.62}$$

$$\equiv 4\lambda_1\eta\bar{\eta}\frac{d}{dt}\delta\left(\lambda_1 - t\frac{2}{B\bar{l}\gamma}\right). \tag{5.63}$$

Above, we have just Fourier transformed the Dirac delta (neglected the c term), expanded *in the Grassmann pair* and used the "trick" of writing the expansion as a derivative of the delta function[19]. The two λ_1 factors in Eq. (5.63) and Eq. (5.59) will compensate the $1/\lambda_1^2$ in the measure, Eq. (5.54), and this ultimately justifies the neglecting of all the *bounded* λ terms: as they would multiply some $1/\lambda_1 \sim \gamma \to 0$ factor left over, their contribution would vanish. Now the integration can be done very easily: the λ integral produces a factor of 2, the angles ϕ, χ, which have disappeared from the integrand produce a $(2\pi)^2$, and the Grassmann integration has to be made with the anti-commutation rules in mind (they produce a global minus sign). As the end result we write

$$f_{\tilde{Q}}(t) = -\frac{\Delta\bar{l}}{4\pi}\mathrm{str}\Lambda\Pi_{\mathrm{b}}\xi^\dagger\tilde{\mathcal{Q}}\xi\frac{d}{dt}e^{-S_{\mathrm{k}}-S_t} \tag{5.64}$$

$$= \frac{\Delta\bar{l}}{4\pi}2B\bar{l}\frac{d^2}{dt^2}e^{-S_{\mathrm{k}}-S_t} \tag{5.65}$$

$$= \frac{\bar{l}}{2}\frac{d^2}{dt^2}e^{-S_{\mathrm{k}}-S_t}, \tag{5.66}$$

with

$$S_t = \frac{t}{2B\bar{l}}\mathrm{str}\Lambda\Pi_{\mathrm{b}}\xi^\dagger\tilde{\mathcal{Q}}\xi. \tag{5.67}$$

The universal result is obtained making $\tilde{Q} = \Lambda$. Since $\mathrm{str}\Lambda\Pi_{\mathrm{b}}\Lambda = 2\cdot 2B$, we have

$$f(t)_{\mathrm{u}} = f(t)_\Lambda = \frac{2}{\bar{l}}e^{-\frac{2}{\bar{l}}t}. \tag{5.68}$$

Expanding the action in $\tilde{\mathcal{Q}} - \Lambda$, up to second order in $Z, \tilde{Z}$,

$$S_{\mathrm{k}}^{(2)} + S_t^{(2)} = \mathrm{str}\left(SZS^\dagger\tilde{Z} - Z\tilde{Z} + \frac{t}{2B\bar{l}}4\mathrm{str}\pi_{\mathrm{b}}SZS^\dagger\tilde{Z}\right), \tag{5.69}$$

[19] Of course, a single derivative because the terms $(\eta\bar{\eta})^2$ etc vanish.

we can calculate the Gaussian correction to Eq. (5.68):

$$f(t)_{\Lambda,2} = e^{-\frac{2}{l}t} \int d(Z,\tilde{Z}) e^{-\mathrm{str}\vec{\tilde{Z}}(1-F+\frac{2t}{Bl}F\pi_\mathrm{b})\vec{Z}} \tag{5.70}$$

$$= e^{-\frac{2}{l}t} \mathrm{sdet}^2 \frac{1}{1-F-\frac{2t}{Bl}F\pi_\mathrm{b}} \tag{5.71}$$

$$= e^{-\frac{2}{l}t} \left(1 + \frac{4t}{Bl}\mathrm{tr}\frac{F}{1-F} + O\left(\frac{1}{B}\mathrm{tr}\frac{F}{1-F}\right)^2\right). \tag{5.72}$$

Chapter 6

Alternative quantization of digraphs

6.1 Introduction

Kottos and Smilansky approach to quantizing a graph, in [3], consists in solving a Schrödinger equation on the graph. The wave function, with wave number k, on a bond b, takes the form[1]

$$\psi_b(x_b; \mathrm{k}) = a_{b,+} e^{\iota \mathrm{k} x_b} + a_{b,-} e^{-i\mathrm{k}x_b}, \tag{6.1}$$

where $x_b \in [0, l_b]$ is the variable assigned to such bond. The bi-directionality of the wave is clear in Eq. (6.1) as, on the one hand, $a_{b,+}, a_{b,-}$ are complex constants which take specific values, $a_{\mathrm{k}_s;b,+}, a_{\mathrm{k}_s;b,-}$ for specific eigenvalues k_s of the QG, but are in no way restricted to be zero[2], and on the other hand x_b is the variable associated with the bond irrespective of direction. For comparison, the wave traveling through the arc ij, in a QdG, will have the form

$$\psi_{ij}(x_{ij}; \mathrm{k}) = a_{ij} e^{\iota \mathrm{k} x_{ij}} + 0 \cdot e^{-\iota \mathrm{k} x_{ij}}, \tag{6.2}$$

where the restriction in direction has been made explicit in the second term on the r.h.s. If there exists an arc ji (as it is necessary in a *symmetric* digraph), two

[1] We ignore here magnetic fields.

[2] The vanishing of one of the constants would make the wave effectively mono-directional in the bond. This could be the case for some wave number of the spectrum, but it is not true in general.

different functions, of two different variables, will correspond to the antiparallel arcs ij and ji, as shown in the table 6.1.

TABLE 6.1: Nomenclature referring to the unidirectional waves moving across the two anti-parallel arcs connecting the vertices i and j.

arc	variable	range	wave	amplitude
ij	x_{ij}	$[0, l_{ij}]$	$\psi_{ij} = a_{ij}e^{\iota \mathrm{k} x_{ij}}$	a_{ij}
ji	x_{ji}	$[0, l_{ji}]$	$\psi_{ji} = a_{ji}e^{\iota \mathrm{k} x_{ji}}$	a_{ji}

It is convenient to point out here that in the quantum graph literature, and more generally in the treatment of differential operators on graphs, the word *directed* is sometimes used to reflect the fact that not only a "weight" is given to every edge ij, i.e. the length $l_{ij} > 0$, but an *interval* $[a, a + l_{ij}]$ which naturally enthuses ij with the direction $a \to a + l_{ij}$. This is necessary in order to have "well defined first derivatives" [66] on the bonds, but it does *not* restrict the sign of the derivatives a priori. Our use of the word *directed*, in this sense, implies that the sign of $\psi_{ij}(x_{ij})$ is equal to the sign of $\frac{1}{\iota}\psi'_{ij}(x_{ij}) = \mathrm{k}\psi_{ij}(x_{ij})$, as it is obvious from the table above, and unlike in Eq. (6.1), where this sign would depend on the dominant amplitude in the r.h.s. It is possible that general treatments like Carlson's [66, 67] can account for directed graphs in our sense, for example considering pairs of bi-directional edges in the place of our pairs of antiparallel arcs (each edge, of course, with a different length) and enforcing the appropriate direction of the wave (that is, the appropriate sign of $\frac{1}{\iota}\psi'$) through appropriate boundary conditions. However, we do not follow this general approach here, as we only aim to find boundary conditions that will allow us to generalize the Robin's boundary conditions employed in [3] and consistently recover Neumann type scattering matrices, Eq. (3.67).

Kottos and Smilansky impose *continuity* of the wave function *at the nodes*. This means that, if two bonds b and b' are connected to the same vertex v, and, for example $x_b = l_b$ and $x_{b'} = l_{b'}$ at this vertex, then[3]

$$\psi_b(l_b; \mathrm{k}) = \psi_{b'}(l_{b'}; \mathrm{k}). \tag{6.3}$$

The condition Eq. (6.3) guarantees that $\psi_b(x_b; \mathrm{k})$ takes a *unique* value across the network domain, including at the nodes. Imposing current conservation at the

[3]Obviously, if at the vertex v, $x_b = l_b$ and $x_{b'} = 0$ then $\psi_b(l_b; \mathrm{k}) = \psi_{b'}(0; \mathrm{k})$, etc.

nodes (see subsections 6.2.1 and 6.2.3 for the essentially identical case of the QdG) the authors are able to find the secular equation Eq. (3.78), in which the unitary vertex scattering matrices (see equations Eq. (3.64) to Eq. (3.70)) take the form, in the vertex i,

$$\sigma^{i}_{c_{\text{out}}c_{\text{in}}} \equiv \frac{2}{d^i - \frac{\lambda_i}{\imath \mathrm{k}}} - \delta_{c_{\text{in}}c_{\text{out}}}, \tag{6.4}$$

where λ_i is a positive definite constant that parameterizes the range of possible boundary conditions from Neumann b.c. ($\lambda_i = 0$) to Dirichlet b.c. ($\lambda_i \to \infty$), i.e. the Robin boundary conditions.

We are interested in applying the Neumann b.c. to the symmetric QdG, and nothing prevents us from using Eq. (6.4) directly. The difference from the QG case would simply be that $T(\mathrm{k})_{ij} \neq T(\mathrm{k})_{ji}$ in our case (see Eq. (3.73)). However, imposing continuity for the QG wave functions allows for the derivation of a secular equation different from Eq. (3.78), an equation of the form

$$\det H(\mathrm{k}) = 0, \tag{6.5}$$

where H is a $V \times V$ (as opposed to the much larger $2B \times 2B$ dimensionality of $U(\mathrm{k})$) Hermitian matrix which is better suited for numerical generation of the spectrum. The question then arises whether there exists an equation analogous to Eq. (6.5) for symmetric digraphs with Robin-like scattering matrices, Eq. (6.4), and what the conditions on the directed waves (table 6.1) would be that would allow us to derive such an equation. To this question we turn in section 6.2, where we define what we call *pseudo-continuity* on symmetric QdG, from which we derive an equation of the type Eq. (6.5) which will be the base of the numerical calculations shown in the chapter 7, and re-derive the equation Eq. (3.78) (with Eq. (6.4)).

6.2 Robin boundary conditions for digraphs

6.2.1 Pseudo-continuity and current conservation

The uniqueness of the wave function in a QG is a natural requirement, because $|\psi_b(x_b)|^2$ is interpreted as the probability density distribution representing (considering the QG as a Schrödinger operator on a graph) the likelihood of measuring

the position of an electron in the network and finding it to be x_b, in the bond b[4]. For this reason it is usual to impose Eq. (6.3) and to define ϕ_i as the value taken at the vertex i by the wave function, no matter from which bond (connected to i) we are accessing the vertex.

The situation is not so clear for the digraph. Keeping in mind the notation in the table 6.1 from now on, $|\psi_{ij}(x_{ij})|^2$ would represent the probability density related to finding the electron in x_{ij}, and *and moving from i to j*, hence imposing $|\psi_{ij}(0)| = |\psi_{ik}(0)| = |\psi_{li}(l_{li})| = \dots$ for all $j, k, l, \dots$ connected to i would imply that the events of the electron being located in i and moving towards j, or located in i and moving towards k, and the event of "entering" i from the arc li, etc need to be equally probable. This seems to be too restrictive an unnatural. For the case of a *symmetric* digraph, however, the "trick" of generalizing Eq. (6.3) by coupling antiparallel arcs and considering the sum of the values of their respective wave functions at the two ends will prove useful below.

We define the *pseudo*-continuity (or pseudo-uniqueness) as the property of the QdG wave function that holds under the condition

$$\begin{aligned} \phi_i =& \psi_{ij}(x_{ij} = 0; \mathrm{k}) + \psi_{ji}(x_{ji} = l_{ji}; \mathrm{k}) && (6.6)\\ =& a_{ij} + a_{ji} e^{\iota \mathrm{k} l_{ji}} \quad \text{for all } j \text{ connected to } i, && (6.7) \end{aligned}$$

where for Eq. (6.7) one needs to apply the definitions in the table. To every node i, then, correspond $d^i - 1$ independent equations, arising from the application of Eq. (6.7) to every two pairs of anti-parallel arcs that connect through i:

$$\begin{aligned} a_{ij_1} + a_{j_1 i} e^{\iota \mathrm{k} l_{j_1 i}} =& a_{ij_2} + a_{j_2 i} e^{\iota \mathrm{k} l_{j_2 i}} && (6.8)\\ =& a_{ij_3} + a_{j_3 i} e^{\iota \mathrm{k} l_{j_3 i}} && (6.9)\\ & \dots && (6.10)\\ =& a_{ij_{d^i}} + a_{j_{d^i} i} e^{\iota \mathrm{k} l_{j_{d^i} i}}. && (6.11) \end{aligned}$$

[4]It is natural, but not necessary. Arbitrary vertex propagators can be used, as in chapter 3, for graphs or digraphs, for which the eigenfunctions are not unique (hence not defined) at the vertices. The position of the electron can only be measured up to some degree of accuracy, hence only the probability of finding the electron in a small region around a node is relevant, not at the node itself. And such probability is calculated integrating $|\psi|^2$ over that region without the discontinuity at the node posing any problem.

Hence we have a total of $\sum_{i=1}^{V}(d_i-1)$ equations to be imposed on the $2B$ wave amplitudes. This leaves us with

$$2B-\sum_{i=1}^{V}(d_i-1)=\sum_{i=1}^{V}d_i-\sum_{i=1}^{V}(d_i-1) \tag{6.12}$$

$$=V, \tag{6.13}$$

degrees of freedom : $\phi_1,\phi_2,\ldots,\phi_V$ (exactly as in QGs [4]). In terms of these, the wave amplitudes are

$$a_{ij}=\frac{\phi_i-\phi_j e^{\iota \mathrm{k}(l_{ij}^+-l_{ij}^-)}}{1-e^{2\iota \mathrm{k} l_{ij}^+}}, \tag{6.14}$$

where we have just defined

$$l_{ij}^+\equiv\frac{l_{ij}+l_{ji}}{2}, \tag{6.15}$$

$$l_{ij}^-\equiv\frac{l_{ij}-l_{ji}}{2}. \tag{6.16}$$

We impose now "current conservation". Around the node i, this condition reads

$$\frac{\lambda_i\phi_i}{\iota \mathrm{k}}=\frac{1}{\iota \mathrm{k}}\sum_j\left(\frac{d}{dx_{ij}}\psi_{ij}(x_{ij}=0)-\frac{d}{dx_{ji}}\psi_{ji}(x_{ji}=l_{ji})\right) \tag{6.17}$$

$$=\sum_j\left(a_{ij}-a_{ji}e^{\iota \mathrm{k}(l_{ij}^+-l_{ij}^-)}\right) \tag{6.18}$$

$$=\sum_j\left(\frac{\phi_i-\phi_j e^{\iota \mathrm{k}(l_{ij}^+-l_{ij}^-)}}{1-e^{2\iota \mathrm{k} l_{ij}^+}}-\frac{\phi_j-\phi_i e^{\iota \mathrm{k}(l_{ij}^++l_{ij}^-)}}{1-e^{2\iota \mathrm{k} l_{ij}^+}}e^{\iota \mathrm{k}(l_{ij}^+-l_{ij}^-)}\right) \tag{6.19}$$

where the sum involves all vertices connected to i, and where λ_i is the constant mentioned in the introduction, 6.1, parameterizing the family of Robin b.c. Depending on whether one applies Eq. (6.19) directly, or expresses it in terms of the wave amplitudes using Eq. (6.7), one can derive, respectively, the secular equations Eq. (3.78) and Eq. (6.5).

6.2.2 Vertex secular equation

Re-arranging the sum in Eq. (6.19) so as to separate the "fixed" i term, we have

$$0 = \phi_i \left(\frac{-\lambda_i}{\iota \mathrm{k}} + \sum_j \frac{1 + e^{2\iota \mathrm{k} l_{ij}^+}}{1 - e^{2\iota \mathrm{k} l_{ij}^+}} \right) + \sum_j \phi_j \frac{-2e^{\iota \mathrm{k} l_{ij}^+ - \iota \mathrm{k} l_{ij}^-}}{1 - e^{2\iota \mathrm{k} l_{ij}^+}} \tag{6.20}$$

$$= \phi_i \left(\frac{-\lambda_i}{\iota \mathrm{k}} + \iota \sum_j \cot \mathrm{k} l_{ij}^+ \right) + \sum_j \phi_j \left(-\iota \frac{\cos \mathrm{k} l_{ij}^-}{\sin \mathrm{k} l_{ij}^+} - \frac{\sin \mathrm{k} l_{ij}^-}{\sin \mathrm{k} l_{ij}^+} \right) \tag{6.21}$$

The V linear equations such as Eq. (6.21) can be solved if

$$\det H(k) = 0, \tag{6.22}$$

where the *complex* hermitian matrix H is defined as

$$H_{ij} = \delta_{ij} \left(\frac{\lambda_i}{\mathrm{k}} + \sum_{j'} \cot \mathrm{k} l_{ij'}^+ \right) + (1 - \delta_{ij}) \left(-\frac{\cos \mathrm{k} l_{ij}^-}{\sin \mathrm{k} l_{ij}^+} + \iota \frac{\sin \mathrm{k} l_{ij}^-}{\sin \mathrm{k} l_{ij}^+} \right). \tag{6.23}$$

The matrix $H(\mathrm{k})$ together with the equation Eq. (6.22) generalize Kottos and Smilansky *vertex secular equation*, which can be recovered re-imposing $l_{ij} = l_{ji}$ (thus $l_{ij}^+ = l_{ij}$ and $l_{ij}^- = 0$). We will use this result in the chapter 5 in order to generate the spectrum of full Neumann digraphs.

6.2.3 The quantum map $U(\mathrm{k})$

Our aim is to derive now Eq. (3.78) with Robin-like scattering matrices, Eq. (6.4). We start from Eq. (6.18):

$$\frac{\lambda_i}{\iota \mathrm{k}} \phi_i = \sum_j a_{ij} - \sum_j a_{ji} e^{\iota \mathrm{k} l_{ji}} \tag{6.24}$$

$$= \sum_j \left(\phi_i - a_{ji} e^{\iota \mathrm{k} l_{ji}} \right) - \sum_j a_{ji} e^{\iota \mathrm{k} l_{ji}} \tag{6.25}$$

$$= d^i \phi_i - 2 \sum_j a_{ji} e^{\iota \mathrm{k} l_{ji}}. \tag{6.26}$$

The idea is to write the amplitudes outgoing from i in terms of the amplitudes incoming to that vertex; for that purpose, we choose any node k connected to i,

and use continuity Eq. (6.7) in order to substitute for ϕ_i in Eq. (6.26),

$$a_{ik} = \frac{1}{d^i} \frac{2}{1 - \frac{\lambda_i}{\iota \mathrm{k}}} \sum_j e^{\iota \mathrm{k} l_{ji}} a_{ji} - e^{\iota \mathrm{k} l_{ki}} a_{ki}. \tag{6.27}$$

We can then write, for a vertex i,

$$a_{ik} = \sum_j \sigma^i_{c_{\mathrm{out}}(k) c_{\mathrm{in}}(j)} e^{\iota \mathrm{k} l_{ji}} a_{ji}, \tag{6.28}$$

with σ^i given by Eq. (6.4).

Re-grouping *all* wave amplitudes in the graph in a single vector, as in section 3.4, we find the stationarity condition Eq. (3.77) and the secular equation Eq. (3.78).

Chapter 7

Numerical experiments on large, full Neumann digraphs

7.1 Introduction

It is known (see for example [41] or [68]), that in order to extract any conclusion, through numerical calculations, on the large-size spectral-statistical behaviour of the FNG, one needs to consider graphs of around 30 vertices an beyond. The size must be much larger than the 5-vertex graphs considered, for example, in [4]. Results for such small graphs are quite misleading because their "good behaviour", i.e. their spectral statistics showing already strong similarity to Gaussian RMT ensembles, can induce one to believe that the larger graphs will be even better behaved (as this is what usually happens, and as we expect universal behaviour in the $B \to \infty$ limit) and not worth checking. The curves representing the spectral statistics of *bigger* graphs are actually *further away* from the RMT curves, before starting to converge to (or, at least, approach) universality again as we increase the size beyond a certain point. The situation is not different for FNQdG (see for example Fig. 7.6(a), where deviations from universality increase moving from the 10 to the 20-vertex graph, to diminish again from 30 vertices onwards).

The method to generate the spectrum of the Neumann QdG is identical to the

one used by Kottos and Smilansky ([4])[1], which consists in finding the solutions of the vertex secular equation,

$$\det H(k) = 0, \tag{7.1}$$

where, from Eq. (6.23),

$$H_{ij} = \delta_{ij} \sum_{j'} \cot \mathrm{k} l^{+}_{ij'} + (1 - \delta_{ij}) \left(-\frac{\cos \mathrm{k} l^{-}_{ij}}{\sin \mathrm{k} l^{+}_{ij}} + i \frac{\sin \mathrm{k} l^{-}_{ij}}{\sin \mathrm{k} l^{+}_{ij}} \right) \tag{7.2}$$

The exact equation that one solves, however, reads

$$f(\mathrm{k}) = 0, \quad \text{where} \tag{7.3}$$

$$f(\mathrm{k}) \equiv \prod_{ij} \sin \mathrm{k} l_{ij} \det H(\mathrm{k}). \tag{7.4}$$

The product of sine functions introduced in the r.h.s. of Eq. (7.4) is necessary to compensate for poles in $\det H(\mathrm{k})$, whose presence would not make possible the steps 3 and 4 of the algorithm we explain in the next section (7.2.1).

The large size of the graphs considered in this work posed considerable challenges in minimising the computational effort. The simple approach consisting in discretizing the k-axis according to a *constant*, sufficiently fine mesh, i.e. $\mathrm{k}_0 < \mathrm{k}_0 + \Delta\mathrm{k} < k_0 + 2\Delta\mathrm{k} < \dots$, with $\Delta\mathrm{k}$ being small enough for our purpose, and simply looking for sign changes in f, Eq. (7.4)), becomes unrealistically slow beyond certain size. The algorithm we found to circumvent this problem is the subject of the next section (7.2), but the aim is to *minimize the number of explicit calculations* of $f(\mathrm{k})$, while guaranteing that no zeros are missed and that the actual zeros are determined with adequate accuracy.
Two elements, strongly size-dependent, control the time consumption of obtaining $\det H(\mathrm{k})$, for a given k. One is the calculation of H itself, i.e. the calculation of the trigonometric functions that are applied to each of the $2B$ arc-lengths, which we are calling l generally. This would be extremely time consuming, but it is easily circumvented using basic trigonometry: if we know $\sin \mathrm{k} l$ and $\cos \mathrm{k} l$, we "update" those values to $\mathrm{k} + \Delta\mathrm{k}$ using $\sin(\mathrm{k} + \Delta\mathrm{k}) l = \sin \mathrm{k} l \cos \Delta\mathrm{k} l + \cos \mathrm{k} l \sin \Delta\mathrm{k} l$, etc.

[1] The computational time, however, increases slightly due to a QdG with V vertices having twice the number of bond-lengths as a QG of the same vertex-size. The non-vanishing imaginary parts of the non-diagonal components in H, above, probably also delays the calculations with respect to the analogous, real, matrix in QGs.

The precision, though, has to be kept under control since it is slowly lost at every step. The second "bottleneck", once H is taken care of as just explained, is the calculation of its determinant. Because this is unavoidable, all we can do is find an algorithm that locates and bounds all the zeros of $f(\mathrm{k})$ (in a chosen interval) with as few points,

$$(\mathrm{k}_1, f[\mathrm{k}_1]), (\mathrm{k}_2, f[\mathrm{k}_2]), \ldots, (\mathrm{k}_i, f[\mathrm{k}_i]), \ldots, \tag{7.5}$$

as possible. We generally call a set of coordinates, such as in Eq. (7.5), a "discretisation" [2] of (the graph of) $f(k)$.

The main object which we use to characterize the spectrum[3] is the *(integrated) level spacing distribution* or (i)LSD. For general spectral sequences, we referred to the *level spacing distribution* as $\bar{l}(0; s)$ in Eq. (2.24) page 13 and we commented on its relationship to the 2-point correlation function, Eq. (2.29). For the case of the FNG, an exact analytical expression exists for the LSD [69]. The formula is applicable to systems whose spectrum is given by a secular equation with a quasi-periodic function, and it is suited for graphs with a small number of incommensurate lengths, but for "complex graphs", which the authors of [69] consider to be fully connected Neumann tetrahedrons and pentagons, the formula is not practical. Their *numerical* LSD shows systematic deviations from RMT. The authors note that the deviations are greater for the pentagon, and we know now that they actually increase up to a size where they start decreasing again, probably between 20 and 30 vertices. More recently, the FNG-LSD has been studied as well in [68], in connection with parameter-dependent spectral statistics[4]. The authors show that the *autocorrelation function of level velocities*, for this graph model, is closer to the behaviour predicted by RMT in the 6-vertex case, and then continuously deviates (they work with graphs for up to 30 vertices), and they conjecture a large size limit of this object different than the one predicted by RMT. On the other hand, they find the iLSD to be close to RMT for any graph size. They therefore conclude that the latter magnitude is less affected "by non-universal features of the spectrum and wave functions of the graphs, such as scars...". They also

[2] And we use square brackets when, "[ ]", when referring to the discrete version of f.

[3] However, the data available would allow for other physical quantities as well.

[4] The authors study the statistics of the evolution of the eigen-levels when varying parameters such as bond lengths ("level velocities"). This is a work which relies as well on *ensemble* average, which is an important difference with respect to ours.

study the inverse participation ratio[5], and find a much slower decay then than the $\sim 1/B$ they would expect from the random wave hypothesis. Although they do not mention it, the decay that they obtain seems to be around $1/V$, close to what one would expect according to the results in [41]: taking into account, from 4.4.2.2 or the discussion in page 52, the approximately B eigenvalues of F which are of order $1 - \frac{4}{V}$, simple power counting on Eq. (5.6), page 61 gives a $1/V$.
In our study of the iLSD for the FNdG, we do see an approach towards universality at increasing graph size. Although we cannot conclude that no finite deviations remains at infinite size, a level repulsion corresponding to GUE seems to be present beyond doubt.

In section 7.2 we present a time efficient algorithm to generate the spectrum of large FNdG[6]. In section 7.4 we re-define the LSD in a way that is suitable for its numerical approximation, and the cumulative version, iLSD, and describe the main aspects of the numerical results for these quantities. In section 7.5 we attempt to quantify the decay of the iLSD towards universality as graph-size increases, and we discuss possible explanations for the lack of certainty as to whether the iLSD converges towards RMT-GUE behaviour, or whether it saturates with a small but finite deviation from universality. To finalize, in section 7.6 we describe our finding that the sequences of level spacings seems autocorrelated up to a very long range, a feature that has not been noticed, to the best of our knowledge, in the case of the undirected FNG. If present in the latter model as well, these correlations would, on the one hand, further enlarge the number of non-universal issues of an otherwise "very universal" chaotic model, and on the other hand raise some question about the statistical degree of validity of the previous work done on the subject.

7.2 Algorithm to generate the spectrum of large, full Neumann (di)graphs

7.2.1 A 4-step scheme

It is important to remember that this is intended for *large* graphs, and some of the choices of parameters that are proposed may not be the most suitable for small

[5] And we insist that they use averages other than the spectral average that we use here.
[6] It would equally work for the FNG or other models

samples. In fact, graphs of size up to 20 vertices may be more efficiently dealt with using the "naive", constant interval-grid approach.
The following 4 steps outline the procedure to generate the spectrum (zeros) of $f(k)$.

1. Let $\mathrm{k}_0 < \mathrm{k}_1 < \ldots < \mathrm{k}_{i-1} < \mathrm{k}_i, \mathrm{k}_{i+1} < \ldots < \mathrm{k}_{n-1} < \mathrm{k}_n$ be a "grid" of $n+1$ k-values, such that $[\mathrm{k}_0, \mathrm{k}_n]$ is the interval in the k-axis where we wish to find all the zeros, and such that consecutive k-points are equally spaced by a *rather wide* interval, $\Delta\mathrm{k} = \mathrm{k}_{i+1} - \mathrm{k}_i$. Obviously, $n\Delta\mathrm{k} = \mathrm{k}_n - \mathrm{k}_0$. The **first step** is simply to calculate the table of values $(\mathrm{k}_i, f(\mathrm{k}_i))$ on the grid.
   We have found $\Delta\mathrm{k} = 0.4$ (we refer always to mean level spacing units) to be very effective. It involves only 5 calculations of $f(\mathrm{k})$ for every 2 units, and we (almost) always manage to find all the zeros in the third step that follows.
   As mentioned in the introduction, $H(\mathrm{k}+\Delta\mathrm{k})$ is calculated from $H(\mathrm{k})$ using general "update components", $\sin\Delta\mathrm{k}l, \cos\Delta\mathrm{k}l$, calculated beforehand for every arc length l. An efficient way to control the loss of precision is the following: we start with $H(\mathrm{k}_0)$, which is double precision, and we control the precision of $f(\mathrm{k}_0 + n\Delta\mathrm{k})$ for every step n. When, after a number of steps, m, $f(\mathrm{k}+m\Delta\mathrm{k})$ has been seen to reach a precision as low as single precision, the components of $H(\mathrm{k}+m\Delta\mathrm{k})$ are calculated again at double precision, the corresponding f is re-calculated, $H(\mathrm{k}+(m+1)\Delta\mathrm{k})$ is updated, as usual, from the newly obtained, double precision $H(\mathrm{k}+m\Delta\mathrm{k})$, and the process continues indefinitely.

2. The **second step** consists in counting the number of 2π-periods undergone by the phase, $\Phi(\mathrm{k}) \equiv \arctan f(\mathrm{k})$, running counter-clockwise over a rectangular, complex contour with corners at $\mathrm{k}_0 + 50\iota, \mathrm{k}_0 - 50\iota, \mathrm{k}_n - 50\iota, \mathrm{k}_n + 50\iota$. This number will coincide with the number of zeros in the interval $[\mathrm{k}_0, \mathrm{k}_n]$ (which "cuts the rectangle" in two halves) as f has no poles, and as the spectrum of f *is* the spectrum of a (non-degenerate) self-adjoint operator and hence no zeros outside the real axis are expected.
   The reason for this step is twofold: firstly, not missing any zeros ensures a degree of statistical quality of the set of spacings that we analize (which is convenient in any case, and more so given the fact that the finite, large FNdG deviates only *slightly* form RMT behaviour), and secondly, the known number of zeros that we need to find sets the benchmark for the next step.

This "winding number" calculation is computationally "cheap", because at a "distance" of 50 (imaginary) units from the real axis, $\Phi(\mathrm{k})$ is extremely smooth. In the lower (left to right) and upper (right to left) edges of the contour, $\Phi(\mathrm{k})$ essentially acquires a phase $2\pi(\mathrm{k}_n - \mathrm{k}_0)$ progressively, in a straight line $\Phi(k) \sim \pi \mathrm{k}$, and in practice, taking the lower edge as an example, we find it sufficient to calculate pairs $\Phi(\mathrm{k} - 50\iota), \Phi(\mathrm{k} + 0.01 - 50\iota)$ every 10 units, so as to keep a better control of the slope of Φ. The left and right edges are "where things happen" (where the number of zeros is effectively determined). While close to the extremes of the edge, $\Phi(\mathrm{k})$ is still smooth, it varies much more strongly as we approach the middle section (close to the real axis), and one needs to refine the k-mesh in this region. In practice (this needs to be tested and tuned according to the efficiency), we calculate $\Phi(\mathrm{k})$ every unit from 50ι to 10ι, every 0.1 units from 10ι to 1ι, and every 0.01 units from 1ι to 0[7].

3. The **third step** is the most important one. It consists in calculating "extra" points (i.e. points on top of the original discretisation from the first step) and re-counting the zeros of the discretisation $f[\mathrm{k}]$ (i.e. counting sign changes in the discretization), *until all the zeros (according to the count in the second step) have been localised*. The algorithm to decide where on the k-axis to calculate new data, together with the interval Δk in the first step are tuned to *minimise the total number of calculations* of $f[\mathrm{k}]$ before having localized all the zeros, and it is described in the subsection 7.2.2.

4. The **fourth step** consists in *bounding* the zeros already localised in the previous step, and then giving a final value to such zero through interpolation. We mention the details about this in susbsection 7.2.3.

7.2.2 Choice of the extra points

Let us consider the ordered sequence of wave number values,

$$\mathrm{k}_0 < \mathrm{k}_1 < \ldots < \mathrm{k}_{i-1} < \mathrm{k}_i < \mathrm{k}_{i+1} < \ldots < \mathrm{k}_{n-1} < \mathrm{k}_n,$$

[7]Let us mention that, as one can easily check, $f(\mathrm{k}^*) = f(\mathrm{k})^*$, hence one only needs to count the phase accumulated over the lower, or the upper, half of the contour and multiply by two in order to obtain the total.

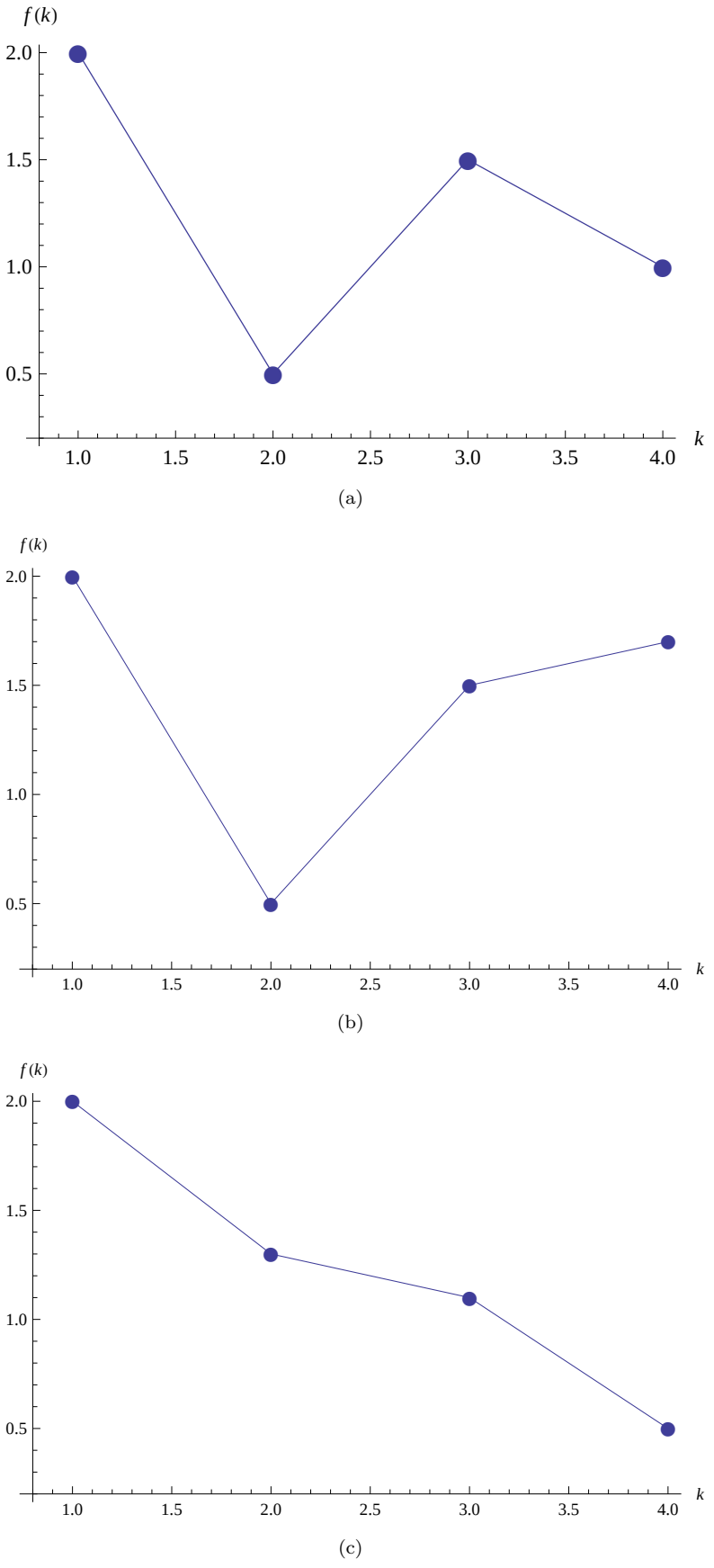

FIGURE 7.1: Three situations where the second derivative of f changes sign *necessarily*, at least once. In (a) and (b), there are also, at least, two and one sign changes in f'. In (c), the derivative could in theory be always negative and no zeros be hidden, but in practice this configuration often does not reflect the true shape of $f(k)$.

for which we dispose of the values $f[\mathrm{k}_0], f[\mathrm{k}_1], \ldots$ of our spectral generating function, $f(\mathrm{k})$. Although the algorithm starts working from a k-sequence, generated by a previous program with a fixed distance $\mathrm{k}_{i+1} - \mathrm{k}_i$, the sequence will change as we insert new data on it in order to find the "missing" zeros. The algorithm decides for which extra value of k to calculate f according to the currently available discretization $(\mathrm{k}_i, f[\mathrm{k}_i])$, therefore $\mathrm{k}_{i+1} - \mathrm{k}_i$ is generally not equal to $\mathrm{k}_{j+1} - \mathrm{k}_j$ for arbitrary $i \neq j$. In order to have an idea of the "smoothness" of any given discretization, we will use *first* and *second discrete derivatives*. We define discrete derivatives of any order n through

$$f^0[\mathrm{k}_i] \equiv f[\mathrm{k}_i], \tag{7.6}$$

$$f^n[\mathrm{k}_i, \mathrm{k}_{i+1}, \ldots, \mathrm{k}_{i+n}] \equiv f^{n-1}[\mathrm{k}_{i+1}, \mathrm{k}_{i+2} \ldots, \mathrm{k}_{i+n}] - f^{n-1}[\mathrm{k}_i, \mathrm{k}_{i+1}, \ldots, \mathrm{k}_{i+n-1}]. \tag{7.7}$$

In the definitions above, the derivatives are not weighted according to any increments in the abscissa, but these are not relevant since we will be only be interested in *sign changes* of derivatives. Let us note that the nth derivative takes $n + 1$ consecutive k values as variable, for example, we need a "triplet" $(f[\mathrm{k}_i], f[\mathrm{k}_{i+1}], f[\mathrm{k}_{i+2}])$ to make up a discrete second derivative, and hence a quadruplet to find a sign-change affecting this derivative (or a "zero of the second discrete derivative", as we may call it). From Eq. (7.7),

$$f'[\mathrm{k}_i, \mathrm{k}_{i+1}] = f[\mathrm{k}_{i+1}] - f[\mathrm{k}_i], \tag{7.8}$$

$$f''[\mathrm{k}_i, \mathrm{k}_{i+1}, \mathrm{k}_{i+2}] = f[\mathrm{k}_{i+2}] - 2f[\mathrm{k}_{i+1}] + f[\mathrm{k}_i], \tag{7.9}$$

$$f'''[\mathrm{k}_i, \mathrm{k}_{i+1}, \mathrm{k}_{i+2}, \mathrm{k}_{i+3}] = f[\mathrm{k}_{i+3}] - 3f[\mathrm{k}_{i+2}] + 3f[\mathrm{k}_{i+1}] - f[\mathrm{k}_i], \tag{7.10}$$

$$\ldots = \ldots, \tag{7.11}$$

$$f^n[\mathrm{k}_i, \ldots, \mathrm{k}_n] = \sum_{m=0}^{n} (-1)^{n+1} \binom{n}{m} f[\mathrm{k}_{i+n-m}]. \tag{7.12}$$

By the Mean Value Theorem, there exists *some* value k, $\mathrm{k}_i < \mathrm{k} < \mathrm{k}_{i+1}$, such that $f'(\mathrm{k}) = f'[\mathrm{k}_i, \mathrm{k}_{i+1}]/(\mathrm{k}_{i+1} - \mathrm{k}_i)$. But let us suppose that the discretization $(\mathrm{k}, f[\mathrm{k}])$ is fine enough so as to reflect the sign of the derivative, i.e. suppose that

$$\operatorname{sgn} f'(\mathrm{k}) = \operatorname{sgn} f'[\mathrm{k}_i, \mathrm{k}_{i+1}] \text{ for all } \mathrm{k}_i < \mathrm{k} < \mathrm{k}_{i+1}. \tag{7.13}$$

Then obviously, since no value of k exists in that interval for which $f'(\mathrm{k}) = 0$, there are no relative extrema and f is bounded by the end points of the interval,

$$f(\mathrm{k}_i) < f(\mathrm{k}) < f(\mathrm{k}_{i+1}) \text{ for all } \mathrm{k}_i < \mathrm{k} < \mathrm{k}_{i+1}, \tag{7.14}$$

which means (we are assuming that Eq. (7.13) holds!) that *a zero of f exists iff* $\operatorname{sgn} f(\mathrm{k}_i) \neq \operatorname{sgn}(f(\mathrm{k}_{i+1}))$ (by the Intermediate Value Theorem), and indeed *only one* zero, since more would break the condition Eq. (7.13) as well. Let us now assume that a "peak" exists in the discretazation, i.e. a point k_i for which $\operatorname{sgn} f'[\mathrm{k}_{i-1}, \mathrm{k}_i] \neq \operatorname{sgn} f'[\mathrm{k}_i, \mathrm{k}_{i+1}]$ (a zero of the first discrete derivative). By application of the Intermediate Value Theorem on the derivative, for some value k_0, with $k_{i-1} < k_0 < k_{i+1}$, we will have $f'(k_0) = 0$, hence the condition Eq. (7.13) cannot be applied (if the minimum is to the left of k_i, for example, then Eq. (7.13) is necessarily violated in the interval $[\mathrm{k}_{i-1}, \mathrm{k}_i]$ and so on). Now, we can still imagine a condition similar to Eq. (7.13), but related to k_0,

$$\operatorname{sgn} f'(\mathrm{k}) = \operatorname{sgn} f'[\mathrm{k}_{i-1}, \mathrm{k}_0] \text{ for all } \mathrm{k}_{i-1} < \mathrm{k} < \mathrm{k}_0 \tag{7.15}$$

$$\operatorname{sgn} f'(\mathrm{k}) = \operatorname{sgn} f'[\mathrm{k}_0, \mathrm{k}_{i+1}] \text{ for all } \mathrm{k}_0 < \mathrm{k} < \mathrm{k}_{i+1}. \tag{7.16}$$

And we would reason as before and say that a zero exists between k_{i-1} and k_0 *iff* $\operatorname{sgn} k_{i-1} \neq \operatorname{sgn} k_0$, and so forth.
The conditions Eq. (7.15), Eq. (7.16) are actually equivalent to stating that, when the condition on the sign of the first derivative, Eq. (7.13), cannot be applied, then we assume that our grid is fine enough so as to reflect the sign of f'':

$$\operatorname{sgn} f''(\mathrm{k}) = \operatorname{sgn} f''[\mathrm{k}_{i-1}, \mathrm{k}_i, \mathrm{k}_{i+1}] \text{ for all } \mathrm{k}_{i-1} < \mathrm{k} < \mathrm{k}_{i+1}. \tag{7.17}$$

Or in other words, the "smooth" f is convex (concave) along the interval $[\mathrm{k}_{i-1}, \mathrm{k}_{i+1}]$ if the peak is pointing downward (upward).
In the same way as it happens with the first derivatives, there are situations where the above condition Eq. (7.17) cannot be applied *a priori*. The most obvious one is a "double peak" such as in Fig. 7.1(a): two discrete extrema in a row. In this case it is clear, anyway, that the discretization fails completely in outlining the shape of f, since the condition on the first derivative fails at least twice and the condition on the second derivative, as we will explain right below, at least once. A more interesting picture is the one in Fig. 7.1(b). Here we could *a priori* postulate that the first condition holds, i.e. that the derivative is positive as

the discrete derivative; but the condition on the second derivative will necessarily fail at least once: since there is a point in $\mathrm{k} \in [\mathrm{k}_i, \mathrm{k}_{i+2}]$ where $\operatorname{sgn} f''(\mathrm{k}) = \operatorname{sgn} f''[\mathrm{k}_i, \mathrm{k}_{i+1}, \mathrm{k}_{i+2}]$ (Mean Value Theorem applied to the second derivative), and another point $\mathrm{k} \in [\mathrm{k}_{i+1}, \mathrm{k}_{i+3}]$ where $\operatorname{sgn} f''(\mathrm{k}) = \operatorname{sgn} f''[\mathrm{k}_{i+1}, \mathrm{k}_{i+2}, \mathrm{k}_{i+3}]$, but at the same time $\operatorname{sgn} f''[\mathrm{k}_i, \mathrm{k}_{i+1}, \mathrm{k}_{i+2}] = -\operatorname{sgn} f''[\mathrm{k}_{i+1}, \mathrm{k}_{i+2}, \mathrm{k}_{i+3}]$, then, for at least one point $\mathrm{k}_0 \in [\mathrm{k}_i, \mathrm{k}_{i+3}]$ we have $f''(\mathrm{k}_0) = 0$ and the condition Eq. (7.17) is violated in the interval where such k-value lies. We have found in practice that where configurations such as this one (Fig. 7.1(b)) appear, often the condition Eq. (7.13) is *also* violated, with $f(\mathrm{k})$ having local extrema, and these often hide missing (pairs of) zeros.

One could keep considering higher order derivatives, but we have found a very effective procedure that relies on discrete derivatives up to second order only, together with heavy use of polynomial interpolation. The main idea behind this method is that polynomial interpolation over an existing grid of data is computationally *much* more efficient than calculating new data (it is, after all, completely unrelated to the graph size). By way of example, let us count how many "points per zero" we had to calculate in a practical case. This refers to the wave number interval [800000,805000] for a graph with 120 vertices. We first obtain f for a grid of constant separation 0.4, this amounts to $0.4^{-1} \times 5000 = 12500$ data points. We then compare the zeros that we find checking sign changes, 4880, with the zeros that we expect from the complex contour integral (second step in the precedent section) $\int \frac{d\Phi(\mathrm{k})}{d\mathrm{k}} d\mathrm{k}$, which turns out to be 5036. The number of data points calculated on the complex contour is rougly 1000. Applying the algorithm that we are showing below, we only need to calculate 81 new data points (!) to find the remaining zeros. In total, less than 14000 data points were needed to locate 5036, which does not even add up to 3 data points per zero. Of course, these zeros are not yet known with enough accuracy: to bound each zero within an interval of length 0.01, we will need roughly (applying the algorithm in the fourth step, which is outlined in the in the subsection 7.2.3) 2 extra points per zero (usually less), which amounts to around 10000 new points. The total cost is therefore close to 5 data points per zero, and we are guaranteed *all the zeros* inside the 5000-length above mentioned interval, and all located within an interval as small as 0.01 mean level spacing units (i.e. the naive constant grid approach would require 100 points per zero for this accuracy). Ultimately, it is this efficiency that justifies the algorithm.

The process of calculating extra data, making use of the second discrete derivative,

is outlined in the following loop, in which i refers to the "current position" in the existing list of wave number values $\mathrm{k}_0 < \ldots < \mathrm{k}_n$:

1. Check for the existence of a zero of $f''[\ ]$, i.e. if $\operatorname{sgn} f''[\mathrm{k}_i, \mathrm{k}_{i+1}, \mathrm{k}_{i+2}] \neq \operatorname{sgn} f''[\mathrm{k}_{i+1}, \mathrm{k}_{i+2}, \mathrm{k}_{i+3}]$ go to 2, else go to 7.

2. Interpolate 9-degree polynomial

$$P(\mathrm{k}; \{\mathrm{k}_{i-3}, \mathrm{k}_{i-2}, \mathrm{k}_{i-1}, \mathrm{k}_i, \mathrm{k}_{i+1}, \mathrm{k}_{i+2}, \mathrm{k}_{i+3}, \mathrm{k}_{i+4}, \mathrm{k}_{i+5}, \mathrm{k}_{i+6}\}),$$

3. Solve $P(\mathrm{k}; \{\mathrm{k}_{i-3}, \ldots, \mathrm{k}_{i+6}\}) = 0$ and count (real) solutions in the interval $[\mathrm{k}_{i-2}, \mathrm{k}_{i+5}]$. If the number of solutions is *greater* than the number of zeros of the discretization $f[\ ]$, go to 4 and return the solutions that *do not match* with zeros of $f[\ ]$, or "extra zeros", i.e. any pair x_1, x_2 such that $P(x_1) = P(x_2) = 0$ and $\mathrm{k}_j < x_1 < x_2 < \mathrm{k}_{j-1}$, with $\operatorname{sgn} f[\mathrm{k}_j] = \operatorname{sgn} f[\mathrm{k}_{j+1}]$[8], else go to 7.

4. Calculate the derivative of the polynomial and solve $P' = 0$. Return the set S of solutions (within $[k_{i-2}, k_{i+5}]$) that happen to lie between two extra zeros selected in the previous step[9].

5. Calculate and *insert* $(x, f[x])$ for every $x \in S$. If $x < k_{i+3}$, go to 6, else go to 7.

6. Select the correct next "position" i, taking into account the new elements in $f[\ ]$, update i and go to 1.

7. Update position, $i \to i + 1$, go to 1.

To test for zeros of the second derivative (step 1) we need and use four points, $\mathrm{k}_i < ... < \mathrm{k}_{i+3}$. If the test is positive and takes us to the step of interpolation (step 2), we take 6 more points (3 to the left of k_i, 3 to the right of k_{i+3}), and we decide whether to keep testing according to what happens within the 8 innermost points (third step), $[\mathrm{k}_{i-2}, \mathrm{k}_{i+5}]$. One simple reason to expand the original quadruplet to 10 points is that it is costless: we are focusing in this area and interpolating *anyway*, so why not then make use of the data that we already have, to obtain a

[8] Or any x_1, x_2, x_3 such that $P(x_1) = P(x_2) = P(x_3) = 0$ and $\mathrm{k}_j < x_1 < x_2 < x_3 < \mathrm{k}_{j+1}$ with $\operatorname{sgn} f[\mathrm{k}_j] \neq \operatorname{sgn} f[\mathrm{k}_{j+1}]$...

[9] Clearly, if the interpolated polynomial has any extra zeros, some extremum must exist between those zeros.

better polynomial?[10]. Another natural reason, also related to the absence of extra cost, is that this polynomial gives us information over a wider range of data for free, and it turns out that extra zeros of the interpolating polynomial, P, are often found in this region outside the original quadruplet.

We do *not* choose *zeros* of P to calculate new values of f, but *extrema* of P that lie between two of its zeros (step 6). As an example, let us have the pair of values $\mathrm{k}_j < \mathrm{k}_{j+1}$ among our original points, such that $\operatorname{sgn} f[\mathrm{k}_j] = \operatorname{sgn} f[\mathrm{k}_{j+1}]$, two "extra zeros", x_1, x_2, of $P(\mathrm{k})$, i.e. $P(x_1) = P(x_2) = 0$, such that $k_j < x_1 < x_2 < k_{j+1}$. We would then calculate the extremum of P, call it x, such that $x_1 < x < x_2$. The reason for this choice is that we do not want, at this stage, to give a good approximation of the zeros of f, but only *locate*, and choosing the extremum of P as the extra point to calculate f, we expect to find $\operatorname{sgn} f[x] \neq \operatorname{sgn} f[\mathrm{k}_j] = \operatorname{sgn} f[\mathrm{k}_{j+1}]$, hence finding two missing zeros in one go. If $f[x]$, on the other hand, is far from $P(x)$, then we can consider that the polynomial interpolation obtained from the data was far from approximating $f(\mathrm{k})$ and the new data was indeed needed (in fact, the addition of the data will force new tests of second discrete derivative). In any case, the choice of extrema to calculate new points is very convenient.

The algorithm is such that after having worked with the last four points in the discretisation, there is no reason to re-check the entire list, because we know beforehand that no new points will be selected for calculation (either because the test in step 1 fails in every group of four points, which is unusual, or because the test in step three fails when the one in step 1 is positive, which is the usual outcome). This feature is due to the step 6, which ensures that all possible configurations which may have being modified with the addition of data points are checked "on the fly"[11].

If zeros are still missing when calculating the new points according to the above criteria, we run an identical test that looks for "peaks" (zeros of $f'[\ ]$):

1. Check for the existence of a zero of $f'[\ ]$, i.e. if $\operatorname{sgn} f'[\mathrm{k}_i, \mathrm{k}_{i+1}] \neq \operatorname{sgn} f'[\mathrm{k}_{i+1}, \mathrm{k}_{i+2}]$ go to 2, else go to 7.

2. Interpolate 9-degree polynomial

$$P(\mathrm{k}; \{\mathrm{k}_{i-3}, \mathrm{k}_{i-2}, \mathrm{k}_{i-1}, \mathrm{k}_i, \mathrm{k}_{i+1}, \mathrm{k}_{i+2}, \mathrm{k}_{i+3}, \mathrm{k}_{i+4}, \mathrm{k}_{i+5}\}),$$

[10]The computing time difference between cubic and ninth polynomial interpolation is insignificant.

[11]A simpler option would consist in updating the position naively (as in step 7) *every time* until the end, and then re-running the algorithm from the beginning when the last. The entire process would finish when no new points were selected after a run

3. Solve $P(\mathrm{k}; \{\mathrm{k}_{i-3}, \ldots, \mathrm{k}_{i+5}\}) = 0$ and count (real) solutions in the interval $[\mathrm{k}_{i-2}, \mathrm{k}_{i+4}]$. If the number of solutions is *greater* than the number of zeros of the discretisation $f[\,]$, go to 4 and return the solutions that *do not match* with zeros of $f[\,]$, (extra zeros), i.e. any pair x_1, x_2 such that $P(x_1) = P(x_2) = 0$ and $\mathrm{k}_j < x_1 < x_2 < \mathrm{k}_{j-1}$, with $\operatorname{sgn} f[\mathrm{k}_j] = \operatorname{sgn} f[\mathrm{k}_{j+1}]$[12], else go to 7.

4. Calculate the derivative of the polynomial and solve $P' = 0$. Return the set S of solutions (within $[k_{i-2}, k_{i+4}]$) that happen to lie between two extra zeros selected in the previous step.

5. Calculate and *insert* $(x, f[x])$ for every $x \in S$. If $x < k_{i+3}$, go to 6, else go to 7.

6. Select the correct next "position" i, taking into account the new elements in $f[\,]$, update i and go to 1.

7. Update position, $i \to i + 1$, go to 1.

If zeros are still missing, and if there are new points in the discretisation coming from testing the first derivative as above, one can rerun a test on the second derivative, and so forth. But this is highly unusual: normally, the second derivative part of the algorithm finds all the zeros.
As a last detail, we mention that a table of update components, $\sin 0.01l, \sin 0.02l$, etc, calculated beforehand, and a way to combine them, are highly useful in order to be able to "jump" from a point to another point of the k-axis (using trigonometry, as in the first of the four steps of the general algorithm -see 7.2.1). The option of calculating $H(\mathrm{k})$ anew, instead of updating it from the last H calculated and stored, is never acceptable due to the computation time.

7.2.3 Bounding the zeros and giving a definite estimate of the spectrum

At this stage, we have a list of data points,

$$\mathrm{k}_0 < \mathrm{k}_1 < \ldots < \mathrm{k}_{i-1} < \mathrm{k}_i < \mathrm{k}_{i+1} < \ldots < \mathrm{k}_{n-1} < \mathrm{k}_n,$$

[12] Or any x_1, x_2, x_3 such that $P(x_1) = P(x_2) = P(x_3) = 0$ and $\mathrm{k}_j < x_1 < x_2 < x_3 < \mathrm{k}_{j+1}$ with $\operatorname{sgn} f[\mathrm{k}_j] \neq \operatorname{sgn} f[\mathrm{k}_{j+1}] \ldots$

such that for every k, $\mathrm{k}_0 < \mathrm{k} < \mathrm{k}_n$, for which $f(\mathrm{k}) = 0$, a pair of consecutive wave numbers $\mathrm{k}_j < \mathrm{k}_{j+1}$ are available such that $\mathrm{k}_j < \mathrm{k} < \mathrm{k}_{j+1}$ and $\operatorname{sgn} f[\mathrm{k}_j] \neq \operatorname{sgn} f[\mathrm{k}_{j+1}]$. To further "zero in" the unknown k, we obtain the cubic interpolation, $P(\mathrm{k})$, over $\mathrm{k}_{j-1} < \mathrm{k}_j < \mathrm{k}_{j+1} < \mathrm{k}_{j+2}$, calculate the solution of $P(\mathrm{k}_s) = 0$ in the interval $[\mathrm{k}_j, \mathrm{k}_{j+1}]$, and calculate $f[\mathrm{k}_s]$. If the sign of $f[\mathrm{k}_s]$ equals the sign of $f[\mathrm{k}]$, we calculate $f[\mathrm{k}_s + 0.01]$, and $f[\mathrm{k}_s + 0.02]$, etc[13], until the sign of f changes to $\operatorname{sgn} f[\mathrm{k}_{j+1}]$. Most usually, the sign changes already after a single step, i.e. $\operatorname{sgn} f[\mathrm{k}_s] \neq \operatorname{sgn} f[\mathrm{k}_s + 0.01]$, very rarely one or two more steps are needed, and often *no* step is needed because an existing data point acts as a bound.

One more detail are worth mentioning. The level of error smearing caused by a 0.01 uncertainty (which highly overestimates the real lack of accuracy of the position of the zeros, anyway) is *extremely* small (we discuss it explicitly in section 7.5). Therefore, a careful study of the error committed if we were to interpolate the zeros directly on the data obtain in the previous step (subsection 7.2.2) could have led us to infer that the bounding of the zeros that we have just explained was really unnecessary. Skipping this step would save us the calculation of (roughly) two data points per zero, hence leaving the total computational time to only 3 data points per zero (see the example in page 90). This is an important consideration regarding efficiency, particularly when dealing with very large graphs[14].

7.3 The data

Our original intention was to generate around a million eigenvalues for the FNdG with 10,20,30,40 and 50 vertices. The slow decay of the cumulative level spacing distribution towards the universal curve (section 7.5), together with the improvements made on the algorithm "along the way" made us generate a similar amount of data for a 60-vertex graph, and explore graphs of over a 100 vertices. The table 7.1 refers to the "small graphs" (10 to 60 vertices); the exact wave number-intervals for which the function $f[\mathrm{k}]$ of the previous section was calculated (and hence for which the spectrum was found) are shown. The table 7.2 refers to graphs of size 100, 120, 140 vertices. The intervals for which f has been calculated in those cases amount to a total of around 100000 or 200000 mls units, depending on the exact

[13] Obviously, if $\operatorname{sgn} f[\mathrm{k}_s] = sgnf[\mathrm{k}_{j+1}$ the loop runs in the opposite direction.

[14] Another point to make is that the procedure outlined here is quite flexible, in the sense that one can always use existing data to improve the accuracy of the zeros *a posteriori*, if needed.

TABLE 7.1: Data generated for small size graphs.

Size (vertices)	k-interval
10	[10000,990000]
20	[10000,990000]
30	[20000,1000000]
40	[10000,900000]
50	[50000,950000]
60	[50000,990000]

graph, *but* they are intended to *span* the same range of wave numbers that we have for the small graphs, i.e. up to around k = 1000000, as can be seen in table 7.2. The reason why we have tried to cover the k-axis over a million mls (apart from the obvious outcome of noise reduction in the 10 to 60 vertices case, where we effectively cover between 900000 and 1000000 mls *in total*), is that unexpected, very long-range, level spacing-to-level spacing correlations appeared, and we have estimated that they are exhausted after the first million (see section 7.6).

TABLE 7.2: Data generated for large graphs.

size (Vertices)	100	120	140
k-intervals	$[60000, 65000]$ $[75000, 80000]$ $[100000, 110000]$ $[135000, 140000]$ $[165000, 170000]$ $[185000, 190000]$ $[205000, 215000]$ $[245000, 255000]$ $[265000, 270000]$ $[300000, 310000]$ $[335000, 340000]$ $[355000, 360000]$ $[380000, 390000]$ $[445000, 450000]$ $[465000, 470000]$ $[500000, 510000]$ $[595000, 605000]$ $[640000, 650000]$ $[690000, 700000]$ $[725000, 730000]$ $[775000, 785000]$ $[805000, 810000]$ $[830000, 835000]$ $[890000, 900000]$ $[925000, 930000]$ $[950000, 955000]$ $[985000, 995000]$	$[100000, 110000]$ $[205000, 215000]$ $[300000, 310000]$ $[380000, 390000]$ $[500000, 510000]$ $[595000, 605000]$ $[690000, 700000]$ $[775000, 785000]$ $[890000, 900000]$ $[985000, 995000]$	$[80000, 85000]$ $[110000, 115000]$ $[165000, 170000]$ $[205000, 210000]$ $[245000, 250000]$ $[320000, 325000]$ $[360000, 365000]$ $[405000, 410000]$ $[450000, 455000]$ $[495000, 500000]$ $[530000, 535000]$ $[570000, 575000]$ $[605000, 610000]$ $[640000, 645000]$ $[710000, 715000]$ $[745000, 750000]$ $[800000, 805000]$ $[875000, 880000]$ $[920000, 925000]$ $[935000, 940000]$ $[990000, 995000]$
total length	195000	100000	105000

7.4 The level spacing probability and its cumulative distribution

From the spectral sequence with $N + 1$ consecutive eigenvalues, corresponding to our V-vertex graphs, we extract and order the N differences between every two consecutive zeros,

$$s_1 \leq s_2 \leq \ldots \leq s_{i-1} \leq s_i \leq s_{i+1} \leq \ldots \leq s_N, \tag{7.18}$$

and define (assuming an arbitrarily large sample) the *level spacing distribution*, LSD, as

$$L_V(s) \equiv \lim_{\Delta s \to 0} \left(\lim_{N \to \infty} L_V(s; \Delta s > 0) \right), \tag{7.19}$$

where

$$L_V(s; \Delta s) \equiv \frac{j - i + 1}{N \Delta s}, \text{ with } s_{i-1} < s - \frac{\Delta s}{s} \leq s_i \leq s_j < s + \frac{\Delta s}{2} \leq s_{j+1}. \tag{7.20}$$

The innermost limit in Eq. (7.19), i.e. $\lim_{N\to\infty} L_V(s; \Delta s)$, represents the *probability that the distance between two consecutive zeros of the FNdG with V vertices lies within* $\left[s - \frac{\Delta s}{2}, s + \frac{\Delta s}{2}\right)$*, divided by the bin length* Δs, the outermost limit producing then a probability density. The double limit converges because the positive integer $j - i + 1$ (in Eq. (7.20)) is proportional to both N and the small, positive "bin length" Δs. On the other hand, the second and third inequalities, together with the fourth, *strict* inequality, in Eq. (7.20) ensure proper counting.

We naturally do not have an infinite sample, and work with the approximated LSD as defined in Eq. (7.20). The numerical values of the LSD are obtained considering bins of length $\Delta s = 0.05$ (always mls units), and no further average is performed. The resulting $L_V(s; 0.05)$, for $V = 10, 20, \ldots$ is compared with the "universal" LSD form the Gaussian Unitary Ensemble , $L_{\mathrm{GUE}}(s)$, which we can express analytically to great accuracy from [50] up to $s \approx 2.3$, and beyond this number we interpolate over tabulated values from Mehta's book ([49]).
Apparent convergence towards universality occurs from $V = 20$ onwards (see Fig. 7.2), although a plot of the deviations (Fig. 7.3(b)), i.e. $L_V(s; 0.05) - L_{\mathrm{GUE}}(s)$, already anticipates the difficulties, at large size and low frequency, that we will find in the next section. Fig. 7.4, on the other hand, shows the 10-vertex graph-LSD to be closer to the GUE-LSD, in the neighborhood of $s \sim 0.5$ and of $s \sim 1.5$, than the larger, 20-vertex graph (in fact, the observation, below, of the cumulative LSD shows the 10-vertex graph to be *globally* closer to universal behaviour than the 20-vertex one). This type of small-size anomaly is known to affect the (undirected) FNG (see for example [68]) and is probably due to the increasing back-scattering amplitude with increasing graph size being the most important mechanism affecting spectral correlations in the small size region. The maximum deviation away from universality probably occurs with a graph with size $V_{\max} \in [10, 20]$, and then from $V_{\max}$ onwards, the increase of the "system dimension", B, takes over as dominant effect. Different quantities, however, may have different behaviours: the

authors in [68] claim, for the time reversal invariant FNG, that the autocorrelation of level velocities moves further away from universal when going from 6-vertex to 30-vertex graphs, and seems to converge to a limiting curve which is not given by the RMT-GOE predictions.

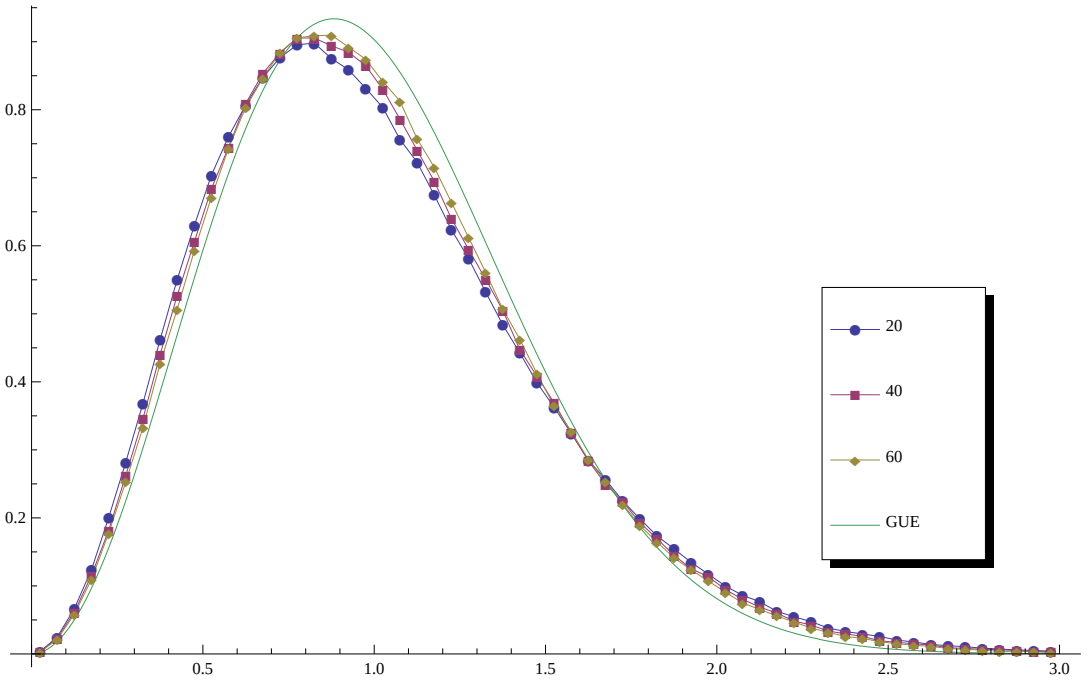

(a)

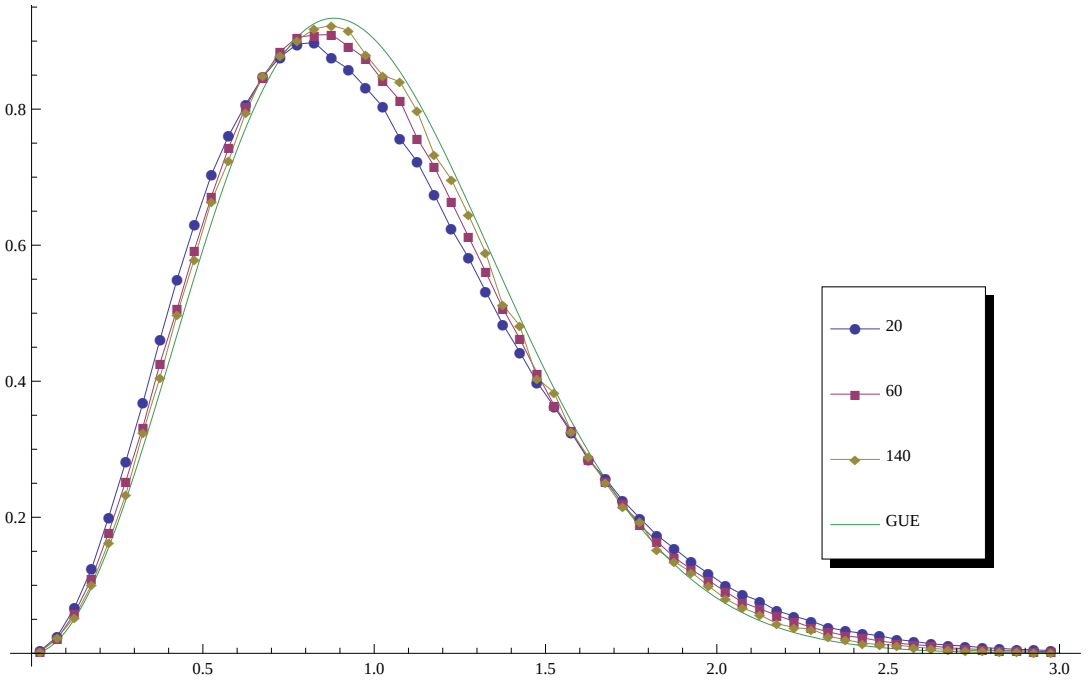

(b)

FIGURE 7.2: Numerical LSD for several graph sizes.

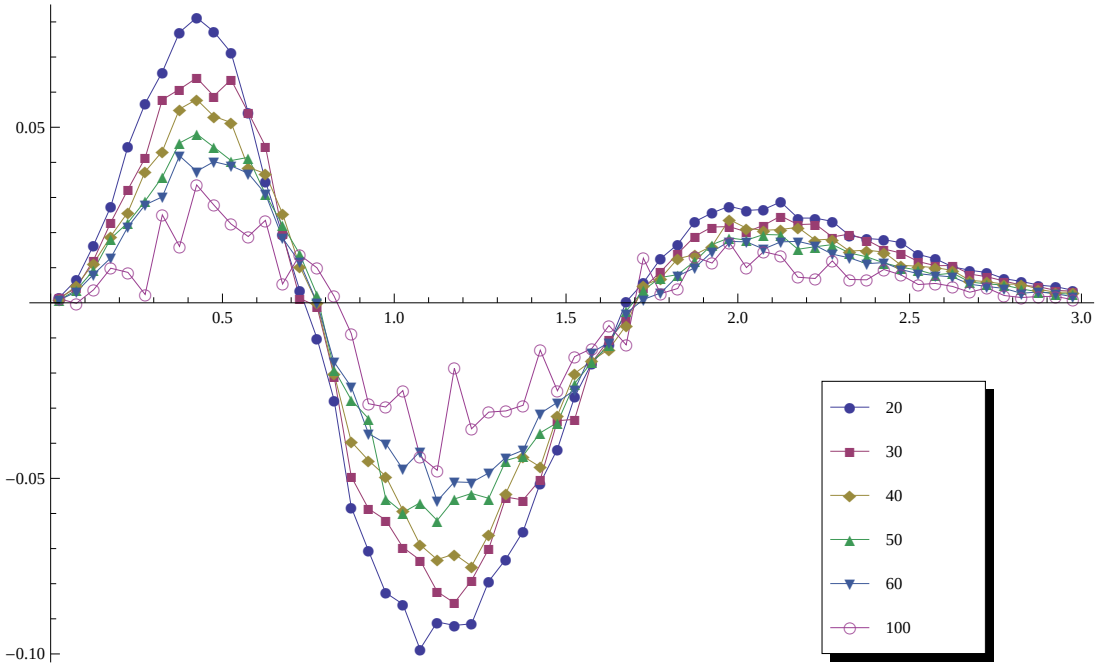

(a)

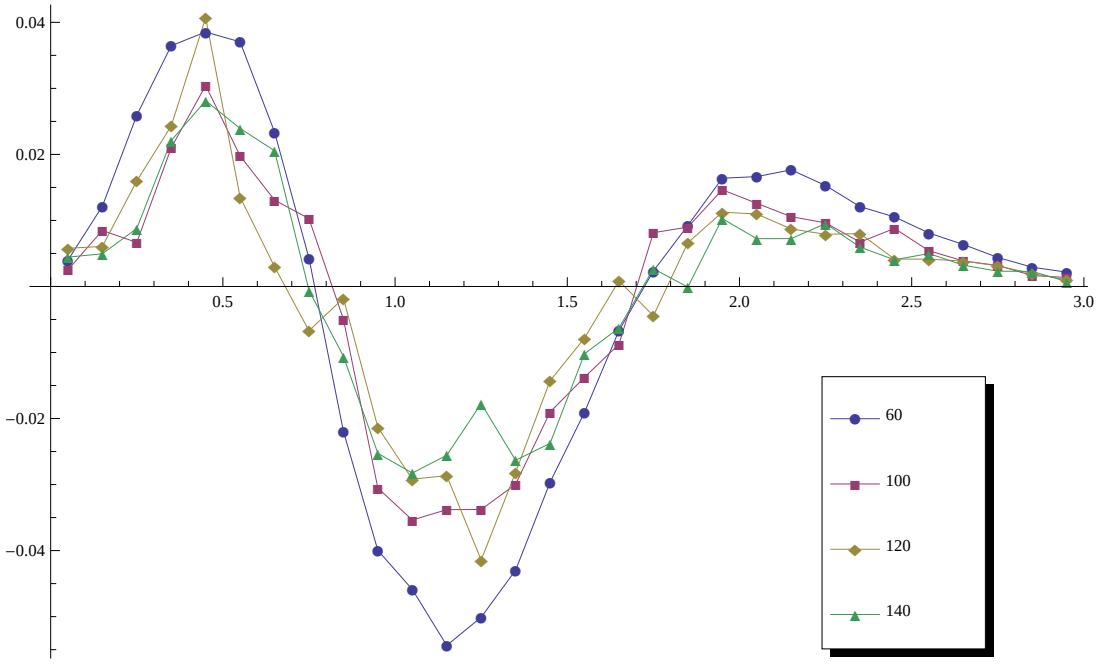

(b)

FIGURE 7.3: LSD deviations from universality, $L_V(s) - L_{\mathrm{GUE}}(s)$ for several graph sizes. In (a), the deviations diminish going from 20 to 100; in (b) the behavior appears not so clear for the three largest graphs.

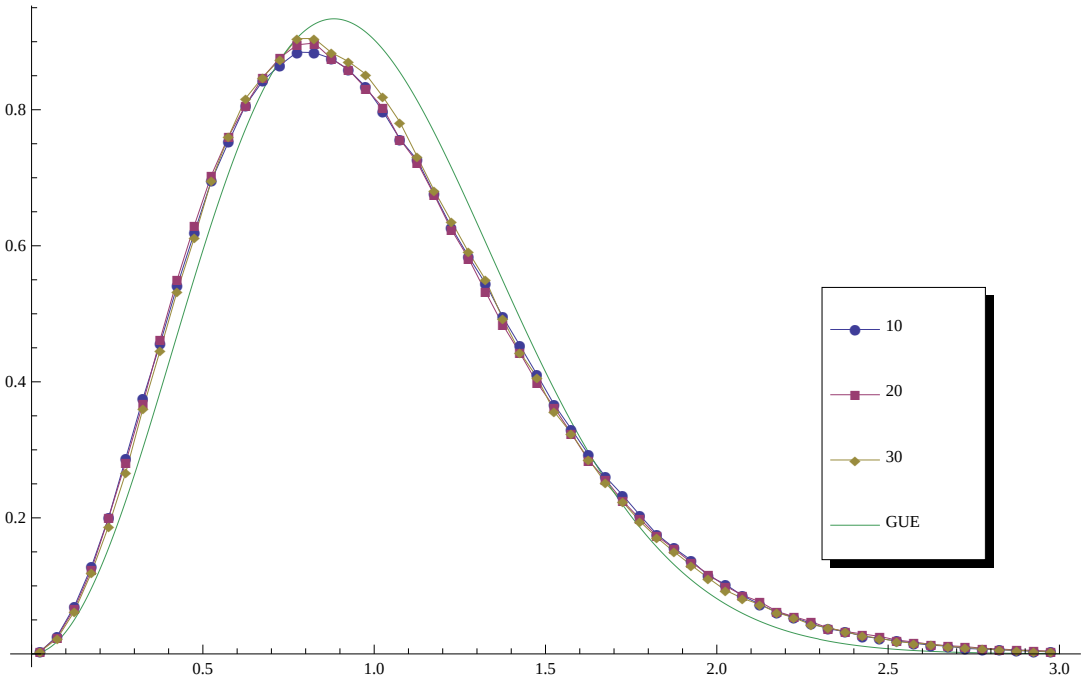

(a)

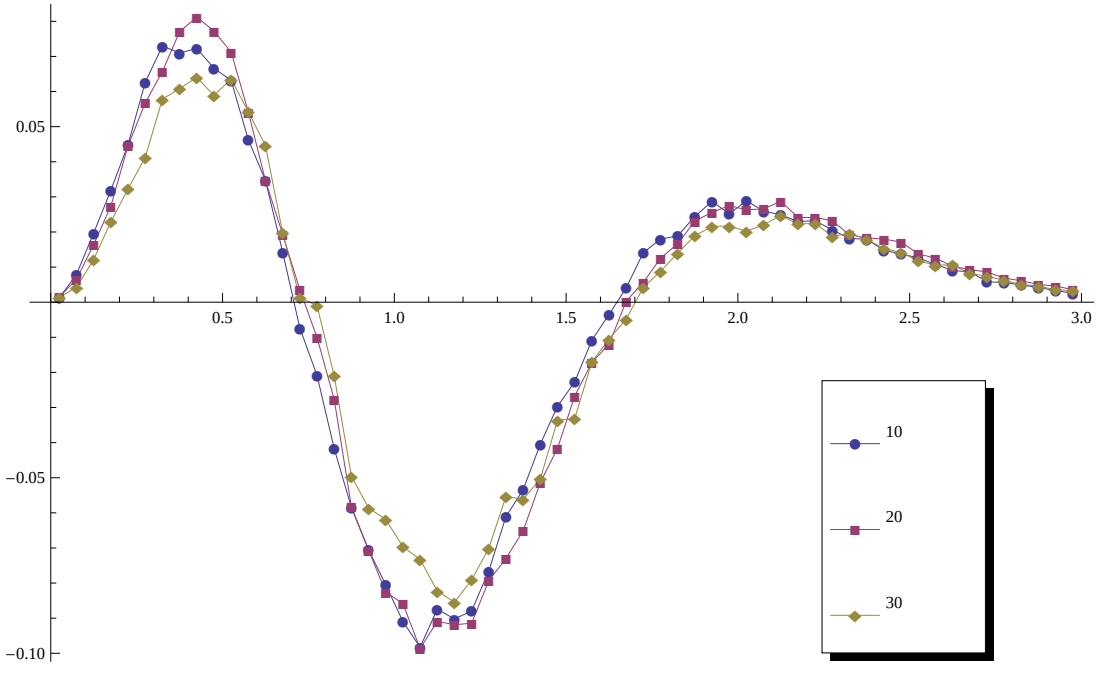

(b)

FIGURE 7.4: The small size effect in the LSD of the FNdG: the smallest graph, 10 vertices, is closer to GUE than the 20-vertex graph in some regions of the spacing axis.

The *integrated level spacing distribution*, ILSD, for the GUE ensemble is the defined as

$$C_{\mathrm{GUE}}(s) \equiv \int_0^s L_{\mathrm{GUE}}(x)dx, \tag{7.21}$$

and represents the probability that the interval between two consecutive eigenvalues of a matrix obtained from the GUE ensemble be in the region $[0, s]$. The cumulative level spacing distribution of the sequence Eq. (7.18), corresponding to a V-vertex digraph, reads

$$C_V(s_i; N) \equiv \frac{i}{N}. \tag{7.22}$$

The ILSD typically smoothes out the noise of the LSD. In Fig. 7.5 we show the iLSD for some of the digraphs, and the GUE-iLSD for comparison. In Fig. 7.6 the square deviations of C_V from C_{GUE} are shown:

$$D_V^2[s_i] \equiv \left(\frac{i}{T} - C_{\mathrm{GUE}}(s_i)\right)^2. \tag{7.23}$$

The noise reduction allows to fully appreciate the anomaly that we mentioned earlier, as $D_{10}^2(s) < D_{20}^2(s)$ almost everywhere in the s-axis. From $V = 20$ to $V = 100$, D_V^2 clearly diminishes, but for the three largest graphs a constant deviation becomes apparent in the region from half to one mls units. We try to give some explanation to this fact in the next section.

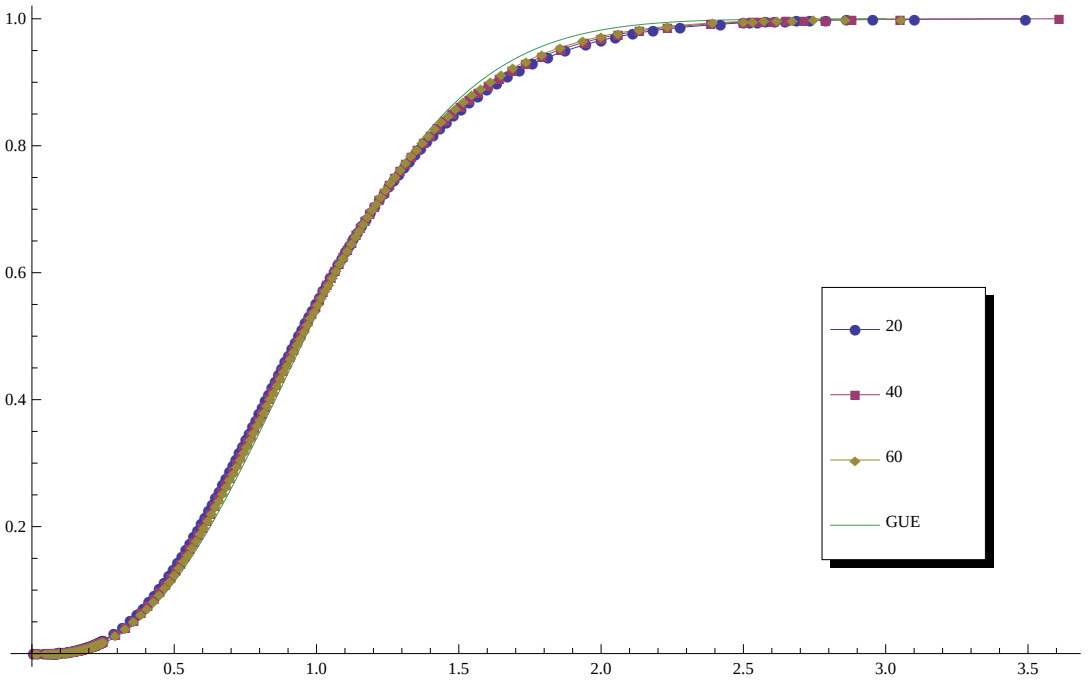

(a)

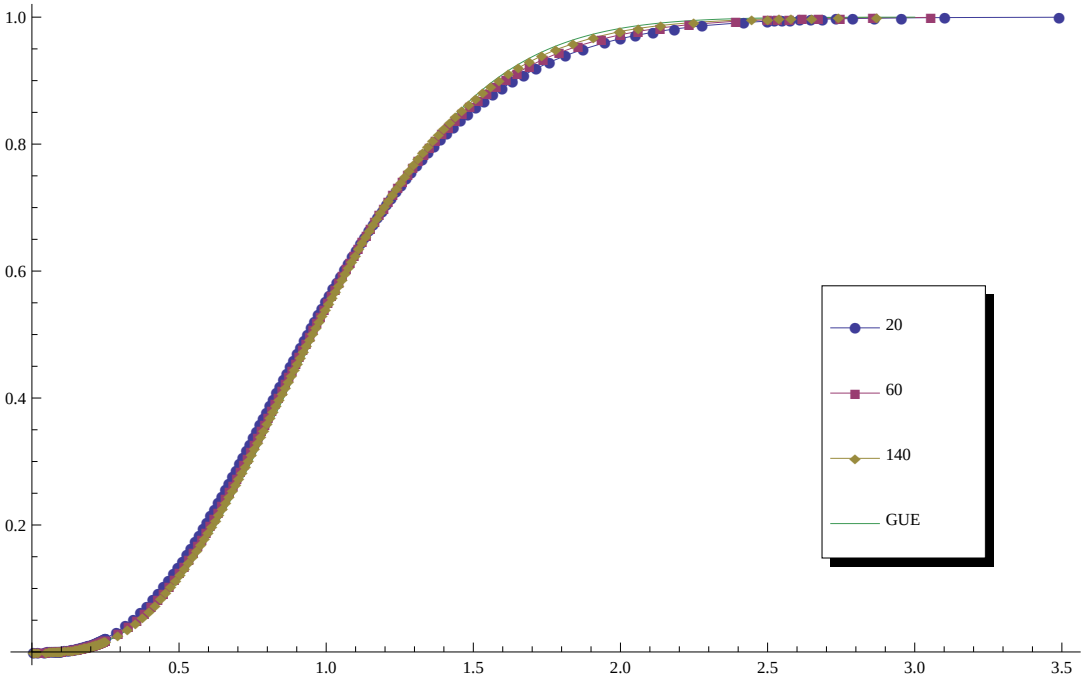

(b)

FIGURE 7.5: iLSD for several graph sizes.

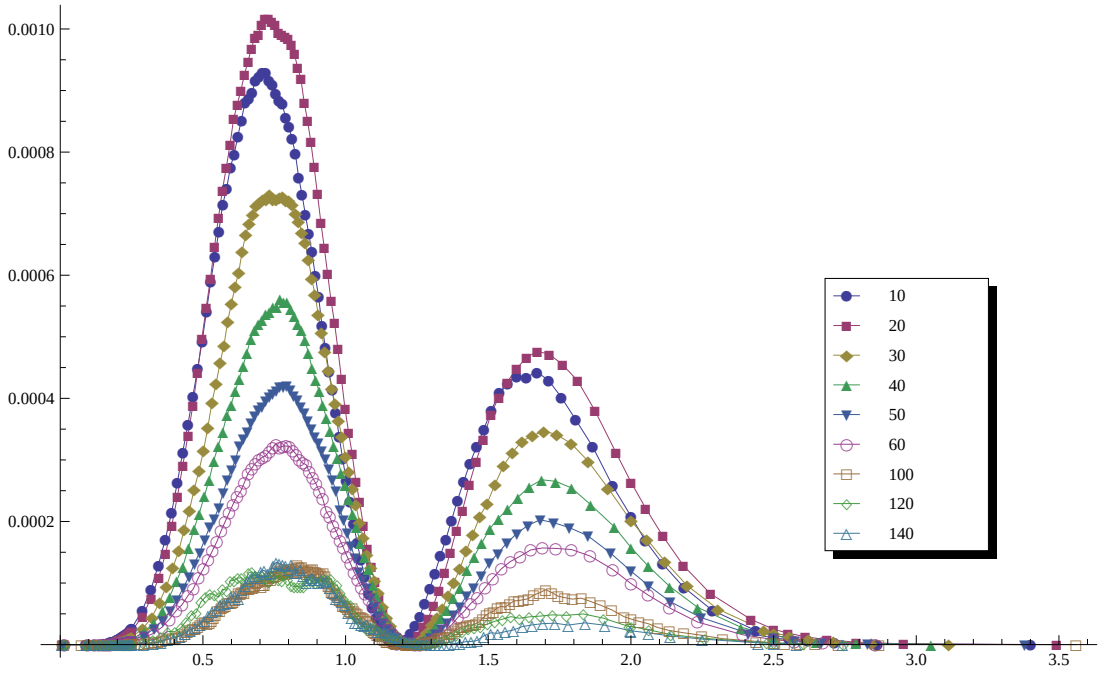

(a)

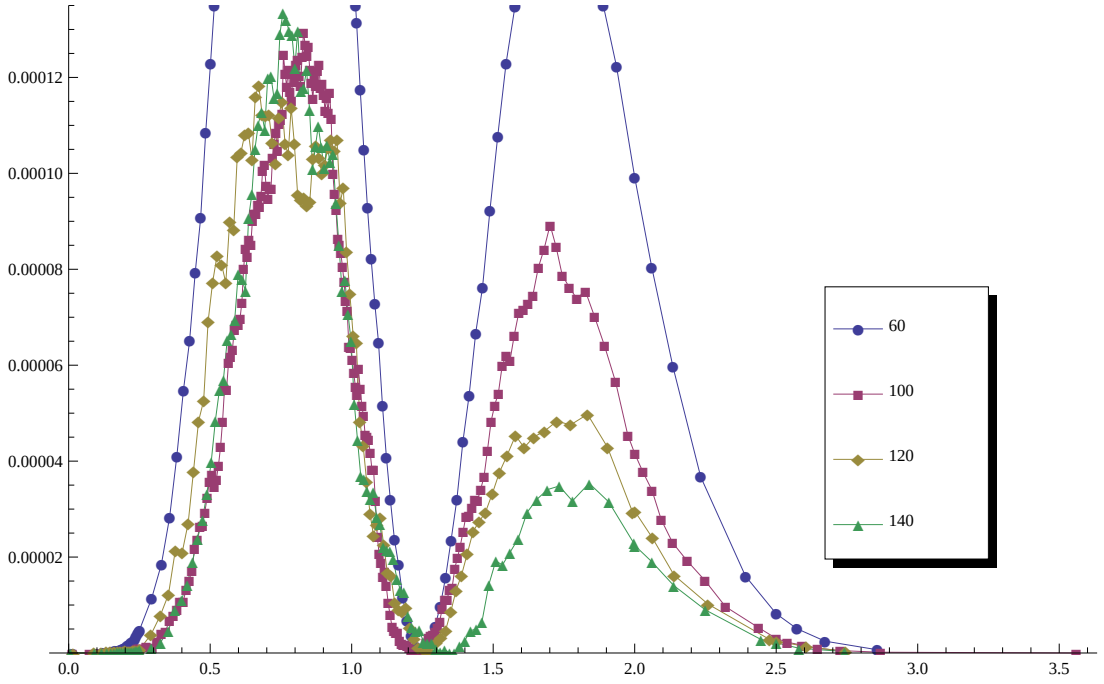

(b)

FIGURE 7.6: In (a), $D_V^2(s)$ for all graphs. In (b), the "collapse" of the deviations at large sizes.

7.5 The decay of the iLSD

We define

$$I(V;s) \equiv \int_0^s D_V^2(x)dx. \tag{7.24}$$

With the data at our disposal, we work with the values of $I(V;3.5)$, which are shown in the table 7.3.

TABLE 7.3: Integrated square deviations of the iLSD.

V	$I(V;3.5)$
10	0.000705568
20	0.000790133
30	0.000566096
40	0.000429932
50	0.000317688
60	0.000250091
100	0.000102912
120	0.0000929369
140	0.0000777149

Fitting a polynomial in powers of $1/V$ to these values produces systematically a negative constant when we allow a term linear in $1/V$ (see Table 7.4), therefore we reject this possibility and try to fit a polynomial with powers not lower than $1/V^2$[15]. The result is in the Table 7.5, where we can see, moreover, that the (now positive) constant term is of the same order as

$$I(100;1.1) = 0.0000545716, \tag{7.25}$$

which is the area under the leftmost "toe" of the curve to which the large graphs seem to collapse, in Fig. 7.3.

[15] we are *not* including the 10-V data point in the fits, since $I(V;3.5)$ increases from $V = 10$ to $V = 20$

TABLE 7.4: Unrestricted polynomial fits resulting in negative constant terms.

1	$\frac{1}{V}$	$\frac{1}{V^2}$	$\frac{1}{V^3}$	sum of square residuals
-0.000040744	0.0173247			4.68702×10^{-9}
-0.000102751	0.0237345	- 0.116208		1.09238×10^{-9}
-0.0000881952	0.0211627		- 1.42886	8.59553×10^{-10}
-0.0000488523	0.0146092	0.280961	- 4.75852	6.31345×10^{-10}

TABLE 7.5: Polynomial fits without $1/V$ term.

1	$\frac{1}{V^2}$	$\frac{1}{V^3}$	$\frac{1}{V^4}$	sum of square residuals
0.000142059	0.290403			4.76657×10^{-8}
0.0000414796	0.892612	-11.89868		1.73883×10^{-9}
0.0000577567	0.647465		-142.546	3.47979×10^{-9}
0.0000129266	1.36532	-35.6529	291.246	3.29711×10^{-10}

Of course, these fits far from conclusive. The two highest order terms of the curves fitted (see Table 7.5), i.e. the constant and the $1/V^2$ term, are of the same order when one substitutes $V = 100, 120 \ldots$, indicating that one would need even larger graphs to confirm this constant as the dominant term. We will later point out other sources for the origine of this constant term.

In the Table 7.6 we show results of curve fitting where we have *imposed* no constant term and no $1/V$ term. In this case, the lowest order term, $1/V^2$, seems to be dominant by a factor of ten over the higher terms, when applied to $V \approx 100$, suggesting that, if the constant term that appears in Table 7.5 (or Eq. (7.25)) is an artifact, the iLSD converges to universality at a rate of $1/V$ (taking into account that we are measuring *square* deviations).

TABLE 7.6: Polynomial fits with no constant nor first order term.

$\frac{1}{V^2}$	$\frac{1}{V^3}$	$\frac{1}{V^4}$	sum of square residuals
0.38012			1.43674×10^{-7}
1.03249	-14.4095		5.73578×10^{-9}
0.774172		-184.88	1.24703×10^{-8}
1.50663	-42.153	366.849	4.9531×10^{-10}

In order to try to justify the appearance of the finite discrepancy, $I(100; 1.1) = 0.0000545716$, as an artifact, we will pose and discuss three arguments :

1. The systematic error in the positioning of the zeros, and hence in the measurements of the level spacings. If we assume that $C_\infty = C_{\mathrm{GUE}}$, there exists a digraph size $V_{\max}$ such that for all $V > V_{\max}$, the error produced by the *finite* accuracy of the zeros will dominate over the difference between C_V and C_{GUE}, and D_V^2 will effectively collapse, at $V > V_{\max}$, to a curve that reflects this error. It is then reasonable to ask whether indeed $V_{\max} \approx 100$ and what we see in Fig. 7.6(b) is the result of this. The answer is negative, as we show below.

2. The finiteness of the sample. The noise in the measurement of $D_V^2[s]$ could be comparable to the difference $D_{100}^2[s] - D_{140}^2[s]$, making the curves in Fig. 7.6(b) effectively indistinguishable, hence making it appear as if the $D_V^2[s]$ is converging to some finite value.

3. The (computational) impossibility to cover the entire "phase space", $\phi_1, \phi_2, \ldots, \phi_{2B}$, $\phi_i \in [0, 2\pi)$, with the "ergodic flow", $\mathrm{k} \to \phi(\mathrm{k}l_1), \phi(\mathrm{k}l_2), \ldots, \phi(\mathrm{k}l_{2B})$, in the case of very large B.

In order to test (and reject) the limited accuracy of the level spacing measurements as the cause of the apparent lack of universality of the large FNdG, let us assume an uncertainty σ for every spacing measurement. Since the zeros that we produce are bounded within an interval of 0.01 mls units (see subsection 7.2.3), σ is of the same order, i.e. we can assume that for ith spacing of the sample, s_i[16],

$$|s_i - s_i^{\mathrm{real}}| < \sigma = 0.01, \tag{7.26}$$

holds, where s_i^{real} is the "infinite precision" version of the measurement s_i. Although we have not checked this systematically, the dispersion Eq. (7.26) is likely to be greatly exaggerated compared to the real one, given the cubic interpolation carried out to find the zeros. In order to isolate the effect of this error, we further assume an *infinite* number of measurements, and also that they arise from the Gaussian Unitary Ensemble. If the deviations $|s_i - s_i^{\mathrm{real}}|$ distribute according to a probability density distribution $P(s_i - s_i^{\mathrm{real}}; \sigma)$, a *modified* spacing distribution will

[16]Small changes to this value do not make any noticeable difference.

result, $\tilde{L}_{\mathrm{GUE}}$, which is a convolution of the theoretical L_{GUE} with the mentioned distribution :

$$\tilde{L}_{\mathrm{GUE}}(s) \equiv \int_{-\infty}^{\infty} L_{\mathrm{GUE}}(|s+x|)P(x)dx. \tag{7.27}$$

Assuming that the error are Gaussian distributed, i.e.

$$P(s_i - s_i^{\mathrm{real}}) = \frac{1}{\sigma\sqrt{2\pi}} \exp\left(-\frac{(s_i - s_i^{\mathrm{real}})^2}{2\sigma^2}\right), \tag{7.28}$$

from Eq. (7.27) we can easily calculate the apparent, finite deviation $D^2_{V_{\max}}(s)$, which reads

$$\left(\tilde{C}_{\mathrm{GUE}}(s) - C_{\mathrm{GUE}}(s)\right)^2 = \left(\int_0^{\infty} L_{\mathrm{GUE}}(u)\left(\frac{1}{2}\left[\mathrm{erf}\left(\frac{s-u}{\sqrt{2}\sigma}\right) + \mathrm{erf}\left(\frac{s+u}{\sqrt{2}\sigma}\right)\right] - \Theta(s-u)\right)du\right)^2, \tag{7.29}$$

and taking $\sigma = 0.01$, the curve to which a system converging to universality should collapse (at $V = V_{\max}$, in the case of a graph) is plotted in 7.7(a), and the order of magnitude is far too small account for the values of $D^2_V(s)$.

Examining the second argument like previous one, i.e. in a clear cut quantitative manner, is not possible: we cannot know the noise affecting the numerically generated curve D^2_{120}, for example. What we can do, is to select from one of the small graphs, for which we have close to 1,000,000 zeros, the zeros lying in the same intervals at our disposal in the case of a big graph, and look at the effect this has on the $D^2_V(s)$ curve. The result is shown in Fig. 7.7(b), where we superpose the curve representing $D^2_{60}(s)$ obtained from the entire data set on the one and, and the one obtained from only the zeros inside the intervals shown in Table 7.2 (referring to the 100-vertex graph) on the other. The difference between the two is more pronounced precisely in the region from $s \sim 0.6$ to $s \sim 0.9$, where a similar discrepancy affecting the $D^2_V(s)$ curves corresponding to the three big graphs could explain the lack of noticeable difference between them. A way to test this hypothesis would be to consider even larger graphs: not existing any reason why the noise should increase, for a large enough graph, with say W vertices, $D^2_W(s)$ should be small enough so that $D^2_{140}(s) - D^2_W(s)$ becomes "visible".

The third argument is a more general one. In a sequence of increasing bond lengths $l_1 < \ldots < l_B$ (whether we have a directed or undirected graph is irrelevant) normalized to one, the *minimal difference, Δl between consecutive bond lengths is not*

greater than $\sim 1/B^2$. The majority of analytical work on QG relies on substituting the flow $\mathrm{k} \to \phi(\mathrm{k}l_b)$ by independent phases $\phi_1, \ldots, \phi_b \ldots$ The phase average, which eventually produces universal statistics, is supposed to mimic the k-average, therefore the numerical evaluation of real QGs should theoretically resemble an average over the entire phase space. Ideally, one would average over a k-interval of length, K, large enough so that $K\Delta l >> 2\pi$, which means that $K \gtrsim 100^4$ for a 100-vertex full graph. The question is then, to which extent the extreme small-size of the phase-space region covered by our spectral average affects the final results.

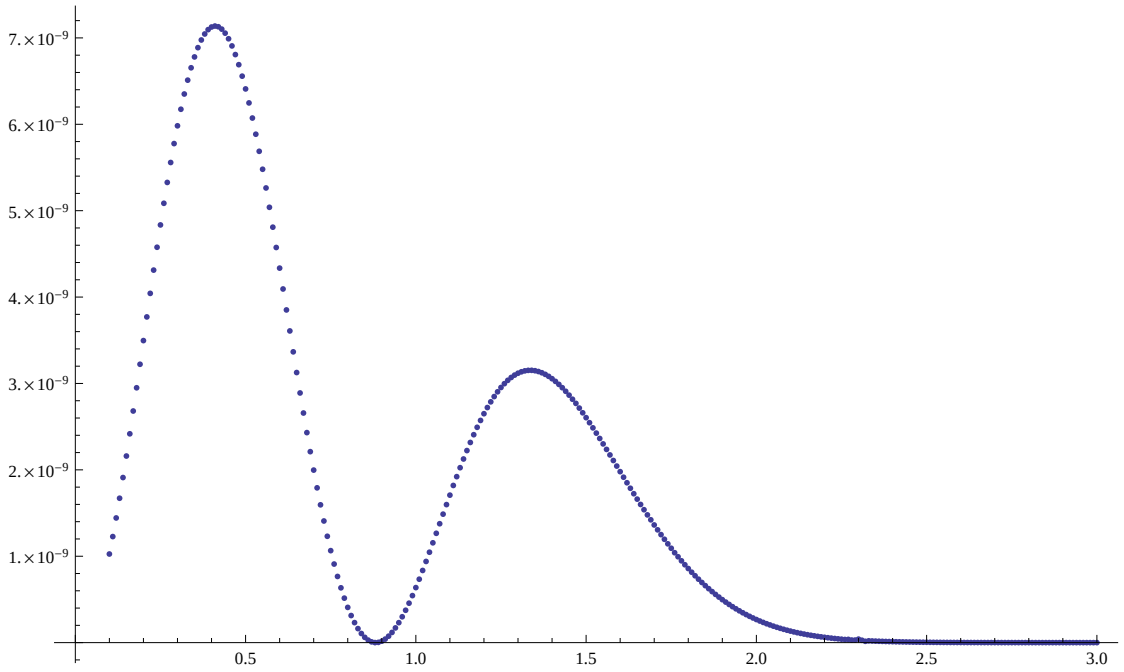

(a)

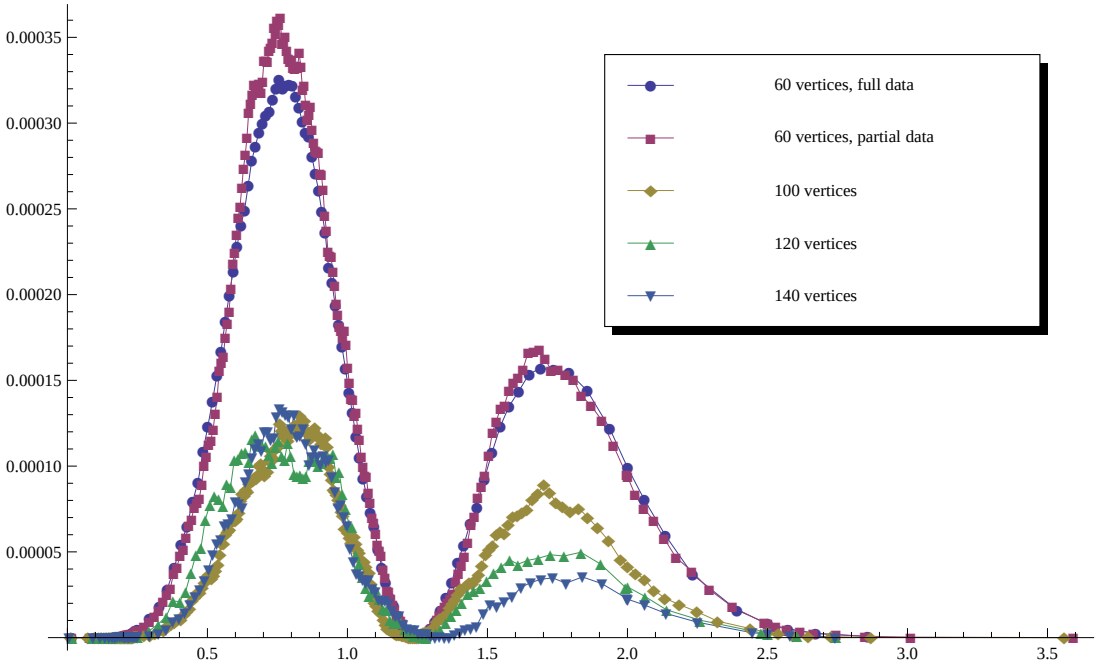

(b)

FIGURE 7.7: In (a), $(\tilde{C}(s) - C_{\mathrm{GUE}}(s))^2$. In (b), we compare the result for $D^2_{60}(s)$ obtained with all the data to the one obtained with data similar to those available for larger graphs. The noise introduced by the reduction of the data could explain the the "mixing" of the curves $D^2_{140}(s), D^2_{120}(s), D^2_{100}(s)$.

7.6 The long range correlation between spacings

When we had to decide the number of zeros that we would attempt to extract from the big graphs, we needed to have an idea about how much "quality" is lost when reducing the k-interval from 1000000 to 100000 mls units length. An unexpected finding was that the result that one obtains for the smaller intervals, besides obviously showing greater noise, seems to strangely depend *on the interval itself*. In Fig. 7.8(a) we show, as an example, the difference that exists between the $D_{60}^2(s)$ curves corresponding to the wave number intervals $[349983, 449984]$ and $[549985, 649979]$, respectively, and between them and the curve drawn from the entire data.

This already suggests that it is better to spread a 100000 mls-long run among small intervals, rather than use consecutive zeros, but it also makes us wonder *how much* should one spread the intervals. In Fig. 7.8(b) we compare the curves for 100000 zeros spread in 10 intervals covering roughly 1000000 mls units from k = 0 to k = 1000000, and spread in 10 intervals ranging from k = 1000000 to k = 10000000 (these are shown in Table 7.7).

Table 7.7: Extra intervals explored for 10-vertex and 60-vertex graph.

$[1100000, 1110000]$
$[2000000, 2010000]$
$[2950000, 2960000]$
$[3975000, 3985000]$
$[5000000, 5010000]$
$[6050000, 6060000]$
$[6990000, 7000000]$
$[8020000, 8030000]$
$[9130000, 9140000]$

The curves obtained from zeros in *separate* intervals (Fig. 7.8(b)) are clearly closer to the curve related to the entire data, than those obtained from the same number of *consecutive* zeros (Fig. 7.8(a)). While the region of the curves below $s \sim 1$ is noisier anyway, (we have discussed the problems related to this region in the previous subsection), the region $s > 1$ is much more stable under removal of data, when this is distributed across a long range of the spectrum.

Spreading the the data over intervals within the *second* million of mls-units shows that there is little difference the corresponding results and those concerning the first million. All this lead us to decide to spread the calculation of zeros over intervals of a 1000000 mls units, and not larger.

This result suggest that there exists a very long range "spacing-to-spacing" correlation, hinting to another departure of the full Neumann graph from RMT statistics which could be further investigated, for example, through the number variance statistics ([49]). One could conjecture that while the level spacing distribution is very close to universal, the correlation between spacings is not, in the exact same way as the level velocity distribution is very close to Gaussian, but the level velocity autocorrelation is strongly size dependent and non-universal, as found by the authors in [68].

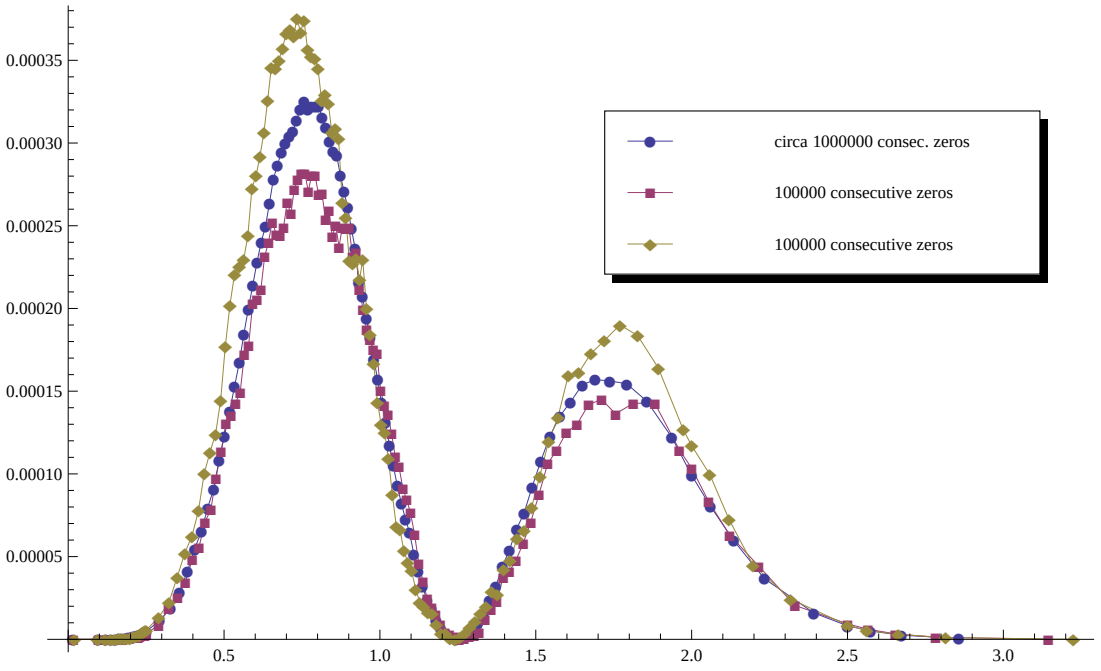

(a)

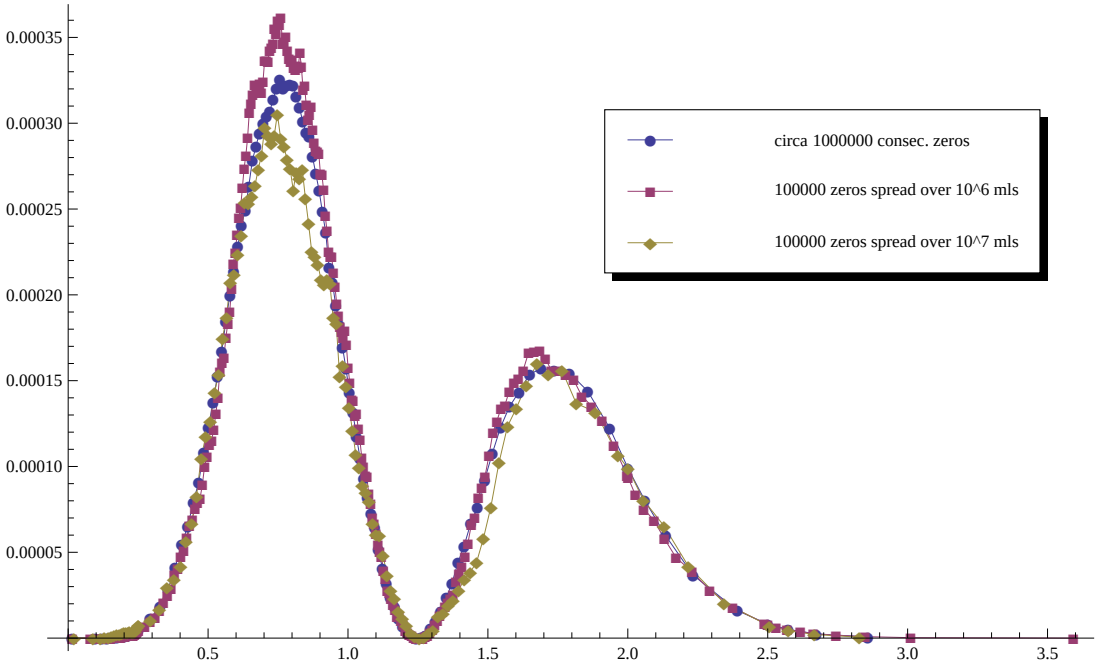

(b)

FIGURE 7.8: In (a) we compare the result for $D_{60}^2(s)$ obtained with all the data to the ones obtained with 100000 *consecutive* zeros belonging to *different* wave number *intervals*. In (b), we show comparison for the cases when the total interval length (around 100000 mls units) is spread over ten smaller intervals that extend over 1000000 mls units or over 10000000.

Chapter 8

Conclusions

We have generalized the notion of wave function *continuity at the nodes* of a quantum graph, to the case when the waves propagating in opposing directions between any two given nodes do so across a pair of antiparallel arcs. The resulting *quantum symmetric digraph* becomes a quantum graph when the two lengths assigned to every pair of antiparallel arcs are made equal, and in this sense the former generalizes the latter. Our pseudo-continuity conditions reduce to the usual continuity conditions when the transition from quantum symmetric digraph to quantum graph is made.

We have introduced a vertex secular equation for QdGs which generalizes the analogous object for QGs introduced by Kottos and Smilansky, and we have used it, together with an original, efficient algorithm, for the numerical generation of the spectra of large, full Neumann digraphs.

We have carried out a systematic study of the decay of the level spacing distribution towards universality at increasing graph size. As a result, and thanks to large data samples, we have confirmed the universality of spectral fluctuations at small frequencies, complementing the knowledge that exists about the universality of the short time form factor. As we find, however, systematic deviations from RMT, full universality of spectral fluctuations cannot be ascertained within our computational means.

The numerical data that were obtained would allow for the exploration of further statistical measures, for example next-to-nearest level spacing distribution and such, that could be compared to the universal equivalent.

The algorithm that we have devised in order to extract the spectrum of large graphs is efficient enough to be further employed, both for graphs and digraphs.

Finally, we suggest here that our quantization scheme, which is based on pseudo-continuity at the nodes and which successfully implements Robin type boundary conditions on symmetric quantum digraphs, could be employed to produce other type of boundary conditions ([44]) on digraphs.

From the work by Gnutzmann and Altland [2], it was not clear that the FNG did *not* fall in the category of graphs for which the saddle point approximation is permitted. A systematic study of the breaking down of the perturbative expansion of the Gnutzmann and Altland field theory (in the case of the FNG) was therefore necessary, and has been carried out.
The reason for splitting a bi-directional bond into two incommensurate arcs with opposite directions was getting rid of the symmetry consisting in associating the same length to both directions in a bond, thereby reducing the number of degrees of freedom of the corresponding field theory and facilitating the analytical treatment (the core of the problem remains when going from the FNG to the FNdG).
Our attempt to a field theoretical, non-perturbative derivation of the universal 2-point correlation function has been based, first, on the simplification just mentioned, and second, on restricting the action to the extensive set of nearly massless modes of Gnutzmann and Altland field theory. As a result, we have obtained a theory whose main variables consist of *sums* of Efetov's type Q-matrices corresponding to arcs attached to a given node. The main difficulty from that point seems to be the fact that interactions exist between these "compound" variables. This is due to every Q_{ij}-matrix being contained both in the compound variable corresponding to node i and that corresponding to node j. It is possible that a different mechanism accounts for the expected universality of the 2-point function, for example a "Higgs mechanism" by which the anti-symmetric modes that we have neglected would generate masses for the symmetric ones.
A number of reasons lead us to suggest that our theory could prove useful when applied to a Neumann *star* graph. On the one hand, a convenient setup of the system, consisting of B mono-directional loops joined together in a single, central point, leads to an action with *no* anti-symmetric modes. On the other hand, the resulting action is much simpler for the star topology than it is for the fully connected graph, because there is obviously only one compound variable, thus the interactions mentioned above do not appear. Since no attempt of using the super-symmetry technique with the Neumann star graph has been made as far as we know and, more generally, applications of Efetov's technique to strongly

non-universal systems (such as the Neumann star) are not frequent, we think this approach could prove interesting.

We have derived an exact functional for wave function statistics in quantum digraphs and studied the universal limit. This work complements the existing understanding on wave function statistics on quantum graphs, and serves to introduce in the quantum graph community a technique used before in the field theoretical treatment of small disordered conductors.

Appendix A

Super-symmetry technique

A.1 Space of Grassmann variables and "super-space"

N "numbers", $\chi_1, \ldots, \chi_N$, and their "complex conjugates", $\chi_1^*, \ldots, \chi_N^*$, satisfying

$$\chi_i \chi_j = -\chi_j \chi_i l \tag{A.1}$$

$$\chi_i \chi_j^* = -\chi_j^* \chi_i \tag{A.2}$$

$$\chi_i^* \chi_j^* = -\chi_j^* \chi_i^*, \tag{A.3}$$

for all i, j, are called *anticommuting*, or *Grassmann*. Complex conjugation of Grassmann numbers has the properties

$$(\chi_i \chi_j)^* = \chi_i^* \chi_j^* \tag{A.4}$$

$$(\chi_i + \chi_j)^* = \chi_i^* + \chi_j^* \tag{A.5}$$

$$(\chi_i^*)^* = -\chi_i. \tag{A.6}$$

A crucial consequence of the anti-commutativity is that products of Grassmann numbers square to zero,

$$(\chi_i \ldots \chi_j)^2 = 0. \tag{A.7}$$

A *supervector*, ψ, and its Hermitian conjugate, are defined as

$$\psi = \begin{pmatrix} \vec{s} \\ \vec{\chi} \end{pmatrix}, \quad \psi^\dagger = \left(\vec{s}^{\,\dagger}, \vec{\chi}^{\,\dagger} \right), \tag{A.8}$$

where the "fermionic" vector $\vec{\chi}$ contains the Grassmann numbers

$$\vec{\chi} = \begin{pmatrix} \chi_1 \\ \vdots \\ \chi_N \end{pmatrix}, \quad \vec{\chi}^{\,\dagger} = (\chi_1^*, \ldots, \chi_N^*), \tag{A.9}$$

and the "bosonic" vector, $\vec{s}$, is simply a N-dimensional complex vector[1], i.e. a "commuting" vector containing "commuting" variables.

The scalar product of two super-vectors is defined in a natural way,

$$\psi_1^\dagger \psi_2 = \vec{s}_1^{\,\dagger} \vec{s}_2 + \vec{\chi}_1^\dagger \vec{\chi}_2, \tag{A.10}$$

and one can see that the "square modulus" of a super-vector is "real", in the sense that $\psi^\dagger\psi = (\psi^\dagger\psi)^*$. Scalar products contain summands of the form $\chi_i^*\chi_j$, which is a *commuting* term, although not an usual, commuting, complex number. Those terms are called *nilpotent*[2].

Super-matrices perform linear operations transforming super-vectors into super-vectors:

$$F\psi = \begin{pmatrix} a & \sigma \\ \rho & b \end{pmatrix} \begin{pmatrix} \vec{s} \\ \vec{\chi} \end{pmatrix} = \begin{pmatrix} a\vec{s} + \sigma\vec{\chi} \\ \rho\vec{s} + b\vec{\chi} \end{pmatrix}, \tag{A.11}$$

where the $2N \times 2N$ super-matrix F contains a *boson-boson* block, a, a *fermion-fermion* block, b, a *boson-fermion* block, σ, and a *fermion-boson* block, ρ. Naturally, the diagonal blocks are commuting numbers and the off-diagonal ones are anti-commuting. If ψ is a super-vector as defined in Eq. (A.8), we see that the super-vector $F\psi$ contains a nilpotent term, $\sigma\vec{\chi}$, in its bosonic part. It is worth mentioning that a bosonic component will in general be the sum of a complex number plus a nilpotent part consisting of a linear combination of *even products*

[1]The fermionic and bosonic spaces need not in general have the same dimension, but they will in our case.

[2]This name can be given to any product of Grassmann numbers, since Eq. (A.7) holds, but it is usually employed to refer to products of an *even* number of factors, which, on the one hand, do not anti-commute with other Grassmann products, but on the other hand are not usual commuting numbers.

of Grassmann numbers, while fermionic components will include a linear combination of *odd products* of anti-commuting numbers[3].

The product of super-matrices is defined in the same way as the usual product of matrices, and the components of a super-matrix can acquire nilpotent parts in a manner similar to that described in the previous paragraph concerning super-vectors.

In order to preserve the property , The *super-transposition* operation is defined as

$$\begin{pmatrix} a & \sigma \\ \rho & b \end{pmatrix}^T = \begin{pmatrix} a^T & \rho^T \\ -\sigma^T & b^T \end{pmatrix}. \tag{A.12}$$

This is highly convenient as, together with Eq. (A.1), it preserves the standard algebraic property

$$(F\psi)^T = \psi^T F^T. \tag{A.13}$$

Moreover, defining super-matrix Hermitian conjugation in the usual way,

$$F^\dagger = (F^T)^*, \tag{A.14}$$

and taking Eq. (A.6) into account, we have

$$(F^\dagger)^\dagger = F, \tag{A.15}$$

while applying Eq. (A.4) and Eq. (A.5) as well, we find

$$(F\psi)^\dagger = \psi^\dagger F^\dagger. \tag{A.16}$$

Super-trace (str) and *super-determinant* (sdet) are defined as

$$\mathrm{str}F = \mathrm{tr}a - \mathrm{tr}b, \quad \mathrm{sdet}F = \frac{\det(a - \sigma b^{-1}\rho)}{\det b}, \tag{A.17}$$

where $\det b$ is assumed not to be nilpotent. The properties

$$\mathrm{str}(F_1F_2) = \mathrm{str}(F_2F_1), \quad \ln \mathrm{sdet}F = \mathrm{str}\ln F, \tag{A.18}$$

hold and generalize the analogous properties of the usual matrix algebra.

[3]Any type of component may equal zero.

A.2 Functions of Grassmann variables, differentiation and integration

Due to the property Eq. (A.7), any function of Grassmann variables, $f(\chi_1, \ldots, \chi_N)$, takes the form of a finite polynomial in those variables:

$$f(\chi_1, \ldots, \chi_N) = c_0 + \sum_i c_1^i \chi_i + \sum_{i<j} c_2^{ij} \chi_i \chi_j + \ldots + c_N \chi_1 \ldots \chi_N, \tag{A.19}$$

where $c_0, c_1^{ij}, \ldots, c_N$ are complex constants. The formula Eq. (A.19) can be obtained from any function by Taylor expansion, although two comments are in order. First, some standard properties of function of a complex variable are not preserved when the function is applied to Grassmann variables, for example, it is obvious that $e^{\chi_i + \chi_j} \neq e^{\chi_i} e^{\chi_j}$ for $i \neq j$. Second, a function $f(x)$ which is non-analytic at $x = 0$ cannot be applied to nilpotents, e.g. $\sqrt{\chi_i}, \frac{1}{\chi_i}, \ln \chi_i$ do not exist. The first of these issues is not usually relevant, because in practice most functions are defined over even products of Grassmann, and we observe that equalities such as $e^{\chi_i \chi_j + \chi_k \chi_l \chi_m \chi_n} = e^{\chi_i \chi_j} e^{\chi_k \chi_l \chi_m \chi_n}$ do hold.

Integration over Grassmann variables is carried out based on the properties

$$\int d\chi_i = 0, \quad \int d\chi_1 \chi_1 = -\int \chi_i d\chi_1 = 1, \tag{A.20}$$

and the fact that the "differentials", $d\chi_i, d\chi_i^*, \ldots$, have the exact same commutation properties as the variables themselves.

The most important use of the super-symmetry technique relies on the validity of formulas for Gaussian integration, such as

$$\int d(\psi^*, \psi) e^{-\psi^\dagger F \psi} = \frac{1}{\mathrm{sdet} F} \tag{A.21}$$

$$\int d(\psi^*, \psi) \psi_i \psi_j^* e^{-\psi^\dagger F \psi} = \frac{1}{\mathrm{sdet} F} \left(F^{-1}\right)_{ij}, \tag{A.22}$$

where

$$d(\psi^*, \psi) = \frac{1}{\pi^N} ds_1^* ds_1 \ldots ds_N^* ds_N d\chi_1^* d\chi^1 \ldots d\chi_N^* d\chi_N. \tag{A.23}$$

The equalities Eq. (A.21) and Eq. (A.22) have the same form as for standard Gaussian integrals, but it is worth mentioning that the order "complex conjugate goes first" in the differential Eq. (A.23), together with "complex conjugate goes

second" in the pair of averaged ψ-components in Eq. (A.22), and the convention Eq. (A.20) make this formulae correct in the case of Grassmann variables (it is irrelevant when averaging over complex-number components). A generalized version of the Wicks theorem can be obtained, allowing for the calculation of the average over any number of super-components. All those averages can be found expanding the following formula on the auxiliary vectors, $\phi, \phi^\dagger$, and equating powers of the same order on these vectors[9]:

$$\mathrm{sdet}F \int_{\cdot} (\psi^*, \psi) e^{-\psi^\dagger F \psi} e^{\psi^\dagger \phi + \phi^\dagger \psi} = e^{\phi^\dagger F \phi}. \tag{A.24}$$

Appendix B

Gaussian integration of super-fields

We consider the second order approximation Eq. (4.28) to the full action Eq. (4.22),

$$S_{\mathrm{k}} = -\operatorname{str}\ln(1 - Z\tilde{Z}) + \operatorname{str}\ln(1 - \Sigma Z\Sigma^{\dagger}\tilde{Z}) \tag{B.1}$$

$$=\operatorname{str}(Z - \Sigma Z\Sigma^{\dagger})\tilde{Z} + O(Z,\tilde{Z})^4 \tag{B.2}$$

for the kinetic action. The source action written as

$$S_{\phi} =\phi_s \operatorname{str}\frac{\Sigma Z\Sigma^{\dagger}\tilde{Z}}{1 - \Sigma Z\Sigma^{\dagger}\tilde{Z}} \tag{B.3}$$

$$+\operatorname{str}\phi_+\frac{\Sigma Z\Sigma^{\dagger}\tilde{Z}}{1 - \Sigma Z\Sigma^{\dagger}\tilde{Z}} + \operatorname{str}\phi_-\frac{\Sigma^{\dagger}\tilde{Z}\Sigma Z}{1 - \Sigma^{\dagger}\tilde{Z}\Sigma Z}, \tag{B.4}$$

has a second order term

$$S^2_{\phi} =\phi_s \operatorname{str}\Sigma Z\Sigma^{\dagger}\tilde{Z} \tag{B.5}$$

$$+\operatorname{str}\phi_+\Sigma Z\Sigma^{\dagger}\tilde{Z} + \operatorname{str}\phi_-\Sigma^{\dagger}\tilde{Z}\Sigma Z. \tag{B.6}$$

The sources $\phi_{\pm}$ are proportional to σ_3^{BF}, and since neither Σ nor ϕ contains non-vanishing Grassmann components, we can see that commuting and anti-commuting variables in the action, at this order, do not multiply each other. Separating both types of variable according to $Z = Z_{\mathrm{D}} + Z_{\mathrm{O}}$, we can re-write the

second order action as

$$S^2 = \mathrm{str}\vec{\tilde{Z}}_{\mathrm{D}}\left(1 - F + \phi_s F + \phi_+ F + \phi_- F\right)\vec{Z}_{\mathrm{D}} \tag{B.7}$$

$$+ \mathrm{str}\vec{\tilde{Z}}_{\mathrm{O}}\left(1 - F + \phi_s F + \phi_+ F - \phi_- F\right)\vec{Z}_{\mathrm{O}}. \tag{B.8}$$

The resulting *independent* gaussian integration of complex and Grassmann Z-components is straightforward:

$$\int d(Z,\tilde{Z})e^{-S^2_{\mathrm{k}}-S^2_{\phi}} = \frac{\det(1 - F + \phi_s F + (\phi_+ - \phi_-)F)}{\det(1 - F + \phi_s F + (\phi_+ + \phi_-)F)}. \tag{B.9}$$

The arguments of the determinants in Eq. (B.9) are not $2B \times 2B$ matrices, but rather $4B \times 4B$, the extra structure on top the arc-structure being inherited from 2×2 *super*-structure of the Z-matrices. Linearizing now in $\phi_\pm$ we find

$$\det(1 - F + \phi_s F + (\phi_+ - \phi_-)F) = \det(1 - F + \phi_s F) \tag{B.10}$$

$$\cdot\left(1 + \mathrm{tr}(\phi_+ - \phi_-)\frac{F}{1-(1-\phi_s)F}\right. \tag{B.11}$$

$$\left. - \frac{1}{2}\mathrm{tr}(\phi_+ - \phi_-)^2\left(\frac{F}{1-(1-\phi_s)F}\right)^2\right), \tag{B.12}$$

$$\frac{1}{\det(1 - F + \phi_s F + (\phi_+ + \phi_-)F)} = \frac{1}{\det(1 - F + \phi_s F)} \tag{B.13}$$

$$\cdot\left(1 - \mathrm{tr}(\phi_+ + \phi_-)\frac{F}{1-(1-\phi_s)F}\right. \tag{B.14}$$

$$\left. + \frac{1}{2}\mathrm{tr}(\phi_+ + \phi_-)^2\left(\frac{F}{1-(1-\phi_s)F}\right)^2\right). \tag{B.15}$$

The sources $\phi_\pm$ are linear in σ_3, in the extra structure, while being proportional to the identity in the arc structure, therefore there is an automatic cancellation of linear terms :

$$\mathrm{tr}\phi_\pm\frac{F}{1-(1-\phi_s)F} = 0. \tag{B.16}$$

They are also linear in the original sources $j_\pm$, and according to the derive-and-take-the-zero-limit procedure, Eq. (4.5), we have another cancellation:

$$\mathrm{tr}\phi^2_\pm\left(\frac{F}{1-(1-\phi_s)F}\right)^2 = 0. \tag{B.17}$$

The final result then reads

$$\lim_{\phi_\pm\to 0}\frac{d^2}{d\phi_+ d\phi_-}\int d(Z,\tilde{Z})e^{-S_{\rm k}^2-S_\phi^2} = 2\lim_{\phi_\pm\to 0}\frac{d^2}{d\phi_+ d\phi_-}{\rm tr}\phi_+\phi_-\left(\frac{F}{1-(1-\phi_s)F}\right)^2 \tag{B.18}$$

$$= 2\left(\frac{\pi}{2B}\right)^2 2{\rm tr}\left(\frac{F}{1-(1-\phi_s)F}\right)^2 \tag{B.19}$$

$$= \left(\frac{\pi}{B}\right)^2 {\rm tr}\left(\frac{F}{1-(1-\phi_s)F}\right)^2. \tag{B.20}$$

The appearance of an extra factor of 2 in Eq. (B.19) is due to the reduction by a half in the dimension of F :

$$\begin{pmatrix} F & 0 \\ 0 & F \end{pmatrix} \to F. \tag{B.21}$$

Bibliography

[1] S. Gnutzmann and A. Altland, *Phys. Rev. Lett.* **93**, 194101 (2004), "Universal spectral statistics in quantum graphs" [arXiv:nlin/0402029].

[2] S. Gnutzmann and A. Altland, *Phys. Rev. E* **72**, 56215 (2005), "Spectral correlations of individual quantum graphs" [arXiv:nlin/0508009].

[3] T. Kottos and U. Smilansky, *Phys. Rev. Lett.* **79**, 4794 (1997), "Quantum chaos on graphs".

[4] T. Kottos and U. Smilansky, *Ann. Phys.* **274**, 76 (1999), "Periodic Orbit Theory and spectral statistics for quantum graphs" [arXiv:chao-dyn/9812005].

[5] V. I. Fal'ko and K. B. Efetov, *Phys. Rev. B* **52**, 17413 (1995), "Statistics of prelocalized states in disordered conductors" [arXiv:cond-mat/9507091].

[6] H. Goldstein, *Classical Mechanics*, (2^{nd} ed.) Addison-Wesley, 1981.

[7] B. Hasselblatt and A. Katok, *A First Course in Dynamics: With a Panorama of Recent Developments.*, Cambridge University Press, 2003.

[8] E. N. Lorentz, *J. Atmos. Sci.* **20**, 140 (1963), "Deterministic nonperiodic flow".

[9] F. Haake, *Quantum Signatures of Chaos*, (corrected 2^{nd} ed.) Springer, Berlin, 2004.

[10] M. Berry, *Phys. Scripta* **40**, 335 (1989), "Quantum chaology, not quantum chaos".

[11] Z. P. Karkuszewski, C. Jarzynski, and W. H. Zurek, *Phys. Rev. Lett.* **89**, 170405 (2002), "Quantum chaotic environments, the butterfly effect, and decoherence" [arXiv:quant-ph/0111002].

[12] L. C. Percival, *J. Phys. B* **6**, L229 (1973), "Regular and irregular spectra".

[13] M. V. Berry and M. Tabor, in *Proc. R. Soc. Lond. A*, volume 349, p. 101, 1976, "Closed orbits and the regular bound spectrum".

[14] M. V. Berry and M. Tabor, in *Proc. R. Soc. Lond. A*, volume 356, p. 375, 1977, "Level clustering in the regular spectrum".

[15] O. Bohigas, M. J. Giannoni, and C. Schmit, *Phys. Rev. Lett.* **52**, 1 (1984), "Characterization of chaotic quantum spectra and universality of level fluctuation laws".

[16] M. C. Gutzwiller, *J. Math. Phys* **12**, 343 (1971), "Periodic orbits and classical quantization condition".

[17] M. C. Gutzwiller, *Chaos in Classical and Quantum Mechanics*, Springer, New York, 1990.

[18] A. Einstein, *Verh. Dt. Phys. Ges.* **19**, 82 (1917), "Zum Quantensatz von Sommerfeld und Epstein".

[19] M. V. Berry, in *Proc. R. Soc. Lond. A*, volume 400, p. 229, 1985, "Semi-classical theory of spectral rigidity".

[20] M. Sieber and K. Richter, *Phys. Scripta* **T90**, 128 (2001), "Correlations between periodic orbits and their role in spectral statistics".

[21] M. Sieber, *J. Phys. A* **35**, L613 (2002), "Leading off-diagonal approximation for the spectral form factor for uniformly hyperbolic systems" [arXiv:nlin/0209016].

[22] S. Müeller, S. Heusler, A. Altland, P. Braun, and F. Haake, *New J. Phys.* **11**, 103025 (2009), "Periodic-orbit theory of universal level correlations in quantum chaos" [arXiv:0906.1960 [nlin.CD]].

[23] K. Efetov, *Supersymmetry in Disorder and Chaos*, Cambridge University Press, 1997.

[24] F. J. Wegner, *Z. Phys. B* **35**, 207 (1979), "The mobility edge problem: Continuous symmetry and a conjecture".

[25] L. Schäfer and F. J. Wegner, *Z. Phys. B* **38**, 113 (1980), "Disordered system with n orbitals per site: Lagrange formulation, hyperbolic symmetry, and Goldstone modes".

[26] J. J. M. Verbaarschot, M. R. Zirnbauer, and H. A. Weidenmüller, *Phys. Rep.* **129**, 367 (1985), "Grassmann integration in stochastic quantum physics: The case of compound-nucleus scattering".

[27] L. P. Gor'Kov and G. M. Eliashberg, *Sov. Phys. JETP* **21**, 940 (1965), "Minute metallic particles in an electromagnetic field".

[28] R. S. Whitney, I. V. Lerner, and R. A. Smith, *Waves Random Media* **9**, 179 (1999), "Can the trace formula describe weak localisation?" [arXiv:cond-mat/9902328].

[29] L. Pauling, *J. Chem. Phys* **4**, 673 (1936), "The diamagnetic anisotropy of aromatic molecules".

[30] K. Ruedenberg and C. Scherr, *J. Chem. Phys* **21**, 1565 (1953), "Free-electron network model for conjugated systems, I. Theory".

[31] P. Exner and O. Post, *J. Phys. A* **42**, 415305 (2009), "Approximation of quantum graph vertex couplings by scaled Schrödinger operators on thin branched manifolds" [arXiv:0811.3707 [math-ph]].

[32] P. Exner, in *Analysis on Graphs and Applications: Proceedings of Symposia in Pure Mathematics*, volume 77, p. 523, 2007, "Leaky quantum graphs: a review" [arXiv:0710.5903 [math-ph]].

[33] S. Gnutzmann and U. Smilansky, *Adv. Phys.* **55**, 527 (2006), "Quantum graphs: applications to quantum chaos and universal spectral statistics" [arXiv:nlin/0605028].

[34] O. Hul, S. Bauch, P. Pakonski, N. Savytskyy, K. Zyczkowski, and L. Sirko, *Phys. Rev. E* **69**, 56205 (2004), "Experimental simulation of quantum graphs by microwave networks" [arXiv:nlin/0404006].

[35] J. P. Rot, in *Lecture Notes in Mathematics: Theorie du Potentiel*, p. 521, Edited by A. Dold and B. Eckmann, SpringerVerlag, 1984.

[36] G. Tanner, *J. Phys. A* **34**, 8485 (2001), "Unitary stochastic matrix ensembles and spectral statistics" [arXiv:nlin/0104014].

[37] G. Berkolaiko, H. Schanz, and R. S. Whitney, *Phys. Rev. Lett.* **88**, 104101 (2002), "Leading off-Diagonal correction to the form factor of large graphs" [arXiv:nlin/0107056].

[38] G. Berkolaiko, H. Schanz, and R. S. Whitney, *J. Phys. A* **36**, 8373 (2003), "Form factor for a family of quantum graphs: an expansion to third order" [arXiv:nlin/0205014].

[39] M. Zirnbauer, in *Supersymmetry and Trace Formula: Chaos and Disorder*, p. 153, Edited by Lerner *et al.*, Kluwer Academic - Plenum Publishers, 1999, "Pair correlations of quantum chaotic maps from supersymmetry" [arXiv:chao-dyn/9812023].

[40] M. Zirnbauer, *J. Phys A* **29**, 7113 (1996), "Supersymmetry for systems with unitary disorder: Circular ensembles" [arXiv:chao-dyn/9609007].

[41] S. Gnutzmann, J. P. Keating, and F. Piotet, *Phys. Rev. Lett.* **101**, 264102 (2008), "Quantum ergodicity on graphs" [arXiv:0808.4110 [nlin.CD]].

[42] S. Gnutzmann, J. P. Keating, and F. Piotet, *Ann. Phys.* **325**, 2595 (2010), "Eigenfunction statistics on quantum graphs" [arXiv:1005.1026 [nlin.CD]].

[43] G. Tanner, *J. Phys. A* **33**, 3567 (2000), "Spectral statistics for unitary transfer matrices of binary graphs" [arXiv:nlin/0001025].

[44] V. Kostrykin and R. Schrader, *J. Phys. A* **32**, 595 (1999), "Kirchhoff's rule for quantum wires" [arXiv:math-ph/9806013].

[45] F. J. Dyson, *J. Math. Phys.* **3**, 166 (1962), "Statistical theory of energy levels of complex systems I, II and III".

[46] E. P. Wigner, in *Proc. Cambridge Phil. Soc.*, volume 47, p. 790, 1951, "On the statistical distribution of the widths and spacings of nuclear resonance levels".

[47] F. J. Dyson and M. L. Mehta, *J. Math. Phys.* **4**, 701 (1963), "Statistical theory of energy levels of complex systems IV".

[48] Y. V. Fyodorov, in *Recent perspectives in random matrix theory and number theory, London Math. Soc. Lecture Note Ser., 322*, p. 31, Cambridge University Press, 2005, "Introduction to the Random Matrix Theory: Gaussian Unitary Ensemble and beyond" [arXiv:math-ph/0412017].

[49] M. L. Mehta, *Random Matrices*, Amsterdam: Elsevier/Academic Press, 2004.

[50] U. Grimm, *Phys. status solidi B* **241**, 2139 (2004), "Series expansions for level-spacing distributions of the Gaussian unitary random matrix ensemble".

[51] P. Pakonski, K. Zyczkowski, and K. Marek, *J. Phys. A* **34**, 9303 (2001), "Classical 1D maps, quantum graphs and ensembles of unitary matrices" [arXiv:nlin/0011050].

[52] F. Barra and P. Gaspard, *Phys. Rev. E* **63**, 066215, "Classical dynamics on graphs" [arXiv:nlin/0011045].

[53] D. R. Cox and H. D. Miller, *The Theory of Stochastic Processes*, Methuen & Co ltd, 1970.

[54] D. Stirzaker, *Stochastic Processes and Models*, Oxford University Press, 2005.

[55] S. Severini and G. Tanner, *J. Phys. A* **37**, 6675 (2004), "Regular quantum graphs" [arXiv:nlin/0312031].

[56] P. Pakonski, G. Tanner, and K. Zyczkowski, *J. Stat. Phys.* **111**, 1331 (2003), "Families of line-graphs and their quantization" [arXiv:nlin/0110043].

[57] C. Itzykson and J. B. Zuber, *J. Math. Phys.* **21**, 411 (1980), "The planar approximation. II".

[58] A. V. Andreev and B. D. Simons, *Phys. Rev. Lett.* **75**, 2304 (1995), "Correlators of spectral determinants in quantum chaos".

[59] T. Guhr, *J. Math. Phys.* **32**, 336 (1991), "Dyson's correlation functions and graded symmetry".

[60] Y. V. Fyodorov and E. Strahov, *Nucl. Phys. B* **630**, 453 (2002), "Characteristic polynomials of random Hermitian matrices and Duistermaat-Heckman localisation on non-compact Kaehler manifolds" [arXiv:math-ph/0201045].

[61] M. V. Berry, *J. Phys. A* **10**, 2083 (1977), "Regular and irregular semiclassical wavefunctions".

[62] L. Kaplan, *Phys. Rev. E* **64**, 36225 (2001), "Eigenstate structure in graphs and disordered lattices" [arXiv:nlin/0101048].

[63] H. Schanz and T. Kottos, *Phys. Rev. Lett.* **90**, 234101 (2003), "Scars on quantum networks ignore the Lyapunov exponent" [arXiv:nlin/0302054].

[64] V. E. Kravtsov and A. D. Mirlin, *JETP Letters* **60**, 656 (1994), "Level statistics in a metallic sample: Corrections to the Wigner-Dyson distribution" [arXiv:cond-mat/9408072].

[65] Y. V. Fyodorov and A. D. Mirlin, *Phys. Rev. B* **51**, 13403 (1995), "Mesoscopic fluctuations of eigenfunctions and level-velocity distribution in disordered metals" [arXiv:cond-mat/9408075].

[66] R. Carlson, *Trans. Am. Math. Soc.* **351**, 4069 (1999), "Inverse eigenvalue problems on directed graphs".

[67] R. Carlson, *Electron. J. Differential Equations* **6**, 1 (1998), "Adjoint and self-adjoint differential operators on graphs".

[68] O. Hul, P. Šeba, and L. Sirko, *Phys. Rev. E* **79**, 066204 (2009), "Departure of some parameter-dependent spectral statistics of irregular quantum graphs from random matrix theory predictions" [arXiv:0907.2794 [nlin.CD]].

[69] F. Barra and P. Gaspard, *J. Stat. Phys* **101**, 283 (2000), "On the level spacing distribution in quantum graphs" [arXiv:quant-ph/0011099].